4

APERTURE DISTRIBUTIONS AND ARRAY SYNTHESIS

Continuous apertures and arrays share similar characteristics. We compute the radiation pattern of the aperture by using the Fourier transform. Array sampling of an aperture distribution leads to a Fourier series analysis for its pattern. We rely on our familiarity with signal processing to give us insights into these processes and their characteristics. We apply aperture theory to the analysis of horns, lens, and reflector antennas, but it also describes array antennas. Since we can design antennas only approximately to produce particular aperture distributions, we often realize them by sampling with an array.

We start with aperture efficiencies developed from the Huygens source approximation of Section 2-2. We apply this method to horns, lens, and reflector antennas for both synthesis and tolerance analysis. The uniform and cosine distributions occur naturally in horns and simple resonant antennas. We use aperture distributions to realize bounds on antenna characteristics given size and excitation distribution.

Taylor developed an aperture distribution based on Dolph's use of the Chebyshev polynomials to produce the narrowest beamwidth for a specified sidelobe level for an array. The Chebyshev array design produces equal-amplitude sidelobes that we discover to be undesirable for large arrays because the equivalent aperture distribution peaks at the ends and the average value of the sidelobes limits the directivity to 3 dB above the sidelobe level. Large edge peaking of the distribution requires a feed network containing a large ratio of coupling values. Mutual coupling between elements causes unwanted excitation for a large ratio of element amplitudes and we lose control. Our usual practice is to sample a Taylor distribution for large arrays. The distribution has limited edge peaking, and large arrays can realize high gains.

Aperture distribution synthesis involves manipulating pattern nulls to achieve desired characteristics. Taylor used the zeros of the Chebyshev array to alter the positions of the inner nulls of the uniform distribution to lower sidelobe levels. Elliott extended this

Modern Antenna Design, Second Edition, By Thomas A. Milligan

idea to iterate the positions of these nulls to produce a linear aperture that radiates individually specified sidelobes. Schelkunoff developed a transformation between the pattern of an array and a polynomial where we combine the roots (or zeros) of the array polynomial in the complex plane with a mapped pattern variable that traverses the unit circle to analyze array patterns. We synthesize arrays by manipulating these polynomial zeros in the complex plane. Similar to Elliott's method of null positioning for the continuous linear aperture, Orchard (and Elliott) developed an iterative method applied to array polynomial zeros to synthesize arrays. The method allows us to specify sidelobes individually and to shape the main beam pattern by moving some zeros off the unit circle. When designing shaped beams, improved synthesis by the Orchard method reduces our use of both array sampling of the Woodward continuous aperture method and direct Fourier series synthesis for linear arrays, but both earlier methods give us insight. We consider the design of series feeding where elements are fed directly from a transmission line for a linear array or continuous linear aperture. This requires specification of the couplers or loading of the transmission line along the array because a portion of the power is extracted at each position with the remaining power dissipated in a load.

We repeat aperture analysis for circular apertures to show limitations of large reflector antennas and for use in sampling with an array. For planar arrays, we reduce many rectangular apertures to the product of two linear distributions. A Chebyshev-type planar array with equal sidelobes can be designed so that the sidelobes in the diagonal planes are not reduced unnecessarily. Convolution synthesis of planar arrays allows manipulation of the pattern zeros in groups of smaller arrays similar to the Schelkunoff method. Finally, we consider aperture blockage and phase errors that lead to gain reduction and increased sidelobes.

4-1 AMPLITUDE TAPER AND PHASE ERROR EFFICIENCIES

When we use the Huygens source approximation, we calculate power radiated by summing (integrating) the magnitude squared of the electric field in the aperture and dividing by the impedance of free space. The average radiation intensity is the radiated power divided by the area of a unit sphere, 4π. To complete the calculation, we compute the maximum radiation intensity by dividing the maximum of the magnitude squared of Eq. (2-24) by the impedance of free space and directivity ($U_{\max}/U_{\text{avg}}$) becomes

$$\frac{\pi(1+\cos\theta)^2}{\lambda^2}\frac{\left|\iint\limits_s E e^{j\mathbf{k}\cdot\mathbf{r}'}\,ds'\right|^2_{\max}}{\iint\limits_s |E|^2\,ds'} \tag{4-1}$$

Equation (4-1) can be used for directivity in any pattern direction, including the maximum of the numerator integral.

An aperture with a uniform amplitude and phase distribution has directivity $4\pi A/\lambda^2$, where A is the area. We separate directivity reductions into individual terms due to

aperture field amplitude and phase variations, and we express the general aperture directivity as

$$\text{directivity} = \frac{4\pi A}{\lambda^2} \cdot \text{ATL} \cdot \text{PEL}$$

where ATL is the amplitude taper efficiency (loss) and PEL is the phase error efficiency (loss). Only amplitude variations contribute to ATL, and only phase variations determine PEL.

We start with a uniform phase distribution in the aperture where the beam peak occurs normal to the aperture ($\theta = 0^\circ$) and PEL = 1. We obtain uniform phase fields by using $|E|$ in Eq. (4-1):

$$\text{directivity} = \frac{4\pi}{\lambda^2} \frac{\left(\iint_s |E|\, ds \right)^2}{\iint_s |E|^2\, ds} = \frac{4\pi A}{\lambda^2} \cdot \text{ATL}$$

where $k_x = k_y = 0$ on the boresight ($\theta = 0^\circ$). On solving for ATL, we derive

$$\text{ATL} = \frac{\left(\iint_s |E|\, ds \right)^2}{A \iint |E|^2\, ds} \tag{4-2}$$

We have forced a constant phase everywhere in the aperture to separate out the amplitude taper effects. We account for nonuniform phase with PEL. The phase error efficiency can be found from

$$\text{PEL}(\theta, \phi) = \frac{\text{directivity}(\theta, \phi)}{(4\pi A/\lambda^2) \cdot \text{ATL}}$$

where we use directivity (θ, ϕ) and PEL (θ, ϕ) depends on the pattern direction $(\theta,\ \phi)$:

$$\text{PEL}(\theta, \phi) = \frac{(1 + \cos\theta)^2}{4} \frac{\left| \iint_s E e^{j\mathbf{k}\cdot\mathbf{r}'}\, ds \right|^2}{\left(\iint_s |E|\, ds \right)^2} \tag{4-3}$$

$$\mathbf{k} = k(\sin\theta\cos\phi\hat{\mathbf{x}} + \sin\theta\sin\phi\hat{\mathbf{y}} + \cos\theta\hat{\mathbf{z}})$$

For an aperture in the $x-y$ plane,

$$\mathbf{k} \cdot \mathbf{r}' = k(x' \sin\theta\cos\phi + y' \sin\theta\sin\phi)$$

We determine maximum PEL to relate it and ATL to directivity. Traditionally, we use the boresight value ($\theta = 0^\circ$) and Eq. (4-3) reduces to

$$\text{PEL} = \frac{\left| \iint_s E\, ds \right|^2}{\left(\iint_s |E|\, ds \right)^2} \tag{4-4}$$

Unless specified, PEL will be Eq. (4-4) and we use Eq. (4-3) for scanned apertures.

Equations (4-2) and (4-4) separate the effects of amplitude and phase variations in the aperture on the directivity at the boresight. If these efficiencies are expressed in decibels, the directivity becomes

$$\text{directivity(dB)} = 10 \log \frac{4\pi A}{\lambda^2} + \text{ATL}_{\text{dB}} + \text{PEL}_{\text{dB}}$$

Expressed in decibels, the efficiencies are called *losses:* amplitude taper loss (ATL) and phase error loss (PEL). It is important to remember that these are the losses at the boresight. A linear phase taper across the aperture scans the beam, but Eq. (4-4) predicts the boresight loss, which could be a null of the pattern. ATL is independent of phase variations that cause squinting of the beam.

4-1.1 Separable Rectangular Aperture Distributions

If the distribution in a rectangular aperture is separable,

$$E(x, y) = E_1(x) E_2(y)$$

the efficiencies also are separable.

$$\text{ATL} = \text{ATL}_x \text{ATL}_y \quad \text{and} \quad \text{PEL} = \text{PEL}_x \text{PEL}_y \tag{4-5}$$

Given a rectangular aperture with an x-axis excursion of $\pm a/2$,

$$\text{ATL}_x = \frac{\left[\int_{-a/2}^{a/2} |E_1(x)|\, dx \right]^2}{a \int_{-a/2}^{a/2} |E_1(x)|^2 dx} \tag{4-6}$$

$$\text{PEL}_x = \frac{\left| \int_{-a/2}^{a/2} E_1(x)\, dx \right|^2}{\left[\int_{-a/2}^{a/2} |E_1(x)|\, dx \right]^2} \tag{4-7}$$

The formulas for the y-axis are the same except for the substitution of y for x.

4-1.2 Circularly Symmetrical Distributions

If a circular aperture has a circularly symmetrical distribution, we easily reduce Eqs. (4-2) and (4-4) to

$$\text{ATL} = \frac{2\left[\int_0^a |E(r)|r\,dr\right]^2}{a^2\int_0^a |E(r)|^2 r\,dr} \tag{4-8}$$

$$\text{PEL} = \frac{\left|\int_0^a E(r)r\,dr\right|^2}{\left[\int_0^a |E(r)|r\,dr\right]^2} \tag{4-9}$$

where a is the radius.

We need a short word on formulas using integrals. They look formidable and seem to have little immediate practical use. In the catalog of distributions to follow, results will be given. A general distribution must be solved by numerical integration. One of the Newton–Cotes methods, such as Simpson's rule or the Rhomberg integration, can be used when evenly spaced values are known. With a known function for the distribution, we use the Gauss–Legendre technique, whereby the method selects the required function values. It is sometimes easier to calculate the integrals numerically instead of writing routines for special functions that arise with circular apertures. Exact expressions are ideal; but unless a distribution is forced by a mode on the structure, it is difficult to achieve the exact distribution. We need only approximations to the accuracy of practical interest.

4-2 SIMPLE LINEAR DISTRIBUTIONS

We assume that rectangular apertures have separable distributions so that we can deal with one coordinate at a time. We compute the pattern in the plane containing the line. By drawing the pattern in k_x (or k_y)-space, we can calculate patterns independent of the aperture size in a way similar to that used for arrays in Chapter 3. In Chapter 2 we derived the k_x-space pattern for a uniform distribution:

$$\frac{a\sin(k_x a/2)}{k_x a/2} \tag{4-10}$$

where a is the aperture width and $k_x = k\sin\theta\cos\phi$. We suppress $\cos\phi$ and consider only patterns in the $\phi = 0^\circ$ plane. Figure 4-1 shows the $k\sin\theta$ space pattern of a uniform distribution. The pattern does not repeat at 2π intervals (radians) as the array does, but the sidelobes continue to decrease at a rate of $1/x$. The first sidelobe is 13.2 dB below the peak. The aperture size a, along with the scanning variable $\sin\theta_0$, determines the visible region in Figure 4-1. It ranges between $\pm ka/2$ centered on $ka/2\sin\theta_0$, since the maximum value of $\sin\theta = 1$.

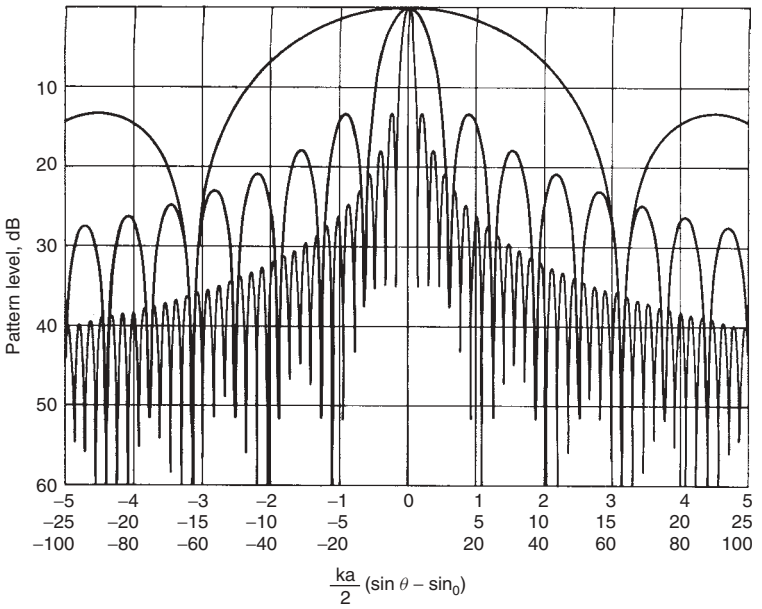

FIGURE 4-1 k_x-space pattern of uniform line-source distribution.

Example An aperture is four wavelengths long. Determine the number of sidelobes between $\theta = \pm 90^\circ$ when $\sin \theta_0 = 0$ (boresight).

The maximum value in ($k \sin \theta$)-space is

$$\frac{2\pi}{\lambda}\frac{4\lambda}{2} = 4\pi \quad \text{or} \quad 12.57$$

There are three sidelobes on each side of the main beam (Figure 4-1) in the visible region. The first sidelobe occurs when $ka/2 \sin \theta_1 = 4.5$, or

$$\theta_1 = \sin^{-1} \frac{4.5\lambda}{a\pi} = 21^\circ$$

We found the half-power beamwidth in Chapter 2:

$$\text{HPBW} = \sin^{-1} \frac{0.4429\lambda}{a} \tag{4-11}$$

valid when we ignore the obliquity factor, $(1 + \cos\theta)/2$. When we approximate $x = \sin x$ (radians) for small angles, we obtain

$$\text{HPBW} = 50.76^\circ \frac{\lambda}{a} \tag{4-12}$$

We use this as the standard and describe other HPBW by their beamwidth factors. The beamwidth factor of the uniform distribution is 1.00. We also consider the null

beamwidth (BW_{null}) of the distribution. The first null occurs at $\pm\pi$ in the $k \sin\theta$ pattern:

$$BW_{null} = 2\sin^{-1}\frac{\lambda}{a} \approx 114.59^\circ\frac{\lambda}{a}$$

We also establish a beamwidth factor for the null beamwidth. When we scan the beam to a direction θ_0, the visible region centers at $\pi a/\lambda \sin\theta_0$ in $(k \sin\theta)$-space.

Example Compute beam edges when $\theta_0 = 30^\circ$ and $a = 6\lambda$ for a uniform distribution.

$$\frac{a}{\lambda}(\sin\theta_{1,2} - \sin\theta_0) = \pm 0.4429$$

$$\sin\theta_{1,2} = \frac{\pm 0.4429}{6} + 0.5$$

$$\theta_1 = 35.02^\circ \qquad \theta_2 = 25.23^\circ$$

The beamwidth is the difference, 9.79°. If we take the beam center as the average between the 3-dB beam edges, we get 30.12° for the beam center. By using the cosine of the beam center times the aperture size, we get 5.19λ, the projected aperture dimension. On substituting this in Eq. (4-11), we calculate HPBW = 9.79°. The actual beam peak is at $\theta = 30^\circ$, but the pattern is asymmetrical about θ_0.

Other simple geometrical distributions on a linear aperture follow the same Fourier transform relation as the uniform distributions with differing transforms in $(k \sin\theta)$-space. Table 4-1 lists the properties of some common distributions.

Example Compute the beamwidth of a 7λ aperture with a cosine distribution.

From Table 4-1, the beamwidth factor = 1.342. The taper increases the beamwidth over that of a uniform distribution:

$$\text{HPBW} = 1.342\frac{50.76\lambda}{a} = 9.73^\circ \quad \text{or} \quad \text{HPBW} = 2\sin^{-1}\left(1.342\frac{0.4429\lambda}{a}\right) = 9.74^\circ$$

We can add distributions and calculate the pattern from the sum of the transforms. Adding a pedestal (uniform distribution) to the cosine-squared distribution decreases

TABLE 4-1 Common Linear Distribution Characteristics

Distribution	f_x	First Sidelobe (dB)	HPBW Factor	BW_{null} Factor	ATR (dB)
Uniform	$\dfrac{\sin(k_x a/2)}{k_x a/2}$	13.2	1.000	1.000	0
Triangular	$\left[\dfrac{\sin(k_x a/4)}{k_x a/4}\right]^2$	26.5	1.439	2.000	1.25
Cosine	$2\pi\dfrac{\cos(k_x a/2)}{\pi^2 - (k_x a)^2}$	23.0	1.342	1.5	0.91
Cosine^2	$\dfrac{\sin(k_x a/2)}{(k_x a/2)[1 - (a/2\lambda)]^2}$	31.5	1.625	2.000	1.76

the beamwidth and the sidelobes of the cosine-squared distribution. The aperture distribution is given by

$$E(x) = \text{PD} + (1 - \text{PD}) \cos^2 \frac{\pi x}{a} \qquad |x| \leq \frac{a}{2}$$

where PD is the voltage pedestal level. The first sidelobe of the uniform distribution lies within the null beamwidth of the cosine-squared distribution. The phase of sidelobes with respect to the main beam alternates between 180° and 0°, and the sidelobe of the pedestal subtracts from the main lobe. The second sidelobe of the pedestal occurs in almost exactly the same k-space location as the first sidelobe of the cosine-squared distribution. These lobes cancel each other to some extent. Table 4-2 gives the required pedestal measured relative to the peak of the distribution for a given maximum sidelobe level. The minimum sidelobes (43.2 dB) occur for a pedestal level of −22.3 dB. At lower pedestal levels, the sidelobes rise and the beamwidth factor increases at a constant rate as the pedestal level decreases.

The amplitude taper efficiency of the cosine squared on a pedestal is

$$\text{ATL} = \frac{2(1 + \text{PD})^2}{3 + 2\text{PD} + 3\text{PD}^2} \qquad \text{ratio} \tag{4-13}$$

Amplitude distributions based on simple functions have limited use. The uniform and cosine distributions or close approximations occur naturally, but the others must be forced on an aperture. An array can sample a distribution to achieve results similar to those for an aperture. A sampled cosine squared on a pedestal is handy for quick tolerance studies of array feed networks, but is far from optimum. Table 4-2 lists the pedestal to achieve a given sidelobe level for this distribution. We consider distributions that allow close control of sidelobes and achieve minimum beamwidths.

The rate of decrease of the far-out sidelobe depends on the functional relation of the distribution at the edges [1]. If α is the exponent of the distribution approximation x_e^{α}, where x_e is the distance from the edge, then the sidelobes decay as $U^{-(1+\alpha)}$, where U

TABLE 4-2 Pedestal Level to Achieve a Given Maximum Sidelobe Level for a Cosine Squared on a Pedestal Distribution

Sidelobe (dB)	Pedestal (dB)	Beamwidth Factor	ATL (dB)
30	−12.9	1.295	0.79
32	−14.2	1.325	0.89
34	−15.7	1.357	0.99
36	−17.3	1.390	1.10
38	−18.7	1.416	1.18
40	−20.0	1.439	1.25
42	−21.4	1.463	1.32
42.7[a]	−21.9	1.471	1.34
43.2[b]	−22.3	1.476	1.36

[a] Hamming distribution.
[b] Minimum sidelobe level.

is a linear function of the k-space variable. Both the triangular and cosine distributions have $\alpha = 1$, and the far-out sidelobes decay as $1/U^2$. The cosine-squared distribution sidelobes decay as $1/U^3$, since $\alpha = 2$. In the case of a cosine squared on a pedestal, the edge functional relation is a step (pedestal, $\alpha = 0$) and the far-out sidelobes decay as $1/U$. The sidelobes of the pedestal eventually overtake the cosine-squared distribution sidelobes, decreasing as $1/U^3$. To achieve uniform sidelobes, α must be -1, which occurs only when the distribution edges are Dirac delta functions, which requires infinite energy in the aperture or design reduction to discrete sources (an array).

We must accept a trade-off between radiated power in the main beam and in the sidelobes. When we narrow the main beam in a fixed size aperture, more power radiates in the sidelobes. We achieve minimum beamwidth in the main beam when all the sidelobes radiate the same power (maximum radiated power in the sidelobes for a given level) and all sidelobes are at the same level. This case leads to the Dolph–Chebyshev array [2], impossible to duplicate in a continuous aperture.

4-3 TAYLOR ONE-PARAMETER LINEAR DISTRIBUTION [3]

The uniform distribution has k-space zeros at (Figure 4-1) $\pm n\pi$, $n = 1, 2, 3, \ldots$. Taylor defines a new variable U to replace $k \sin\theta$:

$$\frac{\sin \pi U}{\pi U} \tag{4-14}$$

where $U = (a/\lambda)(\sin\theta - \sin\theta_0)$ and a is the aperture width. The nulls (zeros) are then located at integer values of U. Taylor adjusted the inner zeros of the uniform distribution to lower the sidelobes while retaining the outer zeros at their locations in the uniform distribution. The zeros are modified by a parameter B the boundary between the two regions in U-space:

$$U_n = \sqrt{n^2 + B^2} \tag{4-15}$$

The pattern has different expressions in two regions:

$$F(U) = \begin{cases} \dfrac{\sinh \pi\sqrt{B^2 - U^2}}{\pi\sqrt{B^2 - U^2}} & |U| \le B \qquad (4\text{-}16a) \\ \dfrac{\sin \pi\sqrt{U^2 - B^2}}{\pi\sqrt{U^2 - B^2}} & |U| \ge B \qquad (4\text{-}16b) \end{cases}$$

The high value of Eq. (4-16a) at the boresight depresses the sidelobes of the uniform distribution, and the parameter B controls all the parameters of the distribution. We compute B from the desired sidelobe level (SLR) by an iterative solution of the equation

$$\text{SLR} = 13.26 + 20 \log \frac{\sinh \pi B}{\pi B} \tag{4-17}$$

Scale 4-1 gives the Taylor single-parameter distribution B for a given sidelobe level.

The aperture distribution over the range -0.5 to 0.5 is given by the equation

$$\frac{I_0[\pi B\sqrt{1 - (2x)^2}]}{I_0(\pi B)} \tag{4-18}$$

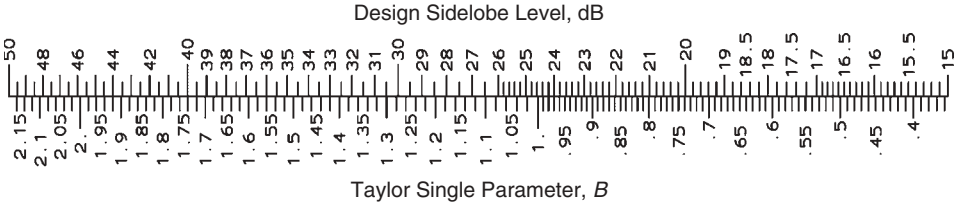

SCALE 4-1 Taylor single-parameter B for a sidelobe level.

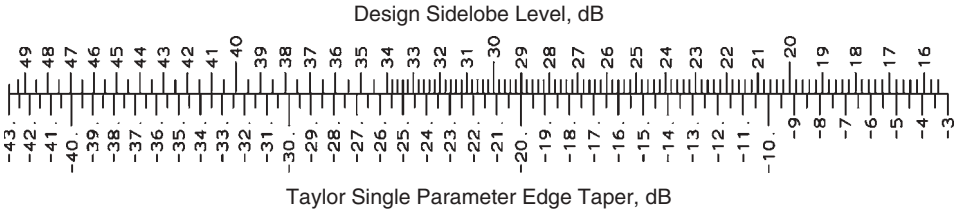

SCALE 4-2 Taylor single-parameter edge taper for a given sidelobe level.

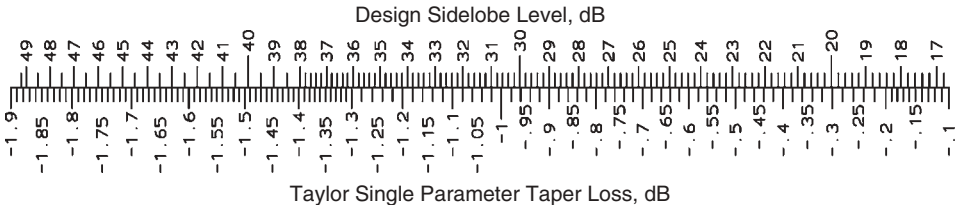

SCALE 4-3 Taylor single-parameter amplitude taper loss for a given sidelobe level.

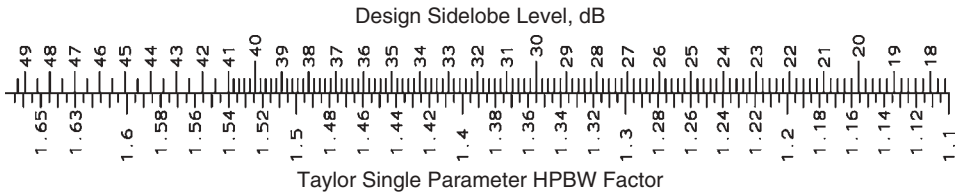

SCALE 4-4 Taylor single-parameter HPBW factor for a given sidelobe level.

Using Eq. (4-18), we calculate aperture edge taper as a function of sidelobe level, given by Scale 4-2. By inserting the expression for the aperture distribution [Eq. (4-18)] into Eq. (4-6), we calculate amplitude taper loss as a function of sidelobe level (Scale 4-3). The HPBW factor can be found from Eq. (4-16) or read easily from Scale 4-4.

Figure 4-2 compares the U-space patterns of the Taylor one-parameter and uniform distributions. Synthesizing aperture distributions and arrays concentrates on the placement of pattern nulls. The one-parameter distribution scaled the locations of the nulls (zeros) by using Eq. (4-15). You should notice that the nulls approach those of the

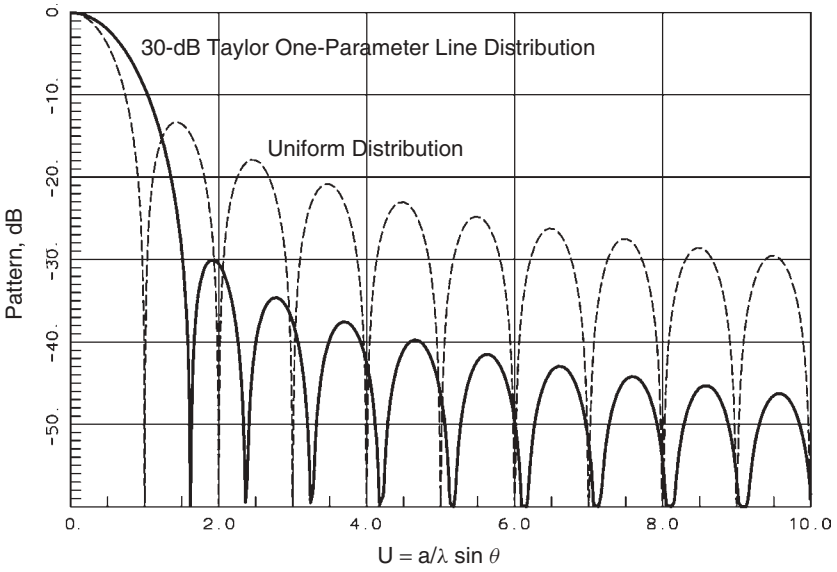

FIGURE 4-2 U-space pattern of 30-dB Taylor one-parameter linear distribution versus uniform distribution.

uniform distribution as U increases. Except for a shift near $U = 0$, the pattern falls off at a $1/U$ rate for far-out sidelobes.

You can use the one-parameter Taylor distribution to estimate the characteristics of a linear distribution for a given sidelobe level. A comparison of this distribution to the cosine squared on a pedestal (Table 4-3) shows that it is not as efficient for moderate sidelobe levels. The cosine squared on a pedestal distribution achieves low sidelobes by canceling sidelobes in two distributions and cannot be extended to any sidelobe level, whereas the one-parameter distribution can produce designs for any sidelobe level. More important, it demonstrates the systematic use of U-space pattern null placement for design. Taylor improved on this distribution by considering the zeros of the Dolph–Chebyshev array to flatten the first few sidelobes of the pattern response and achieved a more efficient distribution.

TABLE 4-3 Comparison Between the Taylor One-Parameter Distribution and Cosine Squared on Pedestal Linear Distribution for Selected Sidelobe Levels

Distribution	Pedestal (dB)	ATR (dB)	HPBW Factor
30-dB one-parameter	−21.13	0.96	1.355
30-dB $\cos^2$ + pedestal	−12.9	0.79	1.295
36-dB one-parameter	−28.49	1.30	1.460
36-dB $\cos^2$ + pedestal	−17.3	1.10	1.390
40-dB one-parameter	−32.38	1.49	1.524

4-4 TAYLOR $\overline{n}$ LINE DISTRIBUTION [1]

The Taylor $\overline{n}$ line-source distribution modifies the location of the inner pattern zeros (nulls) of a uniform distribution to approximate the Dolph–Chebyshev array. The distribution contains a pedestal $\alpha = 0$ and retains the $1/U$ fall-off for the far-out sidelobes. We can modify any number of inner zeros of the pattern to approximate the uniform sidelobe-level array, but we force the aperture voltage to peak at the ends in approximating the Dirac delta functions. We limit the number of altered zeros to keep the distribution practical. After a point, shifting more zeros reduces beamwidth negligibly.

We manipulate the location of pattern zeros to obtain desired patterns. Both aperture and array syntheses depend on zero locations. The number of array elements determines the number of independent zeros ($\overline{n} - 1$), but a continuous aperture has an infinite number of independent zeros. Practical consideration of the distribution edge shape limits the number, but we are free to move zeros. For a given aperture size, we can move zeros out of the invisible region into the visible region and narrow the main beam as much as we want while maintaining low sidelobes. The invisible region represents stored energy in the aperture. When a zero moves out of the invisible region, the amount of stored energy and the Q of the antenna increase. The overall efficiency of the antenna decreases while the antenna becomes more and more narrowband. We call these arrays superdirective because their directivity exceeds that of a uniform distribution. The Taylor line-source distribution retains the zeros in the invisible region and prevents superdirectivity. There is no limit to the directivity achievable on paper for a given aperture, but the theoretical distributions are unrealizable except for very small levels of superdirectivity. The costs of superdirectivity are decreased bandwidth and efficiency.

We will modify the location of the first $\overline{n} - 1$ pairs of inner nulls to lower the sidelobes. Choosing the zeros symmetrically about the origin of U-space gives us a constant phase distribution. We remove the inner zeros by dividing them out of the uniform distribution U-space pattern:

$$\frac{\sin \pi U}{\pi U \prod_{N=1}^{\overline{n}-1} \left(1 - U^2/N^2\right)}$$

We then add new nulls U_n without becoming superdirective:

$$F(U) = \frac{\sin \pi U \prod_{N=1}^{\overline{n}-1} \left(1 - \dfrac{U^2}{U_N^2}\right)}{\pi U \prod_{N=1}^{\overline{n}-1} \left(1 - \dfrac{U^2}{N^2}\right)} \tag{4-19}$$

Because we want to approximate the DoIph–Chebyshev response, we choose the inner zeros from the array:

$$U_N = \overline{n} \frac{\sqrt{A^2 + (N - \frac{1}{2})^2}}{\sqrt{A^2 + (\overline{n} - \frac{1}{2})^2}} \qquad N = 1, 2, \ldots, \overline{n} - 1 \tag{4-20}$$

where A relates to the maximum sidelobe level:

$$\cosh \pi A = b \tag{4-21}$$

in which $20 \log b =$ sidelobe level. Equation (4-19) gives us the U-space (k-space) pattern of the distribution with modified zeros. We determine the aperture distribution by expanding it in a Fourier cosine series:

$$E(x) = \sum_{m=0}^{\infty} B_m \cos 2m\pi x \qquad |x| \le 0.5 \tag{4-22}$$

where the aperture size has been normalized. We calculate the pattern of the distribution from the Fourier transform:

$$f(k_x) = \int_{-1/2}^{1/2} E(x) e^{jk_x x}\, dx \quad \text{or} \quad f(U) = \int_{-1/2}^{1/2} E(x) e^{j2\pi U x}\, dx$$

We substitute Eq. (4-22) for $E(x)$ and reverse the order of summation and integration:

$$f(U) = \sum_{m=0}^{\infty} B_m \int_{-1/2}^{1/2} \cos 2m\pi x \cos 2\pi U x\, dx \tag{4-23}$$

Since the aperture function is an even function, the odd-function part of the integral is zero, as reflected in Eq. (4-23). We calculate coefficients B_m by matching the patterns at integer values of U. The integral [Eq. (4-23)] is zero unless $U = m$:

$$B_0 = f(0) \qquad \frac{B_m}{2} = f(m) \qquad m = 1, 2, \ldots, \overline{n} - 1$$

Since we have only modified the location of the first $\overline{n} - 1$ zeros of the U-space pattern, $f(m) = 0$ for $m \ge \overline{n}$ and the Fourier cosine series has only $\overline{n}$ components:

$$E(x) = f(0) + 2 \sum_{m=1}^{\overline{n}-1} f(m) \cos 2m\pi x \tag{4-24}$$

The coefficients are given by

$$f(0) = 1$$

$$f(m) = \frac{(-1)^m \prod_{N=1}^{\overline{n}-1} \left(1 - m^2/U_N^2\right)}{-2 \prod_{N=1, N\neq m}^{\overline{n}-1} \left(1 - m^2/N^2\right)} \qquad m = 1, 2, \ldots, \overline{n} - 1 \tag{4-25}$$

Equation (4-19) computes the U-space pattern of the Taylor distribution but requires L'Hospital's rule at integer values of U. The finite number of coefficients B_m makes Eq. (4-23) more convenient since the integral is easily solved:

$$f(U) = B_0 \frac{\sin(\pi U)}{\pi U} + \frac{1}{2} \sum_{i=1}^{\overline{n}-1} B_i \left[\frac{\sin[\pi(U - i)]}{\pi(U - i)} + \frac{\sin[\pi(U + i)]}{\pi(U + i)} \right] \tag{4-26}$$

Example Design the Taylor line-source distribution with 30-dB maximum sidelobes and $\overline{n} = 6$.

We use Eq. (4-21) to calculate A:

$$b = 10^{30/20} = 31.6228$$

$$A = \frac{\cosh^{-1} b}{\pi} = 1.3200$$

We substitute this constant into Eq. (4-20) to compute the five $(\overline{n} - 1)$ nulls:

No.	1	2	3	4	5
Null U_N	1.4973	2.1195	2.9989	3.9680	4.9747

The first null value gives us the BW_{null} factor (1.4973). The null beamwidth has been increased almost 50% relative to the uniform distribution. The coefficients of the Fourier cosine aperture distribution are found from Eqs. (4-24) and (4-25) (Table 4-4).

Coefficients of the series are normalized so that the distribution is 1 at $x = 0$, and the amplitude distribution is found by plotting the Fourier cosine series. We calculate the U-space pattern by using Eq. (4-26). We calculate the half-power point and compare it to the uniform distribution to determine the HPBW factor, 1.2611. By using Eq. (4-6), we calculate ATL = 0.66 dB for the distribution.

The U-space plot (Figure 4-3) of the example above shows the 30-dB sidelobe level. The first sidelobe is at 30 dB, and lobes after that fall away from 30 dB. With a higher value of $\overline{n}$, the first unchanged zero, more sidelobes would be nearer 30 dB. The dashed curve gives the pattern of a uniform distribution. Notice that the inner five nulls have been shifted to lower the sidelobes. At the sixth null and higher, the Taylor distribution has the same nulls as the uniform distribution. The $\overline{n}$ distribution has a narrower beamwidth than the one-parameter distribution (Figure 4-2) and a higher taper efficiency of 0.66 dB versus 0.96 dB. Figure 4-4 shows the normalized aperture voltage for 30-dB-maximum sidelobe Taylor distributions. The one-parameter design produces a lower pedestal than the two $\overline{n}$ designs. The $\overline{n} = 20$ design voltage peaks as it approaches the edge. This peaks because the Taylor $\overline{n}$ distribution approximates the Dolph–Chebyshev array that peaks at the edge of the array.

The amplitude taper efficiency was calculated for a number of designs and is given in Table 4-5. The corresponding beamwidth factors are listed in Table 4-6 together with

TABLE 4-4 Fourier Cosine Series Coefficients for Taylor Distribution: 30 dB, $\overline{n} = 6$

No.	B_m	B_m Normalized	Function
1	1.0000	0.64672	1
2	0.5733	0.37074	$\cos 2\pi x$
3	−0.0284	−0.01838	$\cos 4\pi x$
4	−0.000213	−0.000138	$\cos 6\pi x$
5	0.005561	0.003597	$\cos 8\pi x$
6	−0.003929	−0.002541	$\cos 10\pi x$

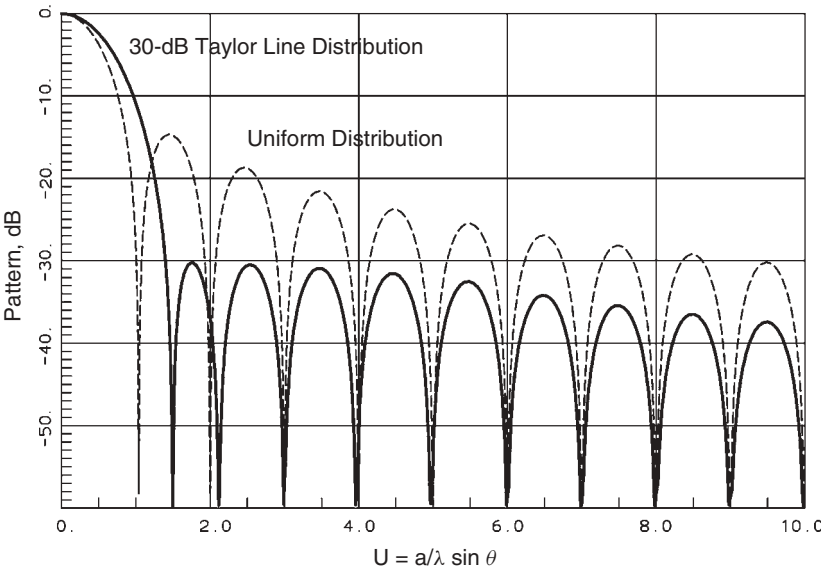

FIGURE 4-3 U-space pattern of 30-dB Taylor $\overline{n} = 6$ linear distribution versus uniform distribution.

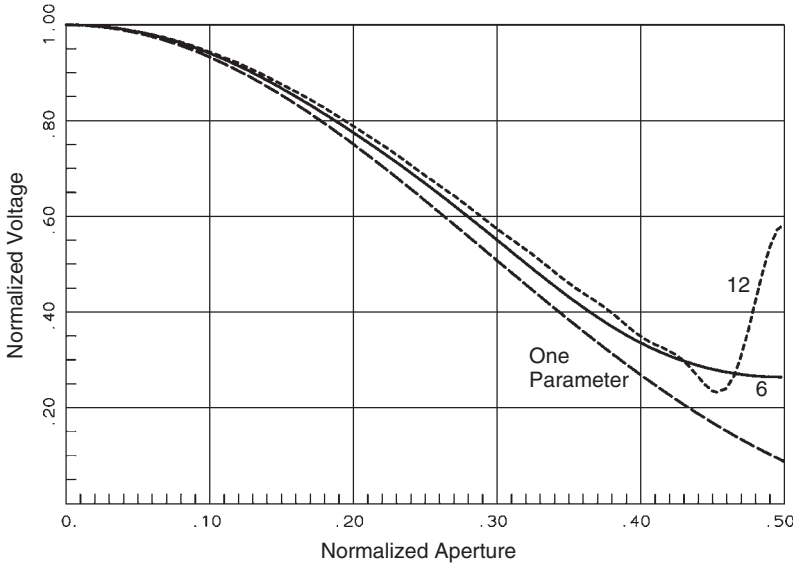

FIGURE 4-4 A 30-dB Taylor linear aperture distribution comparison.

the null beamwidth factors (location of first zero in U-space) in Table 4-7. ATL depends on the sidelobe level (Table 4-5) more than the number of modified zeros. Both the 20- and 25-dB sidelobe levels show that there is an optimum number of zeros. The edge of the distribution peaks toward the Dirac delta function and reduces the amplitude taper efficiency. More than three modified zeros are needed to reduce the sidelobes

TABLE 4-5 Amplitude Taper Losses of Taylor Line-Source Distributions

	Sidelobe Level (dB)						
$\overline{n}$	20	25	30	35	40	45	50
4	0.17	0.43	0.69	0.95			
5	0.15	0.41	0.68	0.93	1.16		
6	0.15	0.39	0.66	0.92	1.15	1.37	
7	0.15	0.37	0.65	0.91	1.15	1.36	1.56
8	0.16	0.36	0.63	0.90	1.14	1.36	1.55
10	0.19	0.34	0.61	0.88	1.13	1.35	1.55
12	0.24	0.34	0.59	0.86	1.11	1.34	1.54
16	0.35	0.35	0.57	0.84	1.09	1.32	1.53
20	0.46	0.27	0.56	0.82	1.07	1.30	1.51

TABLE 4-6 Beamwidth Factor of Taylor Line-Source Distribution

	Sidelobe Level (dB)						
$\overline{n}$	20	25	30	35	40	45	50
4	1.1043	1.1925	1.2696	1.3367			
5	1.0908	1.1837	1.2665	1.3404	1.4065		
6	1.0800	1.1752	1.2611	1.3388	1.4092	1.4733	
7	1.0715	1.1679	1.2555	1.3355	1.4086	1.4758	1.5377
8	1.0646	1.1617	1.2504	1.3317	1.4066	1.4758	1.5400
10	1.0545	1.1521	1.2419	1.3247	1.4015	1.4731	1.5401
12	1.0474	1.1452	1.2353	1.3189	1.3967	1.4695	1.5379
16	1.0381	1.1358	1.2262	1.3103	1.3889	1.4628	1.5326
20	1.0324	1.1299	1.2203	1.3044	1.3833	1.4576	1.5280

TABLE 4-7 Null Beamwidth Factor of Taylor Line-Source Distributions

	Sidelobe Level (dB)						
$\overline{n}$	20	25	30	35	40	45	50
4	1.1865	1.3497	1.5094	1.6636			
5	1.1696	1.3376	1.5049	1.6696	1.8302		
6	1.1566	1.3265	1.4973	1.6671	1.8347	1.9990	
7	1.1465	1.3172	1.4897	1.6632	1.8337	2.0031	2.1699
8	1.1386	1.3095	1.4828	1.6569	1.8306	2.0032	2.1739
10	1.1270	1.2978	1.4716	1.6471	1.8231	1.9990	2.1740
12	1.1189	1.2894	1.4632	1.6392	1.8161	1.9934	2.1705
16	1.1086	1.2783	1.4518	1.6277	1.8051	1.9835	2.1623
20	1.1023	1.2714	1.4444	1.6200	1.7975	1.9760	2.1553

below 40 dB; hence, the blanks represent unrealizable designs. The beamwidth factor (Table 4-6) reduces with increasing $\overline{n}$, but it depends mainly on the sidelobe level.

Example Compute beamwidths and ATL of an 8λ-wide aperture with $\overline{n} = 8$, 40-dB sidelobes, and a Taylor line-source distribution design.

From Table 4-6,

$$\text{HPBW} = \frac{1.4066(50.76^\circ)}{8} = 8.92^\circ$$

From Table 4-7,

$$\text{BW}_{\text{null}} = \frac{1.8306(114.59^\circ)}{8} = 26.22^\circ$$

From Table 4-5, ATL = 1.14 dB. A square aperture with the same distribution in both directions has

$$\text{directivity} = 10 \log \frac{4\pi A}{\lambda^2} - 2\text{ATL} = 26.77 \text{ dB}$$

4-5 TAYLOR LINE DISTRIBUTION WITH EDGE NULLS

Rhodes [4] has shown that it is impossible to have a step discontinuity of the fields at the edge of a physical aperture. Given the radius of curvature of the edge, ρ, the field varies as

$$E_d \sim \frac{C_2}{\rho} d \qquad \text{polarized perpendicular to the aperture edge}$$

$$E_s \sim \frac{C_1}{\rho} d^2 \qquad \text{polarized parallel to the aperture edge}$$

where C_1 and C_2 are constants and d is the distance from the edge. Without the possibility of an edge pedestal, a traditional Taylor line source cannot be realized with a physical aperture. We can sample the distribution with an array or closely approximate it, but we cannot achieve the exact distribution. A Taylor distribution with a null at the edge can be realized in an aperture.

Rhodes [5] extended the Taylor line source by modifying the U-space pattern zeros of the cosine distribution. Since $\alpha = 1$, the far-out sidelobes drop off as $1/U^2$ and the distribution is zero on the edges. The zeros of the cosine distribution occur at

$$(N + 1/2)\pi \qquad N = 1, 2, 3, \ldots \qquad k \text{ space}$$

When the Taylor U-space variable is used, the modified U-space pattern becomes

$$f(U) = \frac{\cos \pi U \prod_{N=1}^{\overline{n}-1} \left(1 - U^2/U_N^2\right)}{[1 - (2U)^2] \prod_{N=1}^{\overline{n}-1} (1 - U^2/(N + \frac{1}{2})^2)} \tag{4-27}$$

We remove the inner $\overline{n} - 1$ zeros at $N + \frac{1}{2}$ and substitute new ones given by

$$U_N = \pm(\overline{n} + \tfrac{1}{2}) \frac{\sqrt{A^2 + (N - \frac{1}{2})^2}}{\sqrt{A^2 + (\overline{n} - \frac{1}{2})^2}} \qquad N = 1, 2, \ldots, \overline{n} - 1 \tag{4-28}$$

When we compare Eqs. (4-28) and (4-20), we see that the nulls are shifted by $(\overline{n} + \frac{1}{2})/\overline{n}$ between the two Taylor distributions. When $\overline{n}$ is large, the nulls are close to the same for the two distributions.

To determine the amplitude distribution in the aperture, we expand the aperture fields in a Fourier cosine series,

$$E(x) = \sum B_m \cos(2m+1)\pi x \qquad |x| \le 0.5 \tag{4-29}$$

Like the Taylor line source, there are only $\overline{n}$ terms in the series whose coefficients are found by equating the pattern from the Fourier transform of Eq. (4-29) to Eq. (4-27). The coefficients are given by

$$B_0 = \frac{2\prod_{N=1}^{\overline{n}-1}\left(1 - \frac{1}{4}/U_N^2\right)}{\prod_{N=1}^{\overline{n}-1}\left[1 - \frac{1}{4}/(N+\frac{1}{2})^2\right]}$$

$$B_m = \frac{(-1)^m(m+\frac{1}{2})\prod_{N=1}^{\overline{n}-1}\left[1 - (m+\frac{1}{2})^2/U_N^2\right]}{[1-(2m+1)^2]\prod_{N=1,N\neq m}^{\overline{n}-1}\left[1-(m+\frac{1}{2})^2/(N+\frac{1}{2})^2\right]} \quad m = 1, 2, \ldots, \overline{n}-1 \tag{4-30}$$

The U-space pattern can be found using the coefficients B_m:

$$f(U) = C_0 \sum_{i=0}^{\overline{n}-1} B_i \left[\frac{\sin[\pi(U-i-\frac{1}{2})]}{\pi(U-i-\frac{1}{2})} + \frac{\sin[\pi(U+i+\frac{1}{2})]}{\pi(U+i+\frac{1}{2})}\right]$$

$$C_0 = 2\sum_{i=0}^{\overline{n}-1} B_i \frac{\sin[\pi(i+\frac{1}{2})]}{\pi(i+\frac{1}{2})} \tag{4-31}$$

Example Design the Taylor line-source distribution with edge nulls for 30-dB maximum sidelobes and $\overline{n} = 6$.

We use Eq. (4-21) to calculate A:

$$b = 10^{30/20} = 31.6228$$

$$A = \frac{\cosh^{-1} b}{\pi} = 1.32$$

the same as the pedestal edge Taylor line-source distribution. We substitute this constant into Eq. (4-28) to compute the five modified nulls:

No.	1	2	3	4	5
Null U_N	1.6221	2.2962	3.2488	4.2987	5.3892

The null locations have increased by $(\overline{n} + \frac{1}{2})/\overline{n} = 6.5/6 = 1.0833$ from the pedestal Taylor line-source design. The null beamwidth factor has also increased by this factor

as well. The coefficients of the Fourier cosine aperture distribution are found from Eq. (4-30) Table 4-8.

The normalized coefficients sum to 1 at $x = 0$. Equation (4-27) determines the U-space pattern given the nulls. On finding the half-power point and comparing it with the uniform distribution half-power point, we compute the beamwidth factor: 1.3581. Tables 4-9 to 4-11 give results for this Taylor line source. As $\overline{n}$ increases, the results approach the result of the pedestal Taylor line source. Since the maximum sidelobe of the cosine distribution is 23 dB, a distribution must have peaking toward the edges to raise the sidelobes above that level. In all distributions the voltage approaches zero linearly at the edges.

TABLE 4-8 Fourier Cosine Series Coefficients for Taylor Distribution with Edge Nulls: 30 dB, $\overline{n} = 6$

No.	B_m	B_m Normalized	Function
1	0.50265	0.94725	$\cos \pi x$
2	0.023087	0.04351	$\cos 3\pi x$
3	0.017828	0.02220	$\cos 5\pi x$
4	−0.010101	−0.02075	$\cos 7\pi x$
5	0.007374	0.01390	$\cos 9\pi x$
6	−0.003245	−0.006116	$\cos 11\pi x$

TABLE 4-9 Amplitude Taper Losses of a Taylor Line Source with Edge Null Distribution

	Sidelobe Level (dB)					
$\overline{n}$	25	30	35	40	45	50
4	0.86	1.13	1.36	1.55	1.71	1.84
6	0.67	0.97	1.24	1.47	1.66	1.84
8	0.56	0.87	1.14	1.39	1.60	1.79
12	0.45	0.74	1.02	1.28	1.51	1.71
16	0.41	0.68	0.96	1.22	1.45	1.66
20	0.39	0.64	0.92	1.17	1.41	1.62

TABLE 4-10 Beamwidth Factor of a Taylor Line Source with Edge Null Distribution

	Sidelobe Level (dB)					
$\overline{n}$	25	30	35	40	45	50
4	1.3559	1.4092	1.4815	1.5443	1.5991	1.6470
6	1.2666	1.3581	1.4407	1.5153	1.5831	1.6448
8	1.2308	1.3242	1.4097	1.4882	1.5608	1.6280
12	1.1914	1.2850	1.3716	1.4522	1.5276	1.5984
16	1.1705	1.2635	1.3500	1.4308	1.5068	1.5785
20	1.1576	1.2502	1.3363	1.4170	1.4930	1.5649

TABLE 4-11 Null Beamwidth Factor of a Taylor Line Source with Edge Null Distribution

	Sidelobe Level (dB)					
$\overline{n}$	25	30	35	40	45	50
4	1.5184	1.6980	1.8715	2.0374	2.1949	2.3433
6	1.4371	1.6221	1.8060	1.9875	2.1656	2.3395
8	1.3913	1.5755	1.7604	1.9450	2.1284	2.3097
12	1.3431	1.5242	1.7075	1.8918	2.0765	2.2610
16	1.3182	1.4971	1.6786	1.8616	2.0455	2.2298
20	1.3031	1.4805	1.6605	1.8424	2.0254	2.2091

4-6 ELLIOTT'S METHOD FOR MODIFIED TAYLOR DISTRIBUTION AND ARBITRARY SIDELOBES [6, pp. 162–165]

Elliott's method separates the distribution nulls into right- and left-hand values in U-space that allows different sidelobe levels in the two regions. By applying a differential expression, the null positions in U-space can be found from the solution of a set of linear equations to produce designs with arbitrary sidelobes. Consider Eq. (4-19) and factor the null location term:

$$1 - \frac{U^2}{U_N^2} = \left(1 + \frac{U}{U_N}\right)\left(1 - \frac{U}{U_N}\right) = \left(1 + \frac{U}{U_{NL}}\right)\left(1 - \frac{U}{U_{NR}}\right)$$

We associate U_{NL} with a nulls on the left side of the origin and U_{NR} with the right side or a positive pattern angle. If we also separate the term in the denominator of Eq. (4-19), we can independently pick the number of nulls to be moved on either side of the pattern:

$$F(U) = C_0 \frac{\sin \pi U \prod_{N=1}^{\overline{n}_L - 1} (1 + U/U_N) \prod_{N=1}^{\overline{n}_R - 1} (1 - U/U_N)}{\pi U \prod_{N=1}^{\overline{n}_L - 1} (1 + U/N) \prod_{N=1}^{\overline{n}_R - 1} (1 - U/N)} \tag{4-32}$$

Equation (4-32) allows different Taylor distributions on the two sides. We add a normalization factor C_0 when we use different distributions. The pattern peak will shift off zero for unbalanced distributions. Since the two sides are not independent, a simple selection of the two levels will not produce the desired sidelobes. Table 4-12 lists the U-space locations of the pattern peaks and sidelobe level for a design with 35- and 30-dB sidelobes. The left distribution lowered the sidelobes on the right and the right one raised the left sidelobes. A few manual iterations produced suitable left and right distributions to give the desired sidelobes. The main beam shifts a little bit. A linear progressive phase shift across the aperture can shift the pattern to broadside.

We expand the aperture distribution in a complex exponential series similar to Eq. (4-22):

$$E(x) = \sum_{i=-\overline{n}_L+1}^{\overline{n}_R - 1} B_i e^{-j2\pi i x} \qquad |x| \le 0.5 \tag{4-33}$$

TABLE 4-12 Modified Taylor Distribution Sidelobes for Independent Left and Right Sidelobe Design Using $\overline{n} = 6$ for Both Sides

Left-Side−35-dB U-Space	Right Side−30-dB Sidelobe (dB)	Left-Side−36-dB U-Space	Right-Side−28.6-dB Sidelobe (dB)
−5.4849	−35.70	−5.4874	−36.00
−4.4905	−35.06	−4.4976	−35.44
−3.5275	−34.66	−3.5399	−35.11
−2.6313	−34.44	−2.6510	−34.97
−1.8997	−34.39	−1.9293	−34.99
−0.0511	0	−0.0758	0
1.7546	−31.05	1.7141	−30.05
2.5372	−31.45	2.5119	−30.55
3.4697	−32.00	3.4544	−31.19
4.4584	−32.74	4.4498	−32.02
5.4711	−33.75	5.4676	−33.13

We calculate the coefficients by the same method used for Eq. (4-25):

$$B(0) = 1$$

$$B(m) = \frac{(-1)^{|m|} \prod_{N=1}^{\overline{n}_L - 1} (1 + m/U_N) \prod_{N=1}^{\overline{n}_R - 1} (1 - m/U_N)}{-\prod_{N=1, N\neq m}^{\overline{n}_L - 1} (1 + m/N) \prod_{N=1, N\neq m}^{\overline{n}_R - 1} (1 - m/N)}$$

$$m = -\overline{n}_L + 1, \ldots, -1, 1, 2, \ldots, \overline{n}_R - 1 \qquad (4\text{-}34)$$

We derive the pattern from the integral of the finite complex exponential:

$$f(U) = C_0 \sum_{i=-\overline{n}_L+1}^{\overline{n}_R - 1} B_i \frac{\sin[\pi(U - i)]}{\pi(U - i)} \qquad (4\text{-}35)$$

We include the normalization factor C_0 for unequal left and right sidelobes.

We control the sidelobes by adjusting the location of the nulls in the U-space pattern. We can iterate the null positions to produce individually selected sidelobes. The peak of each sidelobe given in Table 4-12 was found through a one-dimensional search between pairs of nulls. A search based on the Fibonacci numbers [7, p. 280] computes the peak with the minimum number of evaluations of the pattern using Eq. (4-35). We denote the pattern peaks by U_m^p starting with the peak between $-\overline{n}_L$ and $U_{-\overline{n}_L+1}$, those between nulls, the peak near 0, and the last peak between $U_{\overline{n}_R-1}$ and $\overline{n}_R$ for $\overline{n}_L + \overline{n}_R - 1$.

We adjust the U-space nulls by the differentials δU_N found from the solution of a matrix equation. The terms of the matrix are the differential term of a Taylor series expansion of the numerator of Eq. (4-32) evaluated at the pattern peaks:

$$a_{m,n} = \frac{U_m^p / U_N^2}{1 - U_m^p / U_N} \qquad N = -\overline{n}_L + 1, \ldots, -1, 1, \ldots, \overline{n}_R - 1$$

$$a_{m,0} = 1 \qquad (4\text{-}36)$$

The vector of differential nulls is

$$\delta \mathbf{U} = [\delta U_{-\overline{n}_L+1}, \ldots, \delta U_{-1}, \delta C/C_0, \delta U_1 \ldots, \delta U_{\overline{n}_R-1}]^{\mathrm{T}}$$

where $\delta C/C_0$ is the change in the pattern normalization. We form a vector using the ratio of the desired pattern peak $f_d(U)$ to the actual pattern $f_a(U)$ with terms $[f_d(U_m^p)/f_a(U_m^p)] - 1$. We solve the matrix equation for the null shifts:

$$[a_{m,n}]^{-1} \left[\frac{f_d(U_m^p)}{f_a(U_m^p)} - 1 \right]^{\mathrm{T}} = [\delta U_N] \tag{4-37}$$

We calculate new distribution nulls $U_N + \delta U_N$, substitute the new nulls into Eq. (4-34) to determine the new expansion coefficients B_m, and evaluate the pattern using Eq. (4-35) between the new nulls to compute new pattern peaks. We iterate the process until the sidelobe levels are satisfactory. Notice that $f(U)$ is a voltage.

The Taylor linear distribution produces a pattern with only approximately equal sidelobes. Table 4-13 lists the iteration to produce a distribution with a pattern that has five 30-dB sidelobes. The solution starts with a 30-dB, $\overline{n} = 6$ Taylor distribution. In two iterations the method found a distribution with exactly the desired sidelobes. Table 4-14 gives the results of repeating the example of Table 4-12 of the design for 35- and 30-dB sidelobes. This method can produce a linear distribution with individually

TABLE 4-13 Iteration of Distribution Nulls for a Pattern with 30-dB Sidelobes

Taylor Distribution			First Iteration			Second Iteration		
Null	U-Space	Sidelobe	Null	U-Space	Sidelobe	Null	U-Space	Sidelobe
1.4973	1.7557	−30.22	1.4708	1.7258	−30.00	1.4729	1.7284	−30.00
2.1195	2.5387	−30.46	2.0827	2.4987	−29.99	2.0859	2.5027	−30.00
2.9989	3.4709	−30.89	2.9490	3.4215	−29.96	2.9541	3.4274	−30.00
3.9680	4.4591	−31.53	3.9075	4.4072	−29.86	3.9152	4.4147	−30.00
4.9747	5.4718	−32.48	4.9145	5.4424	−29.63	4.9242	5.4471	−29.99

TABLE 4-14 Iteration for 35- and 30-dB Sidelobes in Linear Distribution

Left-Side−36-dB	Right-Side−28.6-dB		Second Iteration		
U-Space	Sidelobe (dB)	Null	U-Space	Sidelobe (dB)	Null
−5.4874	−36.00	−4.9964	−5.4798	−35.00	−4.9778
−4.4976	−35.44	−4.0169	−4.4859	−35.00	−4.0043
−3.5399	−35.11	−3.0845	−3.5348	−35.00	−3.0829
−2.6510	−34.97	−2.2583	−2.6555	−35.00	−2.2670
−1.9293	−34.99	−1.7008	−1.9410	−35.00	−1.7143
−0.0758	0		−0.1037	0	
1.7141	−30.05	1.4495	1.6615	−30.00	1.4023
2.5119	−30.55	2.0883	2.4475	−30.00	2.0249
3.4544	−31.19	2.9801	3.3839	−30.00	2.9049
4.4498	−32.02	3.9574	4.3839	−30.00	3.8780
5.4676	−33.13	4.9699	5.4313	−29.98	4.9001

selected sidelobes. It may be necessary to design an intermediate distribution if the change in sidelobes is too great for the simple iteration scheme to converge. We will design linear arrays by a similar technique of manipulating pattern nulls to produce arbitrary sidelobes.

4-7 BAYLISS LINE-SOURCE DISTRIBUTION [8]

The Bayliss distribution produces a pattern null on a boresight while controlling the height of the sidelobes. The second dashed curve in Figure 4-5 below is a Bayliss difference pattern also designed to give 30-dB sidelobes when combined with the Taylor distribution. As in the Taylor distribution, the first few sidelobes are nearly the same height, to minimize the beamwidth of the two beams split about the boresight.

A monopulse tracking system uses an auxiliary pattern with a boresight null coincident with the beam peak of the main pattern. The tracking system drives the antenna positioner until the signal in this difference channel nulls so that the main channel (sum) points at the emitter or radar target. The accuracy of the pointing angle is improved, since a null is a more exact direction than the broad sum pattern peak. Noise and receiver sensitivity, along with the slope of the difference pattern, limit the tracking accuracy. Stronger signals can be tracked farther into the null. Because the phase of a pattern shifts by 180° when passing through a null, phase relative to the sum pattern (a reference signal) can be used to give direction. Without monopulse or some other sequential lobing technique, such as conical scan, radar cannot track effectively.

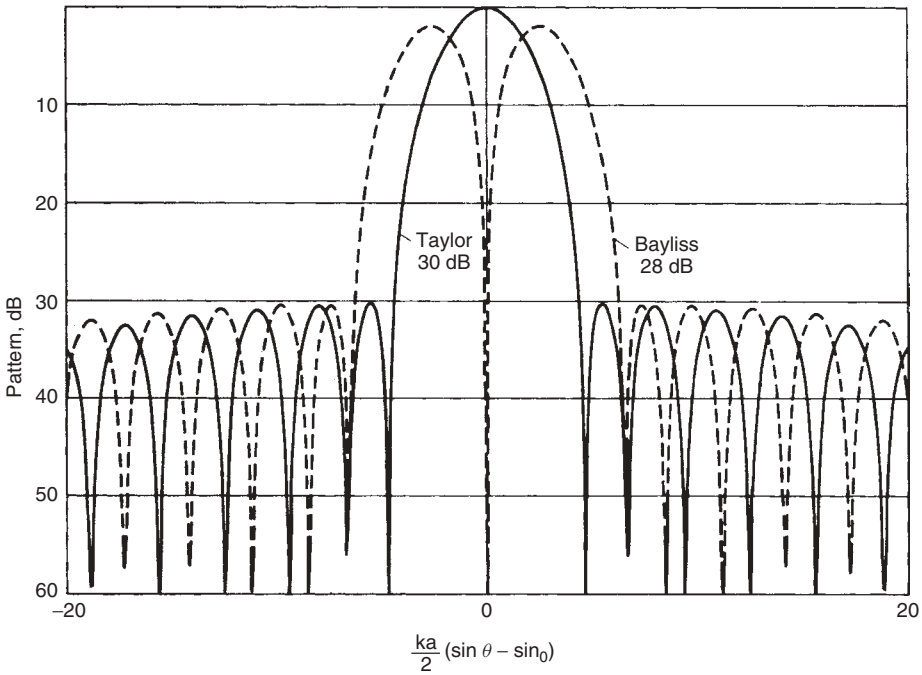

FIGURE 4-5 Taylor and Bayliss line distributions to give 30-dB sidelobes ($\overline{n} = 6$).

Any odd-function distribution produces a null on a boresight. A uniform distribution that switches phase by 180° in the center has the best amplitude taper efficiency but high sidelobes (10 dB). These high sidelobes allow interfering or noise signals to enter the receiver. The Bayliss distribution adjusts the inner nulls of the U-space pattern to lower the sidelobes. Adjusting the zeros to correspond to the Dolph–Chebyshev array does not lower the sidelobes to the same level as it did in the Taylor distribution. Further adjustments of the four inner zeros are required. Bayliss found the proper location through a computer search. We locate the zeros by

$$U_N = \begin{cases} (\overline{n} + \frac{1}{2})\sqrt{\dfrac{\xi_N^2}{A^2 + \overline{n}^2}} & N = 1, 2, 3, 4 \\ (\overline{n} + \frac{1}{2})\sqrt{\dfrac{A^2 + N^2}{A^2 + \overline{n}^2}} & N = 5, 6, \ldots, \overline{n} - 1 \end{cases} \tag{4-38}$$

By using the U-space pattern, we have

$$f(U) = U \cos \pi U \frac{\prod_{N=1}^{\overline{n}-1} \left(1 - U^2/U_N^2\right)}{\prod_{N=0}^{\overline{n}-1} \left[1 - U^2/(N + \frac{1}{2})^2\right]} \tag{4-39}$$

The coefficients were fitted to polynomials depending on the sidelobe level. Given $S = |\text{sidelobe level(dB)}|$:

$$A = 0.3038753 + S(0.05042922 + S(-0.00027989 + S(0.343 \times 10^{-5} - S(0.2 \times 10^{-7})))) \tag{4-40a}$$

$$\xi_1 = 0.9858302 + S(0.0333885 + S(0.00014064 + S(-0.19 \times 10^{-5} + S(0.1 \times 10^{-7})))) \tag{4-40b}$$

$$\xi_2 = 2.00337487 + S(0.01141548 + S(0.0004159 + S(-0.373 \times 10^{-5} + S(0.1 \times 10^{-7})))) \tag{4-40c}$$

$$\xi_3 = 3.00636321 + S(0.00683394 + S(0.00029281 + S(-0.161 \times 10^{-5}))) \tag{4-40d}$$

$$\xi_4 = 4.00518423 + S(0.00501795 + S(0.00021735 + S(-0.88 \times 10^{-6}))) \tag{4-40e}$$

The location of the pattern peak was also fitted to a polynomial:

$$U_{\max} = 0.4797212 + S(0.01456692 + S(-0.00018739 + S(0.218 \times 10^{-5} + S(-0.1 \times 10^{-7})))) \tag{4-41}$$

We obtain the aperture distribution by a Fourier sine series having only $\overline{n}$ terms:

$$E(x) = \sum B_m \sin(m + \tfrac{1}{2})2\pi x \qquad |x| \le 0.5 \tag{4-42}$$

where

$$B_m = \frac{(-1)^m (m+\frac{1}{2})^2}{2j} \frac{\prod_{N=1}^{\overline{n}-1} \left[1-(m+\frac{1}{2})^2/U_N^2\right]}{\prod_{N=0, N\neq m}^{\overline{n}-1} \left[1-(m+\frac{1}{2})^2/(N+\frac{1}{2})^2\right]} \tag{4-43}$$

The phase constant $(-j)$ has little effect on the coefficient B_m except to balance the phase $\pm 90^\circ$ about the null.

Example Design a Bayliss distribution with 30-dB sidelobes and $\overline{n} = 6$.

Use Eq. (4-40) to compute the coefficients.

$$A = 1.64126 \qquad \xi_1 = 2.07086 \qquad \xi_2 = 2.62754 \qquad \xi_3 = 3.43144 \qquad \xi_4 = 4.32758$$

We substitute these constants into Eq. (4-38) to calculate the five $(\overline{n}-1)$ nulls:

No.	1	2	3	4	5
Null U_N	2.1639	2.7456	3.5857	4.5221	5.4990

Equation (4-41) computes the beam peak of the split-beam pattern in U space:

$$U_{\max} = 0.7988 \qquad \frac{ka}{2} \sin\theta_{\max} = \pi U_{\max} = 2.5096$$

where a is the aperture width. We substitute these zeros into Eq. (4-43) to determine the coefficients of the Fourier sine series of the aperture distribution (Table 4-15). By evaluating the series across the aperture, the coefficients can be normalized to give a maximum aperture voltage of 1.

We use Eq. (4-39), after substituting the zeros, to evaluate the pattern. The 3-dB pattern points can be found by searching the pattern:

$$\frac{ka}{2} \sin\theta_1 = 1.27232 \qquad \frac{ka}{2} \sin\theta_2 = 4.10145$$

Figure 4-5 contains the plot of a Bayliss distribution $(\overline{n} = 6)$ designed to have sidelobes 30 dB below the Taylor distribution with 30-dB sidelobes. The losses to the difference pattern are about 2 dB higher than the sum pattern. We design the Bayliss

TABLE 4-15 Fourier Cosine Series Coefficients for Bayliss Distribution: 30 dB, $\overline{n} = 6$

No.	B_m	B_m Normalized	Function
0	0.13421	0.85753	$\sin \pi x$
1	0.081025	0.51769	$\sin 3\pi x$
2	−0.0044151	−0.028209	$\sin 5\pi x$
3	0.001447	0.0092453	$\sin 7\pi x$
4	−0.0003393	−0.0021679	$\sin 9\pi x$
5	−0.000014077	−0.00008994	$\sin 11\pi x$

distribution to have 28-dB sidelobes. If designed for 30-dB sidelobes as in the example above, then, relative to the sum Taylor distribution, the sidelobes would be 32 dB down from the sum pattern peak. The last nulls show that the unmodified zeros of the Taylor distribution occur at $\pm n\pi$, whereas the unmodified zeros of the Bayliss distribution occur at $\pm(n + \frac{1}{2})\pi$.

By using Eq. (4-6), we calculate amplitude taper efficiency of the pattern at the beam peak. When we evaluate the phase error efficiency by using Eq. (4-7), the result is zero because of the boresight null. We use Eq. (4-3) to evaluate the phase error efficiency at the beam peak:

$$\text{PEL} = \frac{\left| \int_{-a/2}^{a/2} E(x) e^{jk \sin \theta_{\max} x} \, dx \right|^2}{\left[\int_{-a/2}^{a/2} |E(x)| \, dx \right]^2} \tag{4-44}$$

Table 4-16 lists results of calculations on Bayliss distributions with $\overline{n} = 10$ for various sidelobe levels. Lower sidelobe levels produce higher distribution losses and push the beam peak out. The position of the beam peak is independent of $\overline{n}$, since the first four zeros are fixed by Eq. (4-40). Like the Taylor distribution, the sidelobe level determines most of the parameters of the Bayliss distribution. Changing $\overline{n}$ has less effect than it has for the Taylor distribution. The values of parameters for distribution with $\overline{n} \neq 10$ will differ little from those in Table 4-16.

Example Compute the beam peak and beam edges for an 8λ-wide aperture excited in a Bayliss distribution with $\overline{n} = 10$ and 30-dB sidelobes.

$$\frac{2\pi}{\lambda} \sin \theta_{\max} \frac{8\lambda}{2} = 2.5096$$

$$\sin \theta_{\max} = \frac{2.5096}{8\pi}$$

$$\sin \theta_1 = \frac{1.263}{8\pi} \qquad \sin \theta_2 = \frac{4.071}{8\pi}$$

$$\theta_{\max} = 5.73^\circ \qquad \theta_1 = 2.88^\circ \qquad \theta_2 = 9.32^\circ$$

TABLE 4-16 Characteristics of a Bayliss Line-Source Distribution with $\overline{n} = 10$ Parameters

Sidelobe Level (dB)	Beam Peak, $ka/2 \sin \theta_{\max}$	3-dB Edge		ATL (dB)	PEL (dB)
		$ka/2 \sin \theta_1$	$ka/2 \sin \theta_2$		
20	2.2366	1.140	3.620	0.50	1.81
25	2.3780	1.204	3.855	0.54	1.90
30	2.5096	1.263	4.071	0.69	1.96
35	2.6341	1.318	4.270	0.85	2.01
40	2.7536	1.369	4.455	1.00	2.04

4-8 WOODWARD LINE-SOURCE SYNTHESIS [9]

In the preceding sections, methods to determine distributions that give the minimum beamwidth for specified sidelobe levels were discussed. Some applications require shaped beams extending over a range of angles. The Woodward synthesis samples the desired k-space pattern at even intervals to determine the aperture distribution. No integrals are required to compute coefficients.

The technique is based on the scanned pattern of a uniform amplitude distribution. Express the pattern in terms of U-space so that when scanned to U_0, it becomes

$$\frac{\sin \pi(U - U_0)}{\pi(U - U_0)}$$

with the nulls of the pattern occurring at integer values of $U - U_0$.

$$U = \frac{a}{\lambda} \sin\theta \qquad U_0 = \frac{a}{\lambda} \sin\theta_0$$

The visible region extends between $+a$ and $-a$, centered about U_0.

Figure 4-6 shows two patterns, scanned to $U_0 = 1$ and $U_0 = 2$. The peak of the curve scanned at $U_0 = 2$ occurs at one of the nulls of the pattern scanned to $U_0 = 1$. If we allow only integer values of U_0, the pattern scanned to U_0 solely determines the pattern at the point U_0 in U-space. The two curves (Figure 4-6) in the regions below $U = 0$ and above $U = 3$ cancel each other to some extent when the distributions are

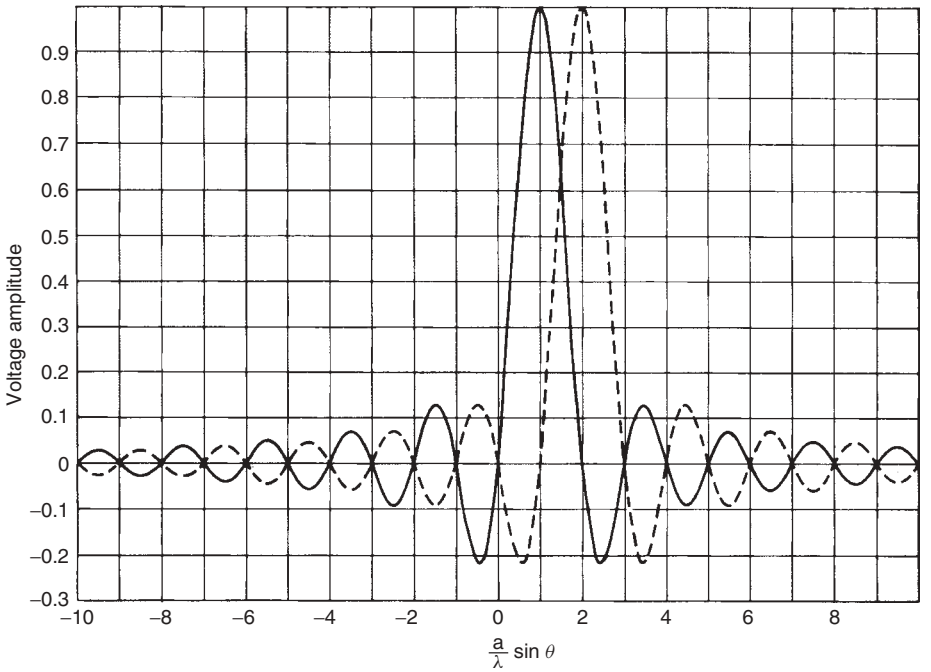

FIGURE 4-6 Scanned uniform distributions: $U_0 = 1$ and $U_0 = 2$.

added. We form the aperture distribution from a sum of $2a/\lambda + 1$ independent sample points of scanned apertures:

$$E(x) = \sum_{i=-N}^{N} E_i e^{-j(i/a)x} \tag{4-45}$$

where $N =$ integer part (a/λ). Each term is a uniform amplitude distribution scanned to an integer value of U. The amplitudes E_i are determined by the sample values of the U-space pattern at those points.

Example Design a 10λ aperture with a constant beam between $\theta = 0^\circ$ and $\theta = 30^\circ$. The nonzero portion of the U-space pattern extends from $U_1 = 10 \sin 0^\circ = 0$ to $U_2 = 10 \sin 30^\circ = 5$.

When we sample the U-space pattern, we discover six nonzero terms:

i	0	1	2	3	4	5
E_i	0.5	1.0	1.0	1.0	1.0	0.5

At $U_1 = 0$ and $U_2 = 5$, we use the average value. The aperture distribution is

$$0.5 + e^{-jx/a} + e^{-j2x/a} + e^{-j3x/a} + e^{-j4x/a} + 0.5e^{-j5x/a}$$

The U-space pattern of this distribution (Figure 4-7) shows some ripple in the beam and the reduction to 6 dB at the beam edges. If we increased the sample level at the edges, $U = 0$ and $U = 5$, the pattern would increase to that level.

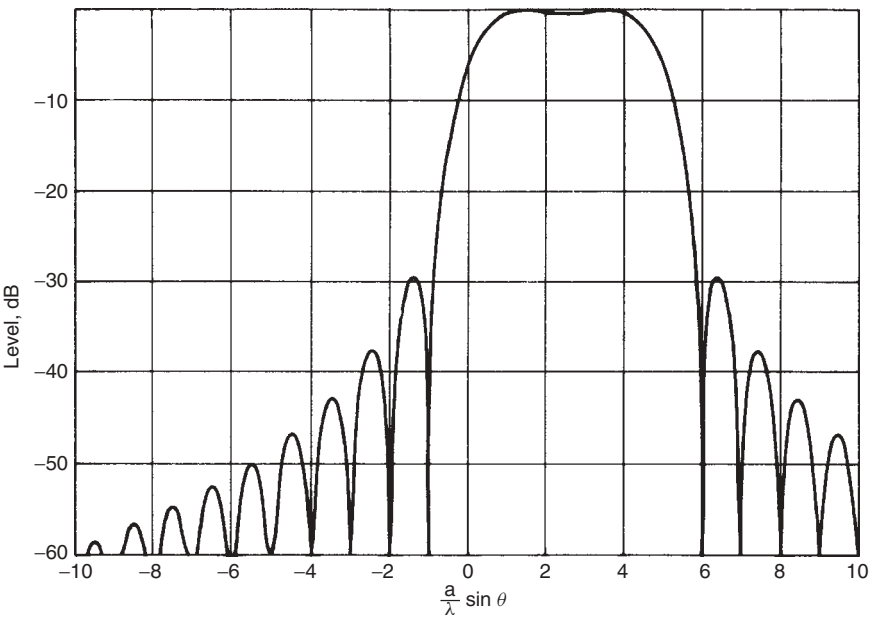

FIGURE 4-7 U-space pattern of Woodward–Lawson sampling for constant beam from 0 to 30° (10λ aperture).

A cosecant-squared power pattern can be designed by the same method as in the preceding example. When an antenna with this pattern on the ground points its maximum toward the horizon, it delivers a constant signal to an aircraft that maintains a constant altitude. The pattern falloff matches the range decrease as the aircraft flies toward the antenna. The voltage pattern is given by

$$E = E_0 \frac{\sin \theta_{\max}}{\sin \theta}$$

where $\theta_{\max}$ is the angle of the pattern maximum. In U-space this becomes

$$E(U) = E_0 \frac{U_m}{U}$$

The amplitudes of the scanned apertures decrease as $1/U$.

Example Design a 10λ aperture with a cosecant-squared pattern from $\theta = 5^\circ$ to $\theta = 70^\circ$ with the maximum at 5°.

There are $2a/\lambda + 1$ possible sample points (21). The nonzero portion of the U-space pattern extends from $U_{\min} = 10 \sin 5^\circ = 0.87$ to $U_{\max} = 10 \sin 70^\circ = 9.4$. We sample only at integer values of U, which gives us nine nonzero terms: $U_m = 0.8716$. The coefficients are given in Table 4-17.

The sum [Eq. (4-45)] for this distribution contains nine terms.

$$E(x) = \sum_{i=1}^{9} E_i e^{-j(i/a)x}$$

Figure 4-8 shows the amplitude and phase of this aperture distribution. The pattern obtained by summing the scanned aperture distributions (Figure 4-9) shows ripple about the desired pattern. Increasing the aperture size increases the number but does not change the level of ripples. The aperture distribution (Figure 4-8) has a negative phase slope to scan the beam off broadside.

4-9 SCHELKUNOFF'S UNIT-CIRCLE METHOD [10]

Schelkunoff's unit-circle method consists of the manipulation of the zeros (nulls) of the array pattern to achieve a desired pattern for a line array. The method is similar to designing networks by specifying the placement of poles and zeros in the complex plane, but the array has only zeros to manipulate. We can use the representation to describe any uniformly spaced array.

TABLE 4-17 Woodward Synthesis Coefficients of 10λ Cosecant-Squared Pattern

i	E_i	i	E_i	i	E_i
1	0.8716	4	0.2179	7	0.1245
2	0.4358	5	0.1743	8	0.1089
3	0.2905	6	0.1453	9	0.0968

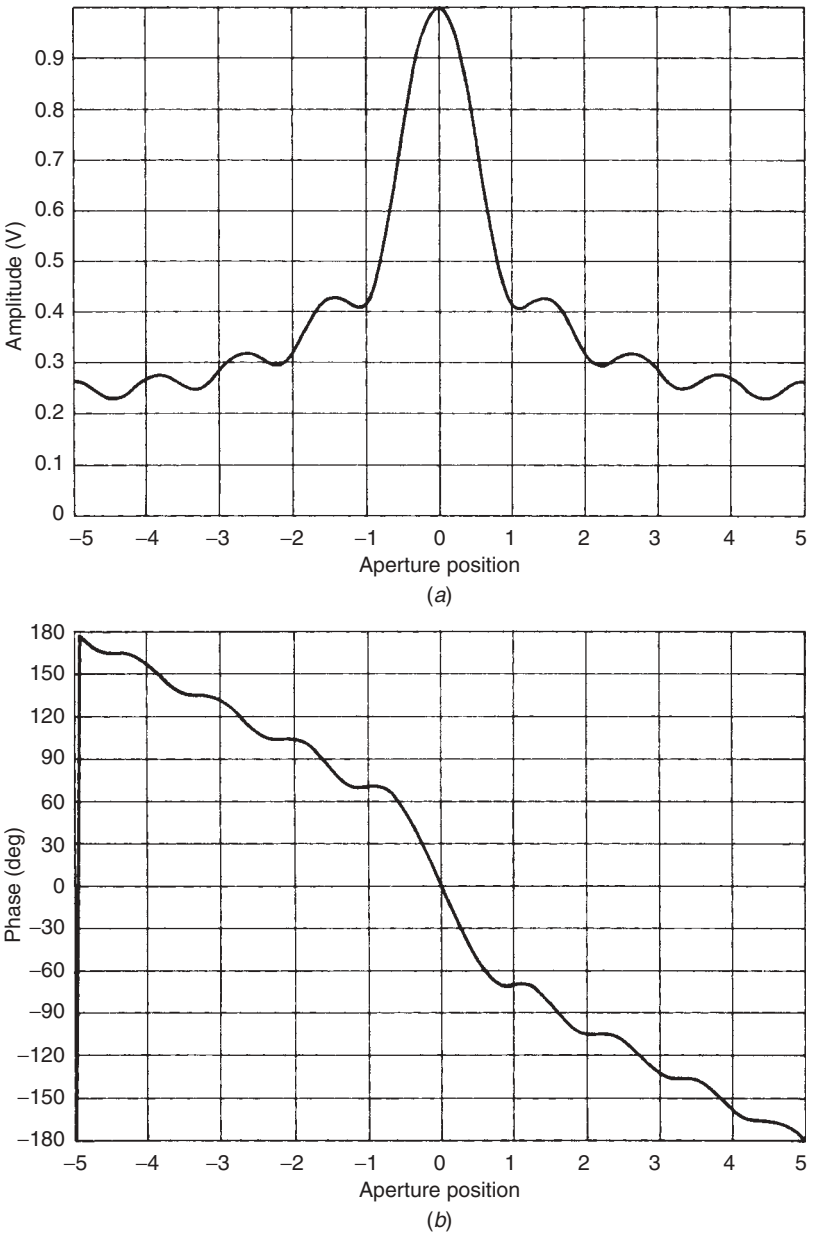

FIGURE 4-8 Aperture distribution of Woodward–Lawson sampling for cosecant-squared pattern (10λ aperture): (*a*) aperture amplitude distribution; (*b*) aperture phase distribution.

Consider a uniformly spaced array along the z-axis with the pattern angle θ measured from the axis. The array response will be symmetrical about the z-axis. If we define the variable $\psi = kd\cos\theta + \delta$, where δ is a fixed progressive phase shift between elements, d the element spacing, and k the wave number $(2\pi/\lambda)$, the pattern of the array is given by

$$E = I_0 + I_1 e^{j\psi} + I_2 e^{j2\psi} + I_3 e^{j3\psi} \cdots \tag{4-46}$$

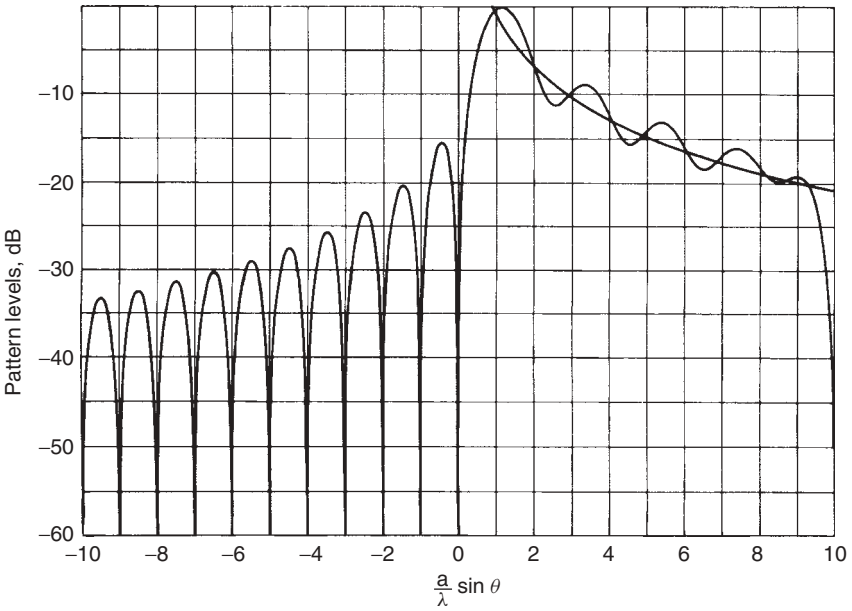

FIGURE 4-9 U-space pattern of 10λ aperture Woodward–Lawson sampling for a cosecant-squared pattern.

where I_i, a phasor, is the excitation of the ith element in the array. We simplify the notation further by defining

$$W = e^{j\psi} \tag{4-47}$$

We then write Eq. (4-46) as

$$E = I_0 + I_1 W + I_2 W^2 + I_3 W^3 + \cdots + I_{N-1} W^{N-1} \tag{4-48}$$

where N is the number of elements in the array. We use the first element as our phase reference point. This array factor (isotropic elements) is a polynomial with $N - 1$ roots (zeros) for N elements.

We denote the roots as W_i and rewrite Eq. (4-48) as

$$E = E_0(W - W_1)(W - W_2) \cdots (W - W_{N-1})$$

We can ignore the normalization E_0 and compute array pattern magnitude as

$$|E(W)| = |W - W_1||W - W_2| \cdots |W - W_{N-1}|$$

where $|W - W_i|$ is the distance from the root W_i to W in the complex plane. W is limited to the unit circle [Eq. (4-47)] because it always has unit value. Both the spacing of the elements and the progressive phase shift δ determine the limits of the phase of W:

$$\begin{aligned} &\theta = 0^\circ \qquad \psi_s = kd + \delta \qquad \text{start} \\ &\theta = 180^\circ \qquad \psi_f = -kd + \delta \qquad \text{finish} \end{aligned} \tag{4-49}$$

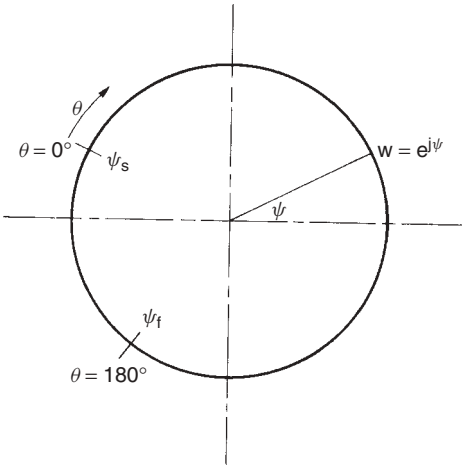

FIGURE 4-10 Unit circle in the W-plane.

As θ increases, ψ decreases and W progresses in a clockwise rotation along the unit circle (Figure 4-10). We have no 2π limitation on either ψ_s or ψ_f. The element spacing determines the number of times W cycles the unit circle as θ varies from 0 to 180°. If $\psi_s - \psi_f$, $2kd$, exceeds 2π, there is a possibility of more than one main beam (grating lobes).

The zeros W_i, suppress the pattern when W moves close to one or more of them. The pattern rises to form a lobe when W is far from the zeros. The main-beam peak occurs at the point with the maximum product of the distances from the zeros. Whenever W passes through that point, another main beam forms. A uniformly fed array has the W-space polynomial

$$f(W) = \frac{1 - W^N}{1 - W} \qquad \text{for } N \text{ elements}$$

The zeros of $f(W)$ are the N zeros of $W^N = 1$ with the zero at $W = 1$ removed: $W_i = e^{j2\pi i/N}$. These are spaced uniformly on the unit circle.

Figure 4-11 shows the unit circle diagram of a 10-element array fed with uniform phase and amplitude. W starts at -1 since $d = \lambda/2$, and it progresses clockwise around the unit circle one revolution to the same point as θ varies from 0 to 180°. At $\theta = 90°$, the product of the distances from the zeros is a maximum. A lobe forms within the space between each pair of zeros. As W moves from the start to the main beam at $W = 1$, it starts at a zero and passes through four additional zeros. These zeros W_i correspond to the nulls in the pattern from $\theta = 0°$ to $\theta = 90°$. An equal number of nulls occur as W moves through the range $\theta = 90$ to 180°.

A uniform-amplitude end-fire array can be represented on the same unit-circle diagram. With antenna elements spaced $\lambda/4$, the excursion from start ψ_s *to* finish ψ_f *is* only $\pi(2kd)$. A progressive phase shift δ of $-kd$ through the array forms an end-fire pattern. From Eq. (4-49), $\psi_s = 0°$ and $\psi_f = 180°$. The end-fire array pattern has only five nulls, including the null at $\theta = 180°$ as θ ranges from 0 to 180°, since only five zeros occur in the visible region.

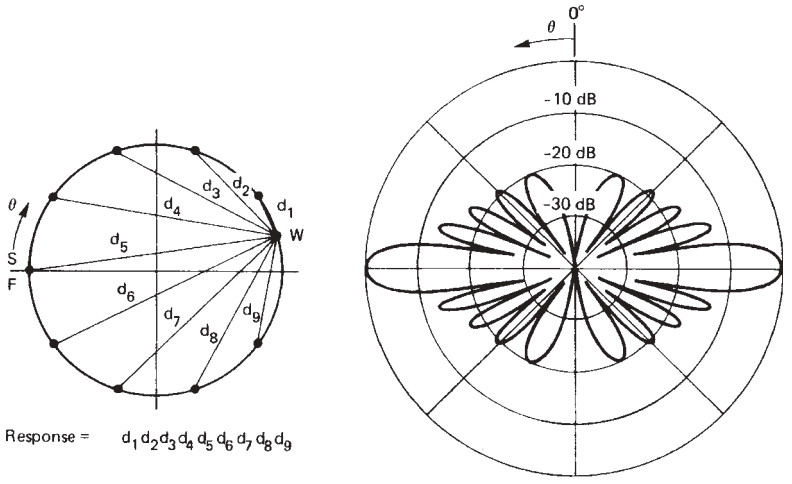

FIGURE 4-11 Unit-circle representation of a 10-element array with λ/2 spacings.

The Hansen and Woodyard increased-directivity end-fire array corresponds to a shift in the start and stop locations on the unit circle. The excursion from start to finish remains π determined by element spacing. Equation (4-49) calculates the start: $\psi_s = 90^\circ - 108^\circ = -18^\circ$. The pattern has five nulls from $\theta = 0$ to 180°.

A binomial array has all its zeros at $W = -1$ and its pattern has no sidelobes, since they occur for points on the unit circle between zeros. Only one beam forms as W traverses the unit circle. The W-space polynomial is $f(W) = (W + 1)^{N-1}$. For an array of given size we can manipulate the location of the nulls either to reduce sidelobes or to place pattern nulls. We reduce a sidelobe by moving the zeros on both sides of it closer together, but either the main-lobe beamwidth increases or the other sidelobes rise. We form a null in the array pattern by moving one of the zeros to that point on the unit circle corresponding to W at the null angle. Given a desired null θ_n,

$$W_i = e^{j(kd\cos\theta_n + \delta)} \tag{4-50}$$

Equation (4-50) gives the phase angle $kd\cos\theta_n + \delta$ of the zero required on the unit circle in W-space.

In the case of an end-fire array in which the spacing between elements is less than λ/2, we can shift zeros from invisible space into visible space to narrow the beam and reduce sidelobes. We thereby form large lobes in invisible space that represent energy storage in the array. The large energy storage reduces the bandwidth and efficiency of the array. This super-directivity method has limited success, although we can produce beautiful patterns on paper.

Example Design a four-element array of broadcast towers to give nearly uniform coverage for $\theta = \pm 45^\circ$ with nulls at $\theta = 270^\circ$ and 135° [11, p. 69].

We will align the array with $\theta = 0^\circ$ to obtain symmetry for the $\pm 45^\circ$ requirement. We actually need only three elements, since only two nulls are specified. Using λ/4 spacings, we set $\delta = -90^\circ$ to get an end-fire array. Equation (4-50) gives the zeros of

the polynomial required for the pattern nulls.

$$W_1: \qquad \psi = \frac{360^\circ}{\lambda}\frac{\lambda}{4}\cos(270^\circ) - 90^\circ = -90^\circ$$

$$W_2: \qquad \psi = \frac{360^\circ}{\lambda}\frac{\lambda}{4}\cos(135^\circ) - 90^\circ = -153.64^\circ$$

We determine the polynomial from the roots:

$$\begin{aligned} f(W) &= (W - e^{-j90^\circ})(W - e^{-j153.64^\circ}) \\ &= W^2 + 1.6994We^{j53.18^\circ} + e^{j116.36^\circ} \end{aligned}$$

We normalize the phase to the first element of the array [constant term of $f(W)$]:

$$f(W) = W^2e^{-j116.36^\circ} + 1.6994We^{-j148.18^\circ} + 1$$

At this point the polynomial representation of the array $f(W)$ does not include the progressive phase factor $\delta = -90^\circ$. We add the factor to the polynomial by adding -90° to the phase of the second element (W term) and -180° to the third element (W^2 term):

$$f(W) = W^2e^{-296.36^\circ} + 1.6994We^{-j148.18^\circ} + 1$$

The coefficients of the polynomial are the voltage (or current) components of the array. No null develops at $\theta = 180^\circ$ because the two available nulls ($N - 1$) were used. Adding the fourth element gives us the freedom to improve the response flatness in the $\pm 45^\circ$ region of θ. Figure 4-12 shows a unit-circle representation and pattern to give a nearly equal ripple response between $\pm 45^\circ$ and the required nulls. We increase

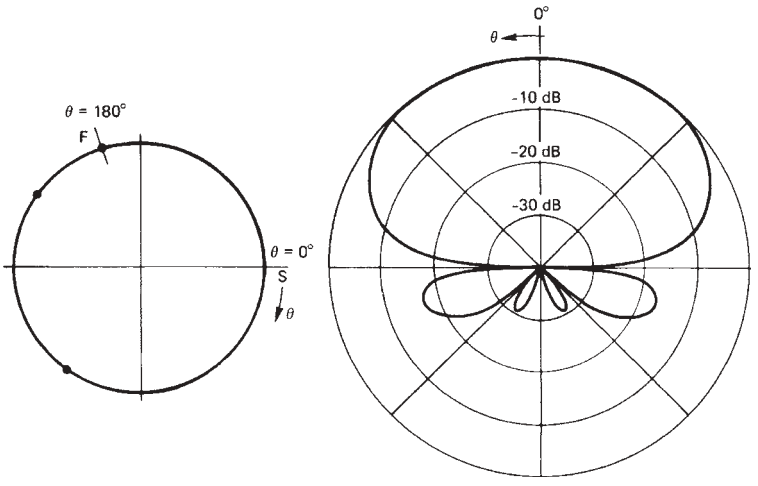

FIGURE 4-12 Four-element linear array with pattern nulls at $\theta = 90$, 135, and 180°. The elements are spaced at 0.35λ to give a flat response $\pm 45^\circ$.

TABLE 4-18 Four-Element 0.35λ Spaced-Array Coefficients for Uniform Beam ±45°

No.	Amplitude (dB)	Phase (deg)
1	−9.50	0.0
2	−4.11	−103.3
3	−4.11	138.4
4	−9.11	35.1

the spacing to 0.35λ and place the pattern nulls at 90°, 135°, and 180°. W starts at +1 on the unit circle or $\psi_s = 0^\circ$ and determines δ:

$$\psi_s = 0 = kd + \delta \quad \text{or} \quad \delta = -kd = -\frac{360^\circ}{\lambda} 0.35\lambda = -126^\circ$$

We compute the phase of the zeros from Eq. (4-50):

$$\psi_1 = 360^\circ (0.35) \cos(90^\circ) - 126^\circ = -126^\circ$$
$$\psi_2 = 360^\circ (0.35) \cos(135^\circ) - 126^\circ = -215.1^\circ \quad (144.9^\circ)$$
$$\psi_3 = 360^\circ (0.35) \cos(180^\circ) - 126^\circ = -252^\circ \quad (108^\circ)$$

By following the same steps as above, we compute the phase and amplitude of the array elements (Table 4-18).

4-10 DOLPH–CHEBYSHEV LINEAR ARRAY [2]

The Chebyshev polynomials have equal ripples in the region $x = \pm 1$, and the amplitude varies between +1 and −1. Outside that region the polynomial value rises exponentially:

$$T_m(x) = \begin{cases} (-1)^m \cosh(m \cosh^{-1} |x|) & x < -1 \\ \cos(m \cos^{-1} x) & -1 \le x \le 1 \\ \cosh(m \cosh^{-1} x) & x > 1 \end{cases}$$

The order of the polynomial m equals the number of roots. Dolph devised a method of relating the Chebyshev polynomials to the array factor polynomial for a broadside array. We scale the polynomial to make the equal-ripple portion the sidelobes and the exponential increase beyond $x = 1$ becomes the main beam. Take an array fed symmetrically about the centerline that has either $2N + 1$ or $2N$ elements. We expand the array factor in a polynomial with factors $\cos(\psi/2)$, where $\psi = kd \cos\theta + \delta$. The beam peak occurs when $\psi = 0$. If we make this correspond to a value x_0, where the Chebyshev polynomial has a value R, the sidelobes will be equal to the ripple at the level $1/R$. By substituting $x = x_0 \cos(\psi/2)$, we use the Chebyshev polynomial for the array polynomial with

$$T_m(x_0) = R \quad \text{or} \quad x_0 = \cosh \frac{\cosh^{-1} R}{m} \tag{4-51}$$

where 20 log R is the desired sidelobe level in decibels. The zeros of $T_m(x)$ are given by

$$x_p = \pm \cos \frac{(2p-1)\pi}{2m} \tag{4-52}$$

By using the equation $x_p = x_0 \cos(\psi/2) = x_0(e^{j\psi/2} + e^{-j\psi/2})$, we calculate the angles of the symmetrical zeros in the W-plane:

$$\psi_p = \pm 2 \cos^{-1} \frac{x_p}{x_0} \tag{4-53}$$

Both values of x_p [Eq. (4-52)] give the same ψ_p pair. Given the zeros in the W-plane, we multiply out the root form of the polynomial to calculate feeding coefficients of the array.

Example Design a 10-element array with 25-dB sidelobes.

The array has nine nulls, so we pick $m = 9$ for the Chebyshev polynomial.

$$\text{[Eq. (4-51)]} \qquad R = 10^{25/20} = 17.7828 \qquad x_0 = 1.0797$$

We need only the first five zeros, since they are symmetrical about zero. We calculate them from Eq. (4-52), divide them by x_0, and use Eq. (4-53) for their angles on the unit circle of the W-plane (Table 4-19). We multiply out the root form of the polynomial for the voltage (current) feeding coefficients of the array. Because the roots are symmetrical about the real axis, all phase angles are zero. We obtain the following coefficients:

Nos.	1, 10	2, 9	3, 8	4, 7	5, 6
Coefficient (dB)	−8.07	−5.92	−2.84	−0.92	0.0

Figure 4-13 shows the unit-circle representation and pattern of the array with λ/2 spacing.

We can estimate the beamwidth of a Chebyshev array by using a beamwidth broadening factor and the beamwidth of a same-length uniformly fed array [12]. The beamwidth broadening factor is given by

$$f = 1 + 0.632 \left[\frac{2}{R} \cosh \sqrt{(\cosh^{-1} R)^2 - \pi^2} \right]^2 \tag{4-54}$$

TABLE 4-19 Chebyshev Polynomial Roots and W-Plane Roots for 10-Element 25-dB Sidelobe Array

p	X_p	ψ_p (deg)
1	0.9848	±48.41
2	0.6428	±106.93
3	0.3420	±143.06
4	0.0	180.00

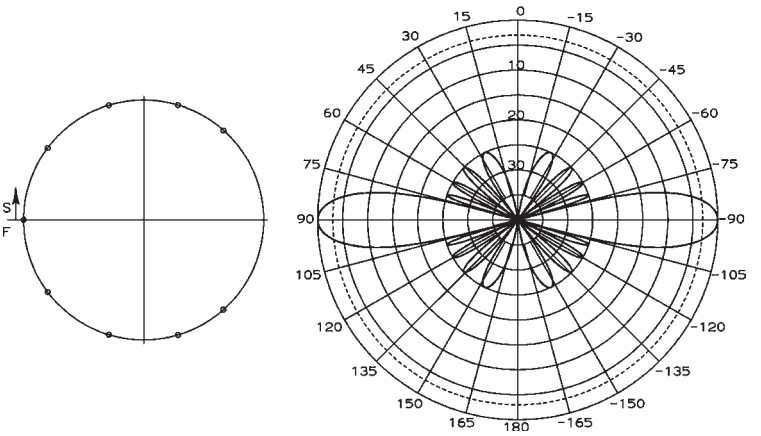

FIGURE 4-13 Ten-element Chebyshev array designed for 25-dB sidelobes.

Equation (4-54) is valid in the range of sidelobe levels from 20 to 60 dB and for scanning near broadside.

Example Compute the broadside beamwidth of a Dolph–Chebyshev array with 61 elements, a 30-dB sidelobe level, and $\lambda/2$ spacings.

Equation (4-54) gives the value 1.144 for f using $R = 10^{30/20}$.

We estimate the beamwidth of the uniform array from $\text{HPBW} = 50.76^\circ\lambda/Nd = 1.66^\circ$, where d is the element spacing:

$$\text{HPBW}_{\text{array}} = (f)\text{HPBW}_{\text{uniform}} = 1.144(1.66^\circ) = 1.90^\circ$$

We use the beam-broadening factor to estimate the array directivity:

$$D = \frac{2R^2}{1 + (R^2 - 1)f\lambda/Nd} \tag{4-55}$$

Example We calculate the directivity of the 61-element array above from Eq. (4-55). $D = 52.0$ (17.2 dB).

If we take its limit as $Nd \to \infty$, Eq. (4-55) becomes $2R^2$. An infinite Dolph–Chebyshev array has a gain 3 dB more than the sidelobe level.

4-11 VILLENEUVE ARRAY SYNTHESIS [13]

Villeneuve devised a method similar to the Taylor distribution that modifies the $\overline{n} - 1$ inner zeros of a uniform amplitude array to lower sidelobes. Since the positions of the outer zeros remain fixed, the outer pattern sidelobes decrease as $1/U$. The uniform distribution W-plane zeros are located uniformly around the unit circle except for $W = 1$:

$$\psi_p = \frac{2\pi p}{N_e} \tag{4-56}$$

The inner zeros correspond to the Chebyshev zeros [Eq. (4-53)] except that we multiply them by a constant factor α dependent on the number of elements, the sidelobe level, and $\overline{n}$:

$$\alpha = \frac{\overline{n}\pi}{N_e \cos^{-1}\left\{(1/x_0)\cos\left[(2\overline{n}-1)\pi/2m\right]\right\}} \tag{4-57}$$

The order of the Chebyshev polynomial $m = N_e/2$. We use Eq. (4-51) to compute x_0.

Example Design a 10-element Villeneuve array containing 10 elements for 25-dB sidelobes and $\overline{n} = 4$.

We determine $\alpha = 1.00653$ using Eq. (4-57). The inner three W-plane zeros are found by multiplying the Chebyshev zeros by α, which occur in pairs, and the next three zeros are found from the uniform amplitude array using Eq. (4-56):

$$\psi_p: \quad \pm 48.73 \qquad \pm 73.82 \qquad \pm 107.63 \qquad \pm 144 \qquad 180$$

Figure 4-14 illustrates the W-plane and pattern of the 10-element Villeneuve array:

Nos.	1, 10	2, 9	3, 8	4, 7	5, 6
Coefficient (dB)	−8.44	−5.85	−2.91	−0.91	0.0

The sidelobes drop off instead of staying constant: −25.08, −25.19, −25.43, −26.14.

4-12 ZERO SAMPLING OF CONTINUOUS DISTRIBUTIONS [14]

We sample continuous distributions, such as the Taylor line source, for large arrays. By using that method, we avoid the numerical difficulties of multiplying out long polynomials. When a small array samples an aperture distribution, its pattern fails to follow the pattern of the distribution. We improve the pattern by matching the zeros of the array to the distribution nulls. The array ψ-space pattern repeats at 2π intervals, but the k-space pattern of the aperture has no repeat. We space elements by $\lambda/2$ to

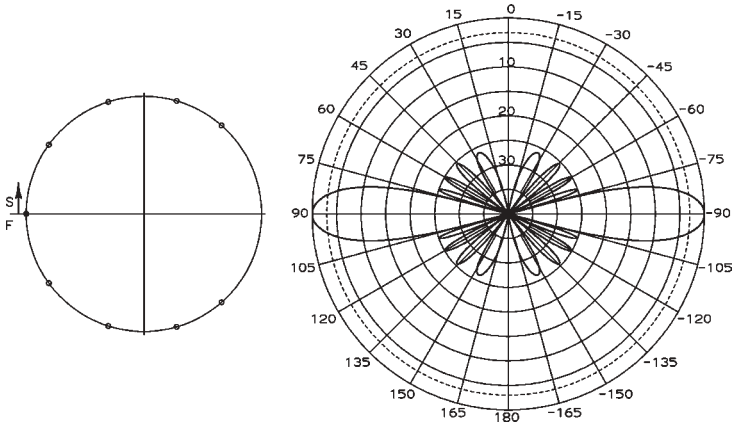

FIGURE 4-14 Ten-element Villeneuve array designed for 25-dB sidelobes, $\overline{n} = 4$.

span the total ψ-space nonrepeating region. We then equate an array with $\lambda/2$ spacings to an aperture of the same length regardless of the actual spacings between elements. Since the array samples a continuous distribution, the aperture is Nd long, where d is the distance between array elements and we consider the array element to be sampling $d/2$ on both sides of its location.

Consider the U-space pattern of a uniform aperture distribution: $\sin \pi U / \pi U$. The aperture zeros occur at integer values of U. The corresponding zeros of the uniformly fed array are $W_i = e^{j2\pi i/N}$, where $i = 1, 2, \ldots, N-1$. The Taylor distribution modifies the location of the zeros of the uniform distribution to U_i, and the sampled zeros of the array must move to follow this pattern:

$$W_i = e^{j2\pi U_i/N} \tag{4-58}$$

Example Given a Taylor line source with 30-dB sidelobes and $\overline{n} = 6$, compute the zeros of an array with 12 elements to sample the distribution.

The array spans 12/2 in U-space. We calculate zeros of the distribution from Section 4-4 and the angles of the array zeros from Eq. (4-58):

U_i	± 1.473	± 2.1195	± 2.9989	± 3.9680	± 4.9747	6
ψ_i	± 44.19	± 63.58	± 89.97	± 119.04	± 149.24	180

We multiply out the root form of the polynomial to compute the array feeding coefficients. The array has 30-dB first sidelobes. A straight sampling of the distribution gives an array whose sidelobes exceed 30 dB.

Figure 4-15 shows the unit-circle diagram of a zero-sampled Taylor line source with 25-dB sidelobes and $\overline{n} = 5$. The method places the zeros on the unit circle close enough together to limit the sidelobe peaks to less than 25 dB when W for a given pattern direction lies between the zeros. The array has higher sidelobes than the equivalent

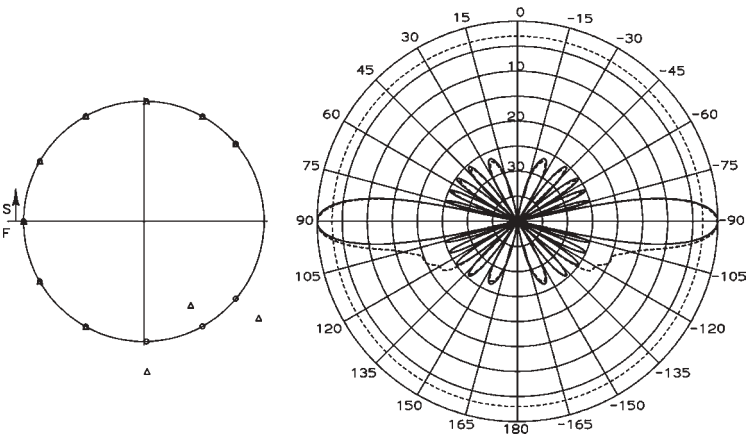

FIGURE 4-15 Twelve-element array designed by zero-sampling 25-dB Taylor distribution: pattern of normal array (solid curve); pattern with null filling by moving three zeros off unit circle (dashed curve and triangles).

aperture, but closer to the specified 25 dB, because the finite array cannot control sidelobes as well as the continuous aperture.

Aperture	25.29	25.68	26.39	27.51	29.63
12-Element Array	25.03	25.07	25.18	25.44	26.41

The dashed plot of Figure 4-15 illustrates pattern behavior when W-space zeros are moved off the unit circle. We can fill pattern nulls and generally shape the pattern. When we place all zeros on the unit circle in the complex plane, it can be proved that the array excitations will have amplitude symmetry about the centerline. Moving the zeros off the unit circle disturbs this symmetry. We can eliminate all pattern nulls by moving all the W-plane zeros off the unit circle. If we start with a uniformly fed array and move all the zeros to the same radius, the distribution taper across the array will be linear in decibels. In the next two sections we explore techniques for moving the zeros systematically to produce shaped patterns from an array.

4-13 FOURIER SERIES SHAPED-BEAM ARRAY SYNTHESIS

The preceding methods seek the narrowest beamwidths for a given sidelobe level. Arrays can also produce shaped beams. We discussed the Woodward line-source method for shaped beams in Section 4-8. We obtain good approximations by sampling the line-source distribution with an array. Beyond sampling a line source, we can apply Fourier series to design an array directly. An array for a shaped beam must be much larger than is required for the beamwidth. The extra size of the array gives us the degrees of freedom necessary for beam shaping. Increasing the array size increases the match between the specified and the actual beam shape.

Because the array pattern is periodic in k-space, we can expand the pattern in a Fourier series. The array pattern for a symmetrically fed array is given by either

$$f(\psi) = 1 + 2\sum_{n=1}^{m} \frac{I_n}{I_0} \cos\frac{2n\psi}{2} \qquad N \text{ odd} \tag{4-59}$$

or

$$f(\psi) = 2\sum_{n=1}^{m} \frac{I_n}{I_0} \cos\frac{(2n-1)\psi}{2} \qquad N \text{ even} \tag{4-60}$$

where $m = (N-1)/2$ (odd) or $m = N/2$ (even) with $\psi = kd\cos\theta + \delta$. Equations (4-59) and (4-60) are Fourier series expansions of the pattern in ψ-space. The elements farthest from the centerline produce the highest harmonics in the series.

In an asymmetrically fed array, we express Eqs. (4-59) and (4-60) as a sum of exponential terms:

$$f(\psi) = \begin{cases} \displaystyle\sum_{n=-m}^{m} a_n e^{jn\psi} & N \text{ odd} \\ \displaystyle\sum_{n=1}^{m} a_n e^{j(2n-1)\psi/2} + a_{-n} e^{-j(2n-1)\psi/2} & N \text{ even} \end{cases} \tag{4-61}$$

Suppose that we have a desired pattern in k-space given by $f_d(\psi)$. We expand it in an infinite Fourier series of the same form as Eq. (4-61) with $m = \infty$. We equate the first m coefficients of the two Fourier series to approximate the desired pattern. As in any Fourier series method, we solve for the coefficients by using the orthogonality of the expansion functions when integrated over a period:

$$a_n = \begin{cases} \dfrac{1}{2\pi}\displaystyle\int_{-\pi}^{\pi} f_d(\psi)e^{-jn\psi}\,d\psi & N \text{ odd} \\ \dfrac{1}{2\pi}\displaystyle\int_{-\pi}^{\pi} f_d(\psi)e^{-j(2n-1)\psi/2}\,d\psi & N \text{ even} \end{cases} \tag{4-62}$$

$$a_{-n} = \frac{1}{2\pi}\int_{-\pi}^{\pi} f_d(\psi)e^{j(2n-1)\psi/2}\,d\psi \qquad N \text{ even} \tag{4-63}$$

We determine the array coefficients directly from the Fourier series coefficients.

Example Design a 21-element array with $\lambda/2$ element spacing with a constant beam $2b$ wide centered in ψ-space.

We use Eq. (4-62) to compute coefficients a_n:

$$a_n = \frac{1}{2\pi}\int_{-b}^{b} e^{-jn\psi}\,d\psi = \frac{\sin nb}{\pi n}$$

Suppose that the constant beam is 45° at broadside: $67.5^\circ \le \theta \le 112.5^\circ$. Then

$$b = \frac{360^\circ}{\lambda}\frac{\lambda}{2}\cos 67.5^\circ = 68.88^\circ$$

We can ignore the constant factor i/π and expand to compute the array coefficients (Table 4-20).

The method fails to some extent when we try it on arrays with spacings greater than $\lambda/2$. The integral does not cover the total visible region. We can, however, use it with

TABLE 4-20 Fourier Series Synthesis Coefficients of 21-Element Array for Pattern of Figure 4-16

n	a_n	Amplitude (dB)	Phase (deg)
0	1.0000	0.00	0
±1	0.9328	−0.60	0
±2	0.3361	−9.47	0
±3	−0.1495	−16.50	180
±4	−0.2488	−12.08	180
±5	−0.0537	−25.40	180
±6	0.1336	−17.48	0
±7	0.1209	−18.35	0
±8	−0.0240	−32.40	180
±9	−0.1094	−19.22	180
±10	−0.0518	−25.72	180

spacings less than $\lambda/2$ with good results. As we increase the number of elements in the array, the match to the desired pattern improves. Of course, tapering the desired pattern reduces the higher harmonics and the subsequent need for more elements.

Example Suppose that we want to scan the beam of the 21-element array with $\lambda/2$ element spacing to 60° with a 45° beamwidth. The beam edges are 37.5° and 82.5°.

We could calculate coefficients by integrating Eq. (4-62) directly with this requirement, but we can use δ, the progressive phase shift between elements, to simplify the problem. The beam edges in ψ-space are

$$\begin{array}{cc} 180^\circ \cos(37.5^\circ) + \delta & \text{and} \quad 180^\circ \cos(82.5^\circ) + \delta \\ 142.8^\circ + \delta & 23.49^\circ + \delta \end{array}$$

We pick δ to center the beam in ψ-space: $b = 142.8^\circ + \delta$, $-b = 23.49^\circ + \delta$. On solving, we have $\delta = -83.15^\circ$ and $b = 59.65^\circ$. We use the formula $\sin(nb)/\pi n$ to compute coefficients of the array and then add the progressive phase shift through the array. Figure 4-16 shows the array pattern.

When we scan the beam to end fire, we must account for the symmetry about $\theta = 0^\circ$. Because we limit the spacings to less than $\lambda/2$ to prevent grating lobes, we have an unspecified region of ψ-space that we can choose in any convenient manner.

Example Design a 21-element end-fire array with a 90° beamwidth and 0.30λ spacings.

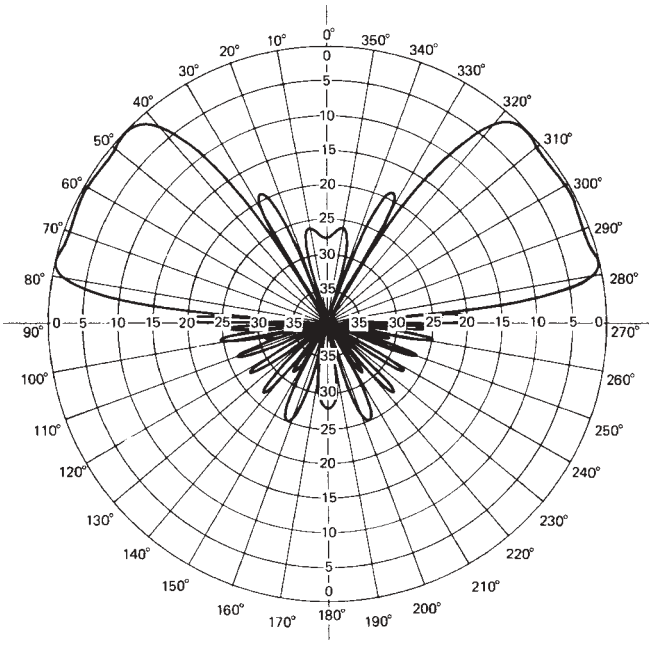

FIGURE 4-16 Twenty-one-element array designed by the Fourier series method to scan to 60° with a 45° beamwidth.

For an end-fire array we pick $\delta = -kd = -108^\circ$. This places the edge of the visible region on the ψ-space origin. We are free to specify the invisible region that will be included in the integral [Eq. (4-62)]. We specify the invisible region as the mirror image of the portion in the visible region and solve for b:

$$-b = 360^\circ(0.3)\cos(45^\circ) - 108^\circ = -31.63^\circ$$

We use the $\sin(nb)/\pi n$ formula to calculate array coefficients and then apply the progressive phase shift δ to the coefficients obtained to get the proper phase to scan to end fire.

We cannot control the sidelobes of an array designed using Fourier series expansion. The initial specification calls for no sidelobes. Sampling a Woodward linear aperture with an array also fails to give control of the sidelobes. The Woodward linear distribution cannot control sidelobes; it provides only ease of design. In the next section we explore a method with direct control of sidelobes of an array.

4-14 ORCHARD METHOD OF ARRAY SYNTHESIS [15]

In Section 4-6 we manipulate the nulls of a continuous linear distribution to control the sidelobes of the radiated pattern individually. In Section 4-9 we show that the nulls of the linear aperture pattern can be related directly to the roots of Schelkunoff polynomial representation of the linear array pattern in W-space. The unit circle method gives us a tool for array synthesis expanded in the Orchard method for the design of arrays with arbitrary patterns. We apply an iterative technique on the W-space zeros to produce the pattern desired. We control all the sidelobes individually and produce shaped patterns for the main beam. The finite size of the array limits the control of the main beam shape as we saw in the Fourier series expansion method. Each array element corresponds to a term in the Fourier series expansion.

We start with the Schelkunoff transformation of the array pattern:

$$f(W) = C_0 \prod_{n=1}^{N} (W - W_n) \tag{4-64}$$

A normalization constant C_0 has been added. We write $W_n = \exp(a_n + jb_n)$. Expansion of Eq. (4-64) produces the feeding coefficients of an array with $N + 1$ elements:

$$W = e^{j\psi} \qquad \text{with} \quad \psi = kd\cos\theta + \delta$$

θ is measured from the array axis. The effect of δ on the unit circle method is to rotate the starting and finishing points when varying W to calculate the pattern using Eq. (4-64). An equally valid method is to rotate the zeros about the origin of the complex plane, which leaves the ψ-space pattern shape unchanged. When designing a shaped beam, we need to rotate the main beam peak to the proper location to calculate the amplitudes because our specification will be in terms of the pattern angle θ relative to the peak.

Figure 4-11 illustrates that the pattern amplitude is the product of distances from each zero to the pattern W point. Expansion of Eq. (4-64) in terms of the product of distances to W gives

$$|f(W)|^2 = C_0^2 \prod_{n=1}^{N} [1 - 2e^{a_n} \cos(\psi - b_n) + e^{2a_n}] \tag{4-65}$$

The Orchard method requires the specification of each sidelobe and additional values located at the minimum ripple points in the shaped region. For a single-beam unshaped pattern, we only specify sidelobes, and all a_n will be zero since all zeros W_n will be on the unit circle. We restrict the array to $\lambda/2$ spaced elements when applying the method so that the entire unit circle is used in the pattern. An array with N zeros has N pattern peaks which lie between the zeros in the W-plane. When we include the normalization constant C_0 to specify the main beam peak and all the zeros, we have $N + 1$ unknowns to find. Without loss of generality we specify the last zero as $W_N = -1$ or $\psi = \pi$ to reduce the number of unknowns to N. Since we rotate the zeros after we determine the proper zero spacing for specified sidelobes, we place the main beam between W_{N-1} and $W_N = -1$. Before starting the iteration technique, we generate a list of sidelobe levels with the main beam as the last one.

The method expands the pattern in a multiple-variable Taylor series using b_n, a_n, and the normalization constant as variables. To facilitate calculating the partial derivatives, we express Eq. (4-65) in decibels:

$$G = \sum_{n=1}^{N-1} \frac{10}{\ln(10)} \ln[1 - 2e^{a_n} \cos(\psi - b_n) + e^{2a_n}] + 10 \log_{10}[2(1 + \cos\psi)] + C \tag{4-66}$$

The second term of Eq. (4-66) is due to the zero $W_N = -1$ and C is the normalization constant of the main beam. The logarithm to the base 10 has been expressed as a natural logarithm for the calculation of derivatives:

$$\frac{\partial G}{\partial a_n} = \frac{M e^{a_n}[e^{a_n} - \cos(\psi - b_n)]}{1 - 2e^{a_n} \cos(\psi - b_n) + e^{2a_n}} \tag{4-67}$$

$$\frac{\partial G}{\partial b_n} = -\frac{M e^{a_n} \sin(\psi - b_n)}{1 - 2e^{a_n} \cos(\psi - b_n) + e^{2a_n}} \tag{4-68}$$

$$\frac{\partial G}{\partial C} = 1 \tag{4-69}$$

The variable $M = 20/\ln(10)$. The multiple-variable Taylor series involves three types of terms:

$$G(b_n, a_n, C) = G_0(b_{n0}, a_{n0}, C_0) + \sum_{n=1}^{N-1} \frac{\partial G}{\partial b_n}(b_n - b_{n0}) + \sum_{n=1}^{N-1} \frac{\partial G}{\partial a_n}(a_n - a_{n0}) + (C - C_0) \tag{4-70}$$

Every nonzero value of a_n fills in the pattern null at $\psi = b_n$. If we specify the desired pattern amplitude at every sidelobe peak, the main beam, and at points between the sidelobe peaks equal to the number of nonzero a_n, we form a square matrix equation. The solution gives the changes in b_n, a_n, and C. Since we expanded Eq. (4-66) as a linear approximation, the solution of Eq. (4-70) gives only an approximate solution. In a few iterations the method converges and we obtain an acceptable pattern.

Suppose that the shaped pattern is limited to a range in W-space so that there are only L nonzero a_n. Given the desired pattern $S_m(\psi_m)$ at ψ_m and the current pattern $G_0(\psi_m)$, one row of the matrix is

$$\left[\frac{\partial G(\psi_m)}{\partial b_1}, \ldots, \frac{\partial G(\psi_m)}{\partial b_{N-1}}, \frac{\partial G(\psi_m)}{\partial a_1}, \ldots, \frac{\partial G(\psi_m)}{\partial a_L}, 1\right]$$

We need $N + L$ rows or pattern points to solve Eq. (4-70) for changes in b_n, a_n, and C:

$$[\delta b_1, \ldots, \delta b_N, \delta a_1, \ldots, \delta a_L, \delta C]^{\mathrm{T}}$$

We require a search routine to locate the pattern peaks between the pattern nulls or minima between peaks in the shaped region for given values of b_n and a_n after we normalize to the current pattern peak. We subtract these from the levels desired:

$$[S(\psi_1) - G_0(\psi_1), \ldots, S(\psi_{N+L}) - G_0(\psi_{N+L})]^{\mathrm{T}}$$

After solving the square matrix equation, we update the W-plane zeros:

$$\begin{aligned} b_1 &= b_1 + \delta b_1 \\ &\vdots \\ b_{N-1} &= b_{N-1} + \delta b_{N-1} \\ &\vdots \\ a_1 &= a_1 + \delta a_1 \\ &\vdots \\ a_L &= a_L + \delta a_L \\ C &= C_0 + \delta C \end{aligned}$$

The iteration alters the beam peak and its location. The pattern peak is normalized after iteration, and for a shaped pattern a new zero rotation is found to line up the beam peak for the pattern-shaping function.

Example Design an eight-element array with its beam peak at 90° and specified sidelobes before the peak of 25, 30, and 25 dB and 20, 25, and 30 dB after the peak.

The sidelobes values begin with the first sidelobe after the peak and rotate to the peak:

$$-20 \qquad -25 \qquad -30 \qquad -25 \qquad -30 \qquad -25 \qquad 0$$

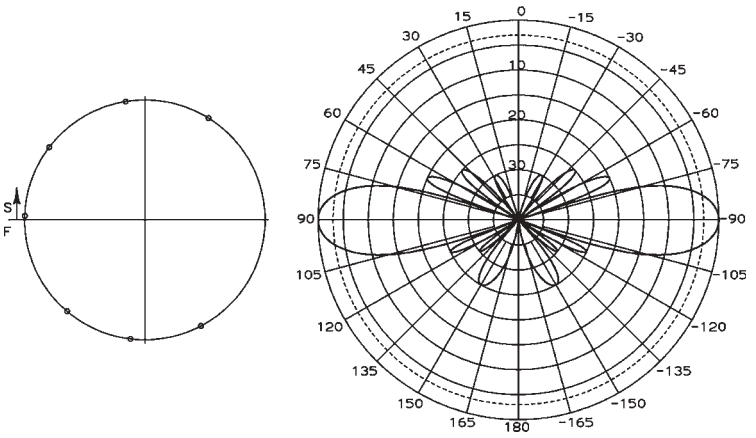

FIGURE 4-17 Eight-element array designed using Orchard synthesis for individually specified sidelobes, $\lambda/2$ spacings.

The solution converges in four iterations after starting with uniformly spaced zeros on the unit circle. Figure 4-17 shows the unit-circle zeros on the left and the corresponding pattern on the right with $\lambda/2$ element spacing:

W-Space Zero (deg)	178.14	142.72	99.26	58.01	−62.18	−96.89	−130.37
Pattern Null (deg)	8.25	37.54	56.53	71.20	110.21	122.57	136.41

The feeding coefficients for the final design are given in Table 4-21.

Although the Orchard method requires the elements to be spaced $\lambda/2$ during synthesis, the completed design can be used at another element spacing. Figure 4-18 gives the unit-circle diagram of the same array with a 0.7λ element spacing. The range of W now exceeds 2π and the sidelobe regions of the unit circle have been used more than once. Sidelobes 3 and 4 occur twice in the pattern. Of course, if we scan the array too far, the pattern would have grating lobes. Figure 4-19 plots the pattern of an end-fire array with $\lambda/4$-element spacing using the same zeros. Only a portion of the unit circle is used, and not all sidelobes are realized. Figure 4-20 illustrates the end-fire case with the elements spaced so that the final position of W occurs at a null. The pattern contains all six sidelobes. The unit-circle analysis mirrors that of

TABLE 4-21 Coefficients of Eight-Element Array of Figure 4-17 Designed by Orchard Synthesis

Element	Magnitude (dB)	Phase (deg)	Element	Magnitude (dB)	Phase (deg)
1	−8.69	8.70	5	0	3.79
2	−3.90	3.22	6	−1.06	7.41
3	−1.06	1.29	7	−3.90	5.48
4	0	4.91	8	−8.69	0

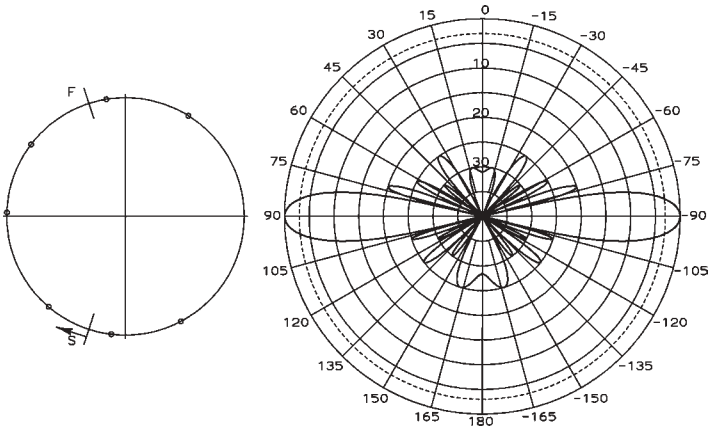

FIGURE 4-18 Eight-element array designed using Orchard synthesis for individually specified sidelobes, 0.7λ spacings.

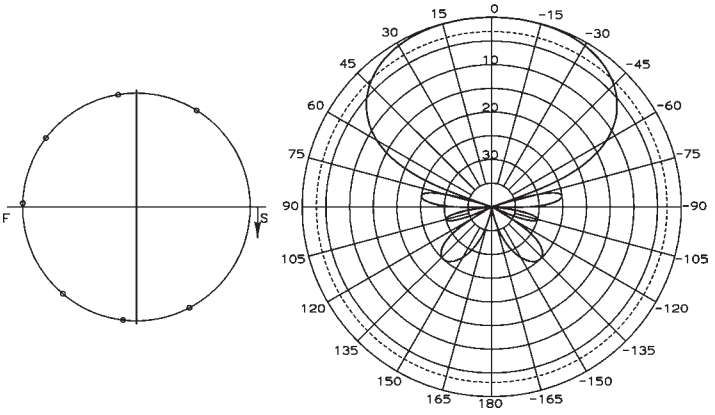

FIGURE 4-19 Eight-element array designed using Orchard synthesis for individually specified sidelobes, λ/4 spacings scanned to end fire.

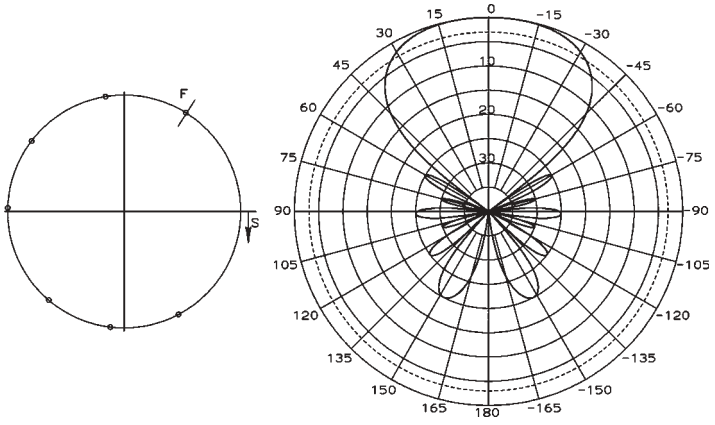

FIGURE 4-20 Eight-element array designed using Orchard synthesis for individually specified sidelobes, 0.42λ spacings scanned to end fire.

the circle diagram in Chapter 3, where increasing the element spacing increases the visible region. In this case the visible region corresponds to rotation about the unit circle. Expansion of Eq. (4-64) produces the array feeding coefficients independent of element spacing, and the progressive phase shift between elements δ affects phase but not amplitude. The four examples given in Figures 4-17 to 4-20 have the same sequence of feed magnitudes.

We can use Orchard synthesis to generate a difference pattern similar to the Bayliss line distribution and control all the sidelobes. A difference pattern has two main beams. Using the same example of an eight-element array, we modify the sidelobe list to include side-by-side main beams. We eliminate the −25-dB lobe next to the original main beam from the values above:

$$-20 \qquad -25 \qquad -30 \qquad -25 \qquad -30 \qquad 0 \qquad 0$$

When we apply the synthesis by placing the last main beam at 90°, we obtain a pattern with two main beams with the null between them at 101.6°, corresponding to a W-plane null at −36.3°. We rotate all W-plane zeros by 36.3° to place the null between the two main beams at 90°. Figure 4-21 shows the W-plane and polar pattern for the final design. Note the placement of the W-plane zero at $W = +1$. Table 4-22 lists the feeding coefficients.

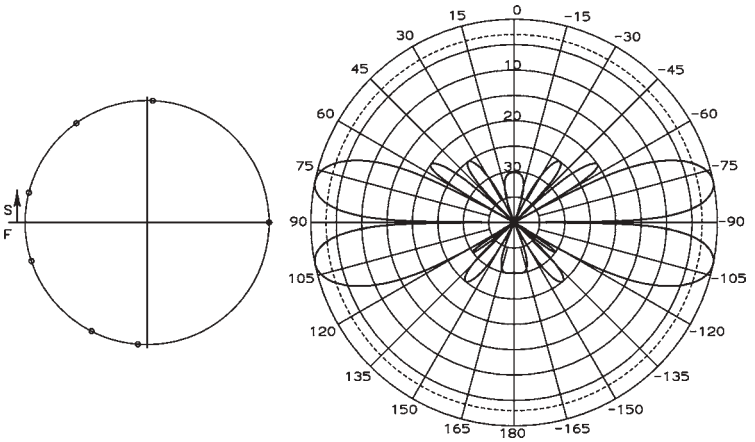

FIGURE 4-21 Difference pattern array using eight-elements designed by Orchard synthesis.

TABLE 4-22 Coefficients of Eight-Element Difference Pattern Array of Figure 4-21 Designed by Orchard Synthesis

Element	Magnitude (dB)	Phase (deg)	Element	Magnitude (dB)	Phase (deg)
1	−6.32	5.39	5	−6.91	178.35
2	−0.35	1.28	6	0.0	184.6
3	0.0	0.8	7	−0.35	184.12
4	−6.91	7.05	8	−6.32	180

We fill in the null between the different lobes to form a flat-topped beam for the eight-element array and use a constant-amplitude shaping function for the pattern desired. The beamwidth of the flat lobe is determined by the lobe spacing, and only certain sizes are possible. Remember that an array is a Fourier series approximation to the pattern desired. With only eight elements the match is poor between the pattern desired and the approximate pattern. We use one nonzero a_n to move the W-plane zero off the unit circle that forms the pattern null between the two beams and add another pattern specification:

$$-20 \qquad -25 \qquad -30 \qquad -25 \qquad -30 \qquad 0 \qquad 0 \qquad -1$$

The last number gives the pattern level at the null relative to the shaped pattern level. This last term uses Eq. (4-67) for its columns. The constant beam design uses a 22°-wide beam centered at 90° for the pattern shape function. We start with $a_n = 0.01$ before iterating. The iteration using the matrix equation computes $a_1 = 0.4435$, which can be either positive or negative without changing the pattern. Rotation of the W-plane zeros placed the zero for minimum ripple along the positive real axis and produced a symmetrical pattern about $\theta = 90°$. Figure 4-22 contains the final design W-space zeros and polar pattern. The iterations produced the sidelobe levels specified (Table 4-23).

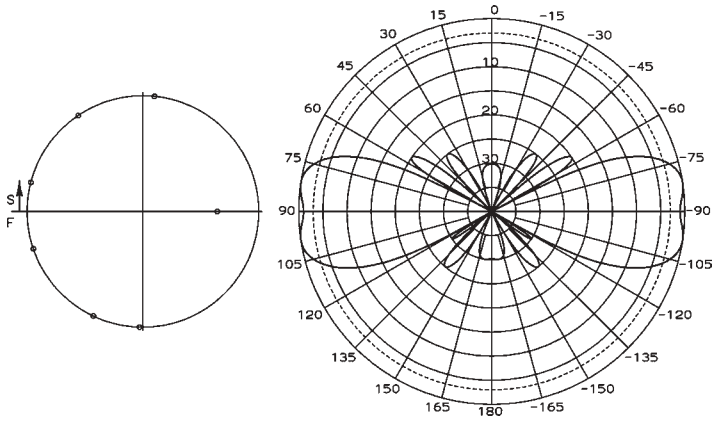

FIGURE 4-22 Flat-topped beam eight-element array designed by Orchard synthesis.

TABLE 4-23 W-Plane Zeros of Eight-Element Flat-Topped Beam of Figure 4-22 Designed by Orchard Synthesis

W-Space Zero (deg)	W-Space Radius	Pattern Null (deg)
165.51	1.0	23.15
123.99	1.0	46.46
84.33	1.0	62.06
0	0.6418	90
−91.65	1.0	120.61
−115.39	1.0	129.87
−161.18	1.0	153.57

TABLE 4-24 Coefficients of Eight-Element Array for Flat-Topped Beam of Figure 4-22 Designed by Orchard Synthesis

Element	Magnitude (dB)	Phase (deg)	Element	Magnitude (dB)	Phase (deg)
1	−12.95	−174.39	5	−1.15	1.54
2	−10.78	178.85	6	0.0	4.37
3	−24.69	167.92	7	−2.26	3.95
4	−7.90	−1.47	8	−9.10	0.0

The radius of the fourth term could be $1/0.6418 = 1.5581$ without affecting the pattern result. Inserting the zeros into Eq. (4-64) and expanding the polynomial produces the feeding coefficients (Table 4-24).

The Fourier series example for a constant beam centered at 60° with a 45° beamwidth using 21 elements spaced $\lambda/2$ (Figure 4-16) was repeated using Orchard synthesis. Fourier series synthesis could not control the sidelobes. First, we need to figure out how many array lobes cover the shaped pattern region. Place the zeros uniformly around the unit circle in the W-plane and determine how many of the roots are within the beam. For a 21-element array six beams and five zeros lie in the $\psi = \pi \cos\theta$ angular region of the constant beam found using Eq. (4-71):

$$\text{beams} = \frac{N(\cos\theta_{\min} - \cos\theta_{\max})}{2} \tag{4-71}$$

The solution to Eq. (4-71) is an integer given N as the number of W-plane zeros. All sidelobes were set at −30 dB and the ripple at −0.9 dB below the constant beam:

Lobes	1–14	15–20	21–25
Sidelobe (dB)	−30	0.0	−0.9

Figure 4-23 gives the final result of the synthesis, an improvement over Figure 4-16, with its uncontrolled sidelobes.

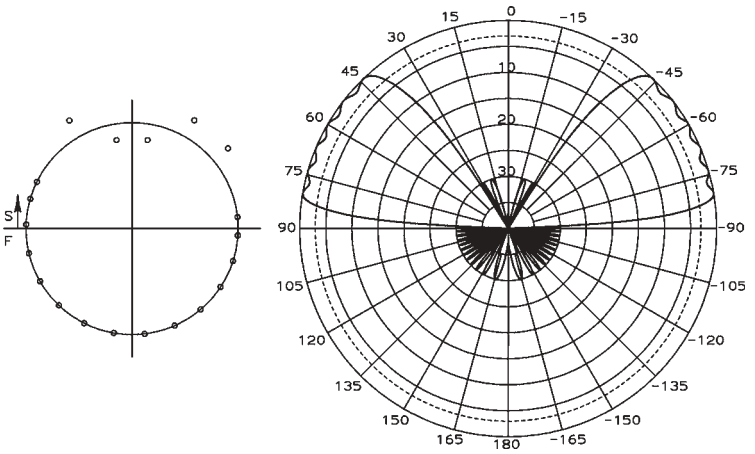

FIGURE 4-23 Twenty-one-element array designed by Orchard synthesis to scan to 60° with a 45° beamwidth.

We must consider the element excitations. The zeros not lying on the unit circle can be either inside or outside the circle and produce the same pattern. Different combinations of zero locations lead to different element amplitudes. The last example has five zeros displaced from the unit circle, which produces $2^5 = 32$ combinations. We need to check the amplitude distribution that results from each case (Table 4-25). Arrays with a large range of amplitudes are difficult to produce. In some cases the range of amplitude available is limited, such as waveguide slot arrays. Mutual coupling between elements also makes it difficult to achieve the desired low amplitudes on some elements because nearby elements will excite them, and compensation for mutual coupling may prove difficult. Figure 4-23 shows one of the combinations of root placements that produced the minimum amplitude variation in the array.

The Fourier series synthesis gave an amplitude variation of 32.4 dB, whereas the Orchard synthesis variation is 13.29 dB. This synthesis produced better patterns with less amplitude variation. Decreasing the ripple depth increases the amplitude variation of the array.

Csc²θ cos θ Pattern This pattern produces constant round-trip signals versus the elevation angle for radar. The pattern from the array axis is given by $\csc^2(\theta - 90^\circ)\cos(\theta - 90^\circ)$. The peak occurs beyond 90° and decreases for greater angles. The shaped pattern function requires the rotation of the W-plane zeros at each step so that the pattern peak calculated from the zeros occurs at the proper angle. The changing zero locations move the beam peak location at each iteration.

Example Design a 16-element $\csc^2(\theta - 90^\circ)\cos(\theta - 90^\circ)$ beam array to operate from 100 to 140° and have 30-dB sidelobes.

Equation (4-71) determines that five beams cover the pattern region and sets the number of nonzero a_n as 4. The 16-element array has 15 zeros, with the first 10 specified as −30 dB, five for the shaped-beam region, and four for the minima between the shaped-beam peaks. We specify the shaped-beam lobes relative to the shape levels. The last lobe is the beam peak.

TABLE 4-25 Coefficients of 21-Element Array for Flat-Topped Beam of Figure 4-23 Designed by Orchard Synthesis

Element	Amplitude (dB)	Phase (deg)	Element	Amplitude (dB)	Phase (deg)
1	−11.85	−65.47	12	−3.48	−115.31
2	−6.89	−146.85	13	−3.01	−158.73
3	−6.23	126.55	14	−2.97	134.01
4	−11.34	4.64	15	−4.93	49.59
5	−5.12	−158.19	16	−7.51	−40.53
6	0.0	108.08	17	−9.64	−111.80
7	−0.01	23.97	18	−9.44	−159.41
8	−6.33	−65.70	19	−8.06	142.99
9	−9.73	86.93	20	−9.26	73.66
10	−2.09	−4.11	21	−13.29	0.0
11	−1.75	−70.12			

Lobe	11	12	13	14	15	16	17	18	19
Amplitude (dB)	1.0	0.8	0.6	0.4	0.2	−0.9	−0.7	−0.5	−0.2

Allowing the ripple to increase in the lower levels of the shaped pattern region decreases the range of element amplitudes. The method converged in 11 iterations to the design given in Figure 4-24. All $2^4 = 16$ combinations of a_n placements inside and outside the unit circle were checked (Table 4-26). The amplitude variation ranged from 11.47 to 25.47 dB.

Figure 4-25 illustrates the design repeated with eight elements (Table 4-27). Although the sidelobes could be controlled at −30 dB, the shaped pattern region shows less pattern control than with 16 elements.

Extensions to the Orchard method make various improvements. By adding balancing zeros inside and outside the unit circle in the W-plane, the feeding coefficients of the array can be made real with only 0 or 180° phases [16]. This adds elements to the array and changes the shape of the beam somewhat. The coefficients are real only if the pattern is symmetrical about $\theta = 90°$. To implement the method you add a term

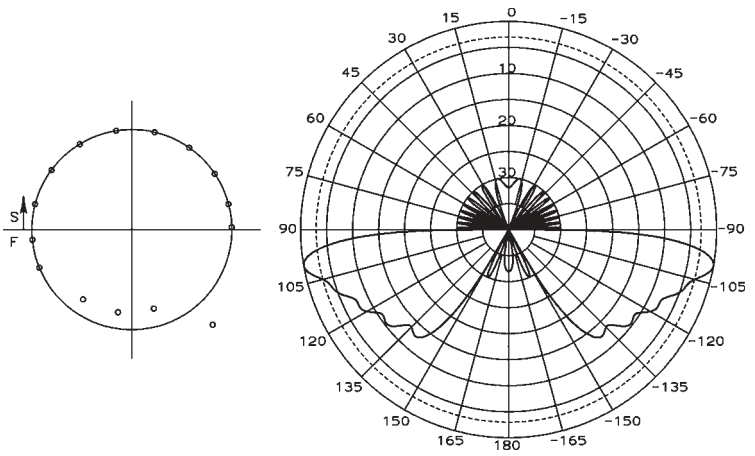

FIGURE 4-24 Sixteen-element array with $\csc^2\theta \cos\theta$ pattern designed by Orchard synthesis.

TABLE 4-26 Coefficients of 16-Element Array for $\csc^2\theta \cos\theta$ Beam of Figure 4-24 Designed by Orchard Synthesis

Element	Magnitude (dB)	Phase (deg)	Element	Magnitude (dB)	Phase (deg)
1	−11.47	−149.27	9	−1.19	149.09
2	−9.84	−100.16	10	−2.71	−177.54
3	−8.07	−69.72	11	−3.53	−131.64
4	−4.79	−40.25	12	−7.82	−52.50
5	−2.65	−0.56	13	−9.46	100.34
6	−2.04	34.20	14	−4.30	−157.29
7	−0.82	65.82	15	−4.55	−76.99
8	0.0	107.07	16	−8.72	0.0

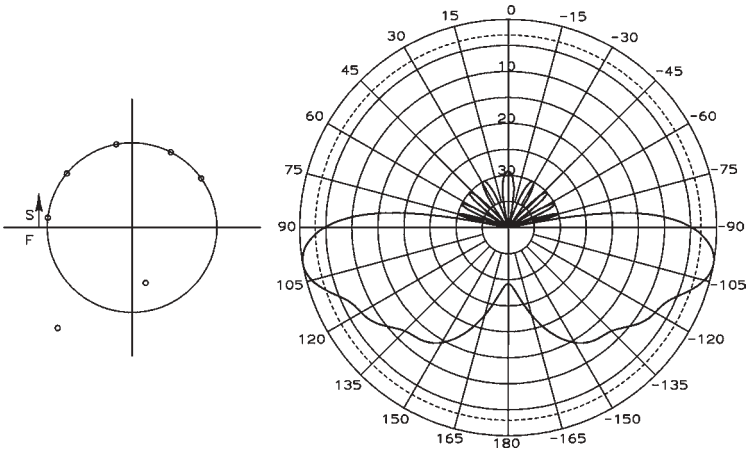

FIGURE 4-25 Eight-element array with $\csc^2\theta \cos\theta$ pattern designed by Orchard synthesis.

TABLE 4-27 Coefficients of Eight-Element Array for $\csc^2\theta \cos\theta$ Beam of Figure 4-24 Designed by Orchard Synthesis

Element	Magnitude (dB)	Phase (deg)	Element	Magnitude (dB)	Phase (deg)
1	−11.62	130.02	5	0.0	−122.98
2	−8.61	−170.78	6	−2.05	−79.05
3	−12.62	179.21	7	−5.73	−44.44
4	−2.61	−173.92	8	−11.54	0.00

to Eqs. (4-67) and (4-68) for the extra elements located off the unit circle. A design of a flat-topped beam centered at 90° using the balanced zeros produced a design with more than 30 dB of variation between the elements similar to a Fourier series expansion that had about the same range of amplitudes. The range of amplitudes in the array can be reduced by placing all the zeros off the unit circle [17, p. 124]. We give up the nulls between the lobes and must now search a large set of possible solutions to select a design with the least amplitude variation. A genetic algorithm sorts through the large set of zero combinations inside/outside all that satisfy the pattern requirements to discover the best design.

4-15 SERIES-FED ARRAY AND TRAVELING-WAVE FEED SYNTHESIS

A series-fed array uses couplers along a line that distribute power to the elements from a single transmission line. A single wave travels along the line with each element removing a portion of the power. A matched load absorbs the remaining power at the end to prevent the reflection of a wave traveling toward the source end. A second backward traveling wave would produce another beam with reduced amplitude indistinguishable from a sidelobe. The coupling could be a physical coupler or it could be just a series or shunt load across the transmission line. Waveguide slots are an example of loads on a transmission line. An array using couplers can have phase shifters between

the couplers and the elements to form a phased array. A second configuration for a phased array places phase shifters in the transmission line between the couplers. This case uses the simple control of identical phase shifters set to the same value to scan the beam. The phase shifters are the progressive phase δ along the array used for scanning.

The array distribution is given by the sequence of radiated powers, P_i. The traveling wave or nonresonant array dissipates a ratio of the input power R in the load:

$$\sum_{i=1}^{N} P_i = P_{\text{in}}(1 - R)$$

We normalize the distribution to the sum of radiated power: $P_0 = \sum_{i=1}^{N} P_i$. The element power becomes $P_i(1 - R)/P_0$ and we use the normalized power distribution to calculate coupling values:

$$C_1 = P_1 \qquad \text{remaining power} = 1 - P_1$$

The coupling to the second element removes power from the remaining power:

$$C_2 = \frac{P_2}{1 - P_1} \qquad \text{remaining power} = 1 - P_1 - P_2$$

The general expression is

$$C_i = \frac{P_i}{1 - \sum_{j=1}^{i-1} P_j} \tag{4-72}$$

If the element electrical model consists of a shunt conductance on a transmission line, such as waveguide slots, the power radiated by each slot $= |V_{\text{inc}}|^2 g_i$ and the normalized $g_i = C_i$. Similarly, an electrical model of an element as a series resistance on a transmission line can be solved in a similar manner. Power radiated $= |I_{\text{inc}}|^2 r_i$ and the normalized $r_i = C_i$.

Some array feeders have significant losses between the elements and we must account for these losses when designing the couplers. Suppose that the feeder has identical losses $L_f = 1 - 10^{-\text{attenuation}/10}$ between couplers. The power balance equation becomes

$$\underset{\text{total}}{P_{\text{in}}} = \underset{\text{load}}{RP_{\text{in}}} + \underset{\text{losses to load}}{(N-1)L_f R P_{\text{in}}} + \underset{\text{antennas}}{\sum_{i=1}^{N} P_i} + \underset{\text{losses to antennas}}{L_f \sum_{j=2}^{N} (j-1)P_j}$$

$$P_{\text{in}} = \frac{L_f \sum_{j=2}^{N} (j-1)P_j + \sum_{i=1}^{N} P_i}{1 - R - (N-1)L_f R}$$

As before, we must normalize the power at each element to the input power P_i/P_{in}. The coupling to the first element is $C_1 = P_1$ and the power left is $1 - P_1$. The transmission medium attenuates the signal between the first and second elements and we compute the power at the second element $= (1 - P_1)(1 - L_f)$. We determine the coupling value from the ratio

$$C_2 = \frac{P_2}{(1 - P_1)(1 - L_f)}$$

and the element removes P_2 power. The remaining power travels to the next element but is attenuated by $(1 - L_f)$. The power removed, P_2, is subtracted from the power at that point and the remaining power is attenuated before reaching the next extraction:

$$C_3 = \frac{P_3}{[(1 - P_1)(1 - L_f) - P_2](1 - L_f)}$$

$$C_4 = \frac{P_4}{\{[(1 - P_1)(1 - L_f) - P_2](1 - L_f) - P_3\}(1 - L_f)} \qquad \text{etc.}$$

The total loss due to attenuation is found from the sum of the normalized powers:

$$\text{loss(dB)} = 10 \log \left(\sum_{i=1}^{N} P_i \right)$$

Continuous Traveling Wave As the wave propagates along the antenna, it loses power continuously. The slots or holes must radiate more and more of the remaining power if the distribution is to be uniform. In general, the holes or slots must load the waveguide increasingly as the wave travels to the termination. The power at any point in the guide is

$$P(z) = P_0 \exp \left[-2 \int_0^z \alpha(z)\, dz \right] \tag{4-73}$$

where P_0 is the power at $z = 0$ and $\alpha(z)$ is the attenuation distribution (nepers/length). Suppose that we have a desired amplitude distribution, $A(z)$ (voltage):

$$P_{\text{in}} = \int_0^L |A(z)|^2\, dz + \int_0^L \rho_L(z)\, dz + P_{\text{load}} \tag{4-74}$$

where P_{load} is the power lost in the termination, $|A(z)|^2$ the radiated power distribution, and $\rho_L(z)$ the ohmic loss in the walls. Let the power into the termination be a ratio of the input power $P_{\text{load}} = RP_{\text{in}}$; then

$$P_{\text{in}} = \frac{1}{1 - R} \int_0^L \left[|A(z)|^2 + \rho_L(z) \right] dz \tag{4-75}$$

The power anywhere along the leaky wave antenna is

$$P(z) = P_{\text{in}} - \int_0^L |A(z)|^2 + \rho_L(z)\, dz \tag{4-76}$$

We differentiate this to get

$$\frac{dP(z)}{dz} = -[|A(z)|^2 + \rho_L(z)] \tag{4-77}$$

We differentiate Eq. (4-73) to relate $\alpha(z)$ to $P(z)$:

$$\frac{1}{P(z)} \frac{dP(z)}{dz} = -2\alpha(z) \tag{4-78}$$

We substitute Eq. (4-75) into Eq. (4-76) for P_{in}. By combining Eqs. (4-76) and (4-77) into Eq. (4-78), we derive the required attenuation distribution [18, p. 153]:

$$\alpha(z) = \frac{\frac{1}{2}|A(z)|^2}{[1/(1-R)]\displaystyle\int_0^L |A(z)|^2 + \rho_L(z)dz - \int_0^z |A(z)|^2 + \rho_L(z)dz} \tag{4-79}$$

If we assume a lossless transmission line, $\rho_L(z) = 0$ and Eq. (4-79) simplifies.

Example Design the attenuation distribution for a uniform distribution along a lossless transmission-line leaky wave antenna.

Substitute $A(z) = 1$ and $\rho_L(z) = 0$ into Eq. (4-79) and perform the integrations:

$$\alpha(z) = \frac{\frac{1}{2}}{[L/(1-R)] - z} = \frac{\frac{1}{2}(1-R)}{L[1 - z(1-R)/L]}$$

Given $R = 0.05$ (5% of the power into the load) for a structure with length 10λ. The initial and final attenuation constants are

$$\alpha_i(0) = \frac{0.95}{20} = 0.0475 \text{ Np}/\lambda \quad \text{or} \quad 0.413\,\text{dB}/\lambda$$

$$\alpha_f(L) = \frac{0.95}{2LR} = 0.95 \text{ Np}/\lambda \quad \text{or} \quad 8.25\,\text{dB}/\lambda$$

We reduce the variation between the initial and final values by dissipating more power in the termination. Given $R = 0.1$,

$$\alpha_i(0) = 0.045 \text{ Np}/\lambda \quad \text{or} \quad 0.39\,\text{dB}/\lambda$$

$$\alpha_f(L) = 0.45 \text{ Np}/\lambda \quad \text{or} \quad 3.9\,\text{dB}/\lambda$$

If we take the ratio of the attenuations at the ends, we have $\alpha(L)/\alpha(0) = 1/R$.

We can normalize Eq. (4-79) to the interval ± 2 and use the linear distributions given above where $x = z/L$ and $\rho_L(z) = 0$. Figure 4-26 shows the attenuation distribution for a Taylor distribution with 30-dB sidelobes and $\overline{n} = 8$ for various levels of power dissipation in the load. Table 4-28 lists the bounds on $\alpha(x)L$ for various Taylor distributions. Changing the number of modified zeros has only a minor effect on the bounds. A $\cos^2$ on a pedestal distribution with a 30-dB sidelobe level has very similar bounds on the attenuation. The 40-dB sidelobe level design requires a greater variation of attenuation than the 30-dB cases. Long structures may not be able to provide the low levels of radiation above the ohmic losses for an effective design. In all cases we decrease the attenuation range on an antenna by decreasing the antenna efficiency though absorbing more power in the termination.

4-16 CIRCULAR APERTURES

Many common apertures conform to circles. The two-dimensional Fourier transform relation for the pattern holds for any aperture rim shape and becomes for the circle

$$f(\theta, \phi) = \int_0^{2\pi} \int_0^a E(r', \phi') e^{jkr' \sin\theta \cos(\phi - \phi')} r'\, dr'\, d\phi' \tag{4-80}$$

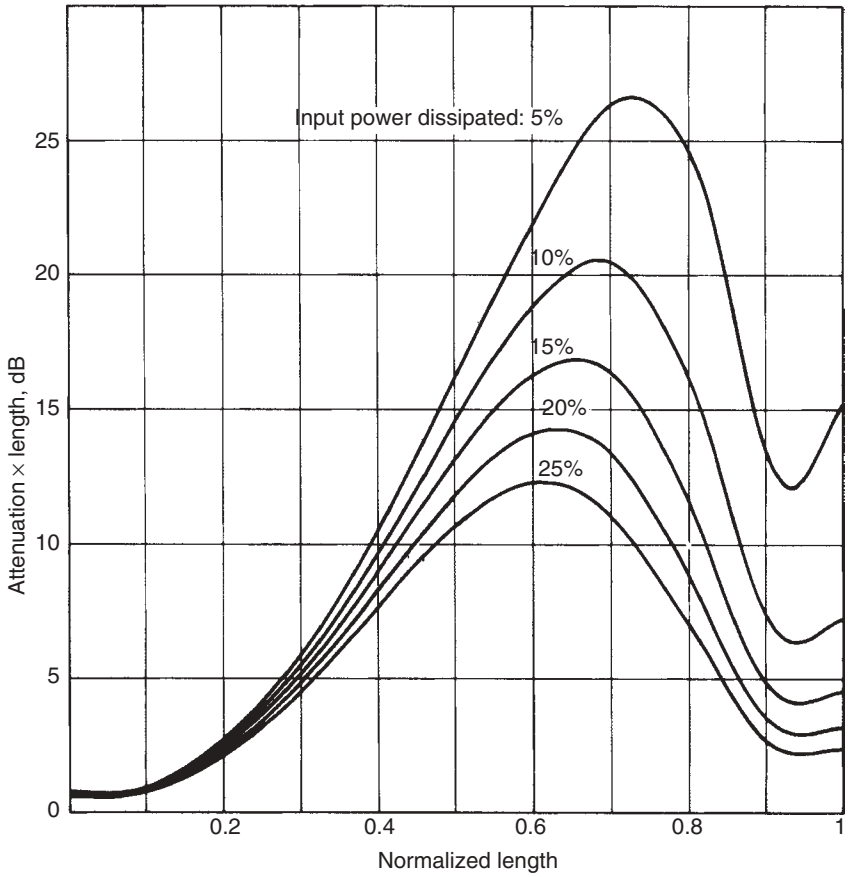

FIGURE 4-26 Leaky wave attenuation distribution for Taylor distribution with 30-dB sidelobes, $\overline{n} = 8$.

TABLE 4-28 Maximum and Minimum Normalized Attenuation $\alpha(z)L$ of a Leaky Wave Taylor Distribution

Termination Power (%)	30 dB				40 dB, $\overline{n} = 8$	
	$\overline{n} = 6$		$\overline{n} = 12$			
	Maximum	Minimum	Maximum	Minimum	Maximum	Minimum
5	27.08	0.59	26.04	0.63	31.61	0.12
6	25.38	0.58	24.54	0.63	29.63	0.12
8	22.70	0.57	22.06	0.61	26.52	0.12
10	20.66	0.56	20.08	0.60	24.12	0.11
12	19.00	0.55	18.46	0.59	22.18	0.11
15	17.00	0.53	16.52	0.57	19.81	0.11
20	14.42	0.50	14.04	0.53	16.78	0.10
25	12.42	0.46	12.09	0.50	14.44	0.10

where a is the radius, r' the radial coordinate, and ϕ' the angle coordinate of the aperture point. The integral leads to a k_r-space.

When the distribution has circular symmetry, the ϕ' integral can be evaluated easily, which reduces Eq. (4-80) to

$$f(k_r) = 2\pi \int_0^a E(r') J_0(kr' \sin\theta) r' \, dr' \tag{4-81}$$

where $J_0(x)$ is the zeroth-order Bessel function of the first kind. All great-circle patterns (constant ϕ) are identical. For a uniform distribution,

$$f(k_r) = \frac{2J_1(ka \sin\theta)}{ka \sin\theta}$$

plotted in Figure 4-27. The zeros occur at the zeros of $J_1(x)$. The 3-dB pattern point of the uniform distribution is

$$\begin{aligned} ka \sin\theta_1 &= 1.6162 \qquad \sin\theta_1 = 0.5145\frac{\lambda}{D} \\ \text{HPBW} &= 2\sin^{-1}\frac{0.5145\lambda}{D} \end{aligned} \tag{4-82}$$

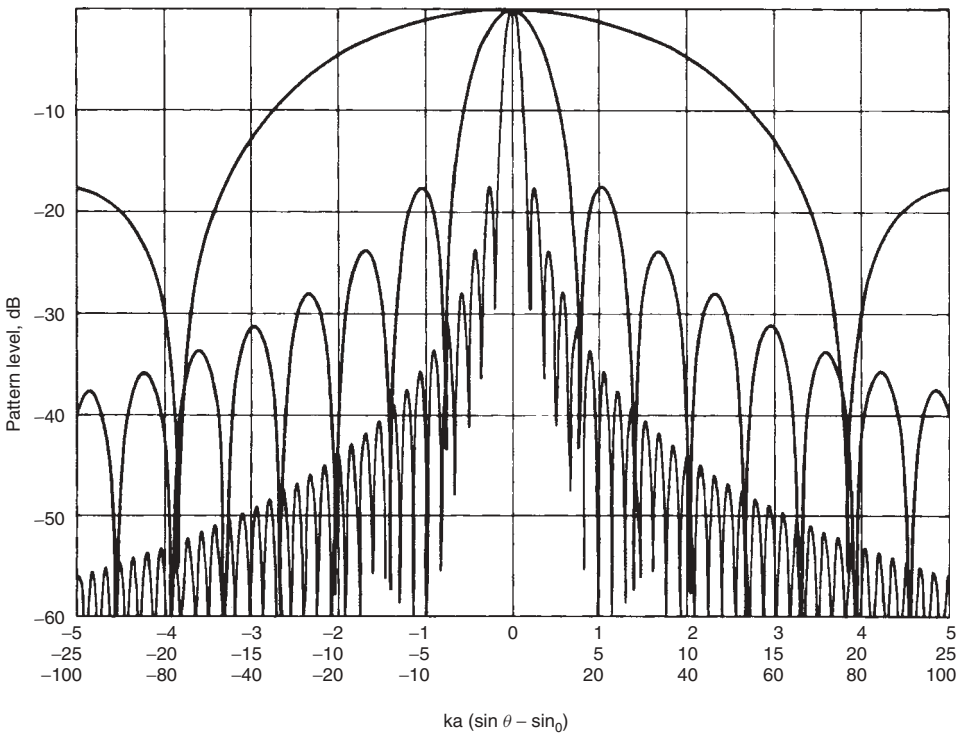

FIGURE 4-27 k_r-space pattern of uniform circular aperture distribution.

where D is the diameter. For large apertures we can approximate $\sin\theta$ by θ (rad). Converted to degrees, the half-power beamwidth becomes

$$\text{HPBW} = 58.95^\circ \frac{\lambda}{D} \tag{4-83}$$

Example Compute the beamwidth of a uniform distribution circular aperture with 10.5λ diameter.

The beamwidths are found from Eqs. (4-82) and (4-83):

$$\text{HPBW} = 2\sin^{-1}\frac{0.5145}{10.5} = 5.62^\circ$$

$$\text{HPBW} = \frac{58.95^\circ}{10.5} = 5.61^\circ$$

The first zero of $J_1(x)$ gives the k-space pattern null point.

$$\begin{aligned} ka\sin\theta_{\text{null}} &= 3.8317 \\ \text{BW}_{\text{null}} &= 2\sin^{-1}\frac{1.2197\lambda}{D} \simeq 139.76^\circ\frac{\lambda}{D} \end{aligned} \tag{4-84}$$

We can also define a null beamwidth factor and relate the beams of other distributions to the uniform circular distribution beamwidth [Eq. (4-84)]. All other circular distributions relate to Eq. (4-82) or (4-83) through a beamwidth factor. The uniform distribution has a unity beamwidth factor.

4-17 CIRCULAR GAUSSIAN DISTRIBUTION [19]

A truncated Gaussian distribution has a simple functional relation:

$$E(r) = e^{-\rho r^2} \qquad |r| \le 1 \tag{4-85}$$

We can easily calculate the edge taper through the conversion between logarithms:

$$\text{edge taper(dB)} = 8.686\rho \tag{4-86}$$

We determine amplitude taper efficiency by substituting Eq. (4-85) into Eq. (4-8) and carrying out the integrations:

$$\text{ATL} = \frac{2(1-e^{-\rho})^2}{\rho(1-e^{-2\rho})} \tag{4-87}$$

Table 4-29 lists designs for various sidelobe levels in terms of the single parameter: edge taper. Equation (4-86) relates the parameter ρ to the edge taper.

Example Estimate the beamwidth of the pattern radiated from a circular distribution with a 13-dB edge taper and radius of three wavelengths.

TABLE 4-29 Circular-Aperture Gaussian Distribution, $e^{-\rho r^2}$ ($|r| < 1$)

Sidelobe Level (dB)	Edge Taper (dB)	ATL (dB)	Beamwidth Factor
20	4.30	0.09	1.0466
22	7.18	0.24	1.0800
24	9.60	0.41	1.1109
25	10.67	0.50	1.1147
26	11.67	0.59	1.1385
28	13.42	0.76	1.1626
30	14.93	0.92	1.1839
32	16.23	1.06	1.2028
34	17.32	1.18	1.2188
35	17.81	1.23	1.2263
36	18.75	1.34	1.2405
38	21.43	1.65	1.2820
40	24.42	2.00	1.3296

We use linear interpolation in Table 4-29 to determine the beamwidth factor. From Eq. (4-82),

$$\text{HPBW} = 2\sin^{-1}\frac{1.1568(0.5145)}{6} = 11.38^\circ$$

From Eq. (4-83),

$$\text{HPBW} = 58.95^\circ\left(\frac{1.1568}{6}\right) = 11.36^\circ$$

The amplitude taper efficiency is calculated from Eq. (4-87):

$$\rho = \frac{13}{8.686} = 1.497$$

$$\text{ATL} = \frac{2(1-e^{-1.497})^2}{1.497(1-e^{-2.993})} = 0.847 \quad (-0.72\,\text{dB})$$

We obtain the same value by interpolating in Table 4-29.

Sidelobes below 40 dB are difficult to obtain with this distribution. The inner sidelobes continue to decrease with a decreasing edge level, but the outer lobes fail to reduce and dominate over the first few sidelobes. Table 4-29 results from a search because no direct method exists for computing the edge taper for a specified sidelobe level.

4-18 HANSEN SINGLE-PARAMETER CIRCULAR DISTRIBUTION [20, 21]

This distribution leads directly from sidelobe level to a single parameter H that relates through closed-form expressions to all other distribution parameters. The pattern of a uniform distribution is modified close in to the main beam. By using the U-space

variable of Taylor, we have $U = (2a/\lambda)\sin\theta$, where a is the radius. The pattern has different expressions in two regions:

$$f(U) = \begin{cases} \dfrac{2I_1(\pi\sqrt{H^2 - U^2})}{\pi\sqrt{H^2 - U^2}} & |U| \le H \qquad (4\text{-}88a) \\ \dfrac{2J_1(\pi\sqrt{U^2 - H^2})}{\pi\sqrt{U^2 - H^2}} & |U| \ge H \qquad (4\text{-}88b) \end{cases}$$

$I_1(x)$ is the first-order modified Bessel function of the first kind.

The high function value of Eq. (4-88a) at the boresight reduces the sidelobes of the uniform distribution [Eq. (4-88b)], 17.57 dB, below the level at $U = H$. The sidelobe level is

$$\text{SLR} = 17.57 + 20\log\frac{2I_1(\pi H)}{\pi H} \qquad (4\text{-}89)$$

Given the sidelobe level [positive (dB)], we use Eq. (4-89) in an iteration scheme to determine H.

The aperture distribution is given by

$$E(r) = I_0(\pi H\sqrt{1 - r^2}) \qquad |r| \le 1 \qquad (4\text{-}90)$$

where I_0 is the zeroth-order modified Bessel function of the first kind. Equation (4-8) can be integrated for this circularly symmetrical distribution [Eq. (4-90)] to derive the amplitude taper efficiency:

$$\text{ATL} = \frac{4I_1^2(\pi H)}{\pi^2 H^2[I_0^2(\pi H) - I_1^2(\pi H)]} \qquad (4\text{-}91)$$

Table 4-30 lists the parameters of the Hansen distribution for various sidelobe levels. At the top, Tables 4-29 and 4-30 are very similar. Any sidelobe level can be achieved with this distribution, subject to tolerance problems generated by any low-sidelobe design. The distribution is not optimum, but it is convenient.

4-19 TAYLOR CIRCULAR-APERTURE DISTRIBUTION [22]

Similar to the line source, the Taylor circular-aperture distribution modifies inner zeros of the uniform amplitude and phase circular-aperture k-space pattern to approximate the Dolph–Chebyshev distribution. By use of the variable $\pi U = ka\sin\theta$ the uniform distribution pattern is found to be $J_1(\pi U)/\pi U$. We remove $\overline{n} - 1$ inner zeros and add those of the Dolph–Chebyshev distribution:

$$f(U) = \frac{J_1(\pi U)\prod_{N=1}^{\overline{n}-1}(1 - U^2/U_N^2)}{\pi U\prod_{N=1}^{\overline{n}-1}(1 - U^2/S_N^2)} \qquad (4\text{-}92)$$

TABLE 4-30 Hansen Single-Parameter Circular-Aperture Distribution

Sidelobe Level (dB)	H	Edge Taper (dB)	ATL (dB)	Beamwidth Factor
20	0.48717	4.49	0.09	1.0484
22	0.66971	7.79	0.27	1.0865
24	0.82091	10.87	0.48	1.1231
25	0.88989	12.35	0.60	1.1409
26	0.95573	13.79	0.72	1.1584
28	1.08027	16.59	0.96	1.1924
30	1.19770	19.29	1.19	1.2252
32	1.30988	21.93	1.42	1.2570
34	1.41802	24.51	1.64	1.2876
35	1.47084	25.78	1.75	1.3026
36	1.52295	27.04	1.85	1.3174
38	1.62525	29.53	2.05	1.3462
40	1.72536	31.98	2.24	1.3742
45	1.96809	38.00	2.68	1.4410
50	2.20262	43.89	3.08	1.5039

Given a zero of $J_1(x)$, $J_1(x_{1N}) = 0$, let $x_{1N} = \pi S_N$. By retaining approximately the same number of zeros in the visible region as in the uniform distribution, we avoid superdirectivity. The new zeros U_N are modified zeros of the uniform distribution:

$$U_N = S_{\overline{n}} \frac{\sqrt{A^2 + (N - \frac{1}{2})^2}}{\sqrt{A^2 + (\overline{n} - \frac{1}{2})^2}} \tag{4-93}$$

where A relates to the maximum sidelobe level, $\cosh \pi A = b$ and $20 \log b =$ sidelobe level(dB). Equation (4-93) is the same as Eq. (4-20) except for the scaling constant $S_{\overline{n}}$, the $\overline{n}$th zero of $J_1(x)$ divided by π.

Equation (4-92) gives the U-space pattern of the new distribution. We expand the aperture distribution in a Fourier–Bessel series:

$$E(r) = \sum_{m=0}^{\overline{n}-1} B_m J_0(\pi S_m r) \qquad r \leq 1 \tag{4-94}$$

We compute coefficients B_m by transforming the Fourier–Bessel series [Eq. (4-94)] into U-space and comparing the far-field pattern with Eq. (4-92). As indicated in Eq. (4-94), the series contains only $\overline{n}$ nonzero terms:

$$\begin{aligned} B_0 &= 1 \\ B_m &= \frac{-\prod_{N=1}^{\overline{n}-1} (1 - S_m^2/U_N^2)}{J_0(\pi S_m) \prod_{N=1, N\neq m}^{\overline{n}-1} (1 - S_m^2/S_N^2)} \qquad m = 1, 2, \ldots, \overline{n} - 1 \end{aligned} \tag{4-95}$$

Example Design a Taylor circular-aperture distribution with 30 dB maximum sidelobes and $\overline{n} = 6$.

We use Eq. (4-21) to calculate the constant A:

$$b = 10^{30/20} = 31.6228$$
$$A = \frac{\cosh^{-1} b}{\pi} = 1.32$$

We substitute this value into Eq. (4-93) to compute the five nulls:

No.	1	2	3	4	5
Null U_N	1.5582	2.2057	3.1208	4.1293	5.1769

The first null of the uniform distribution occurs at

$$x_{11} = 3.83171 \qquad S_1 = \frac{x_{11}}{\pi} = 1.2197$$

We use this with the location of the first zero to determine the null beamwidth factor:

$$\text{BW}_{\text{null}} = \frac{U_1}{S_1} = \frac{1.5582}{1.2197} = 1.2775$$

The coefficients of the Fourier series [Eq. (4-95)] are given in Table 4-31. Figure 4-28 contains the k-space pattern.

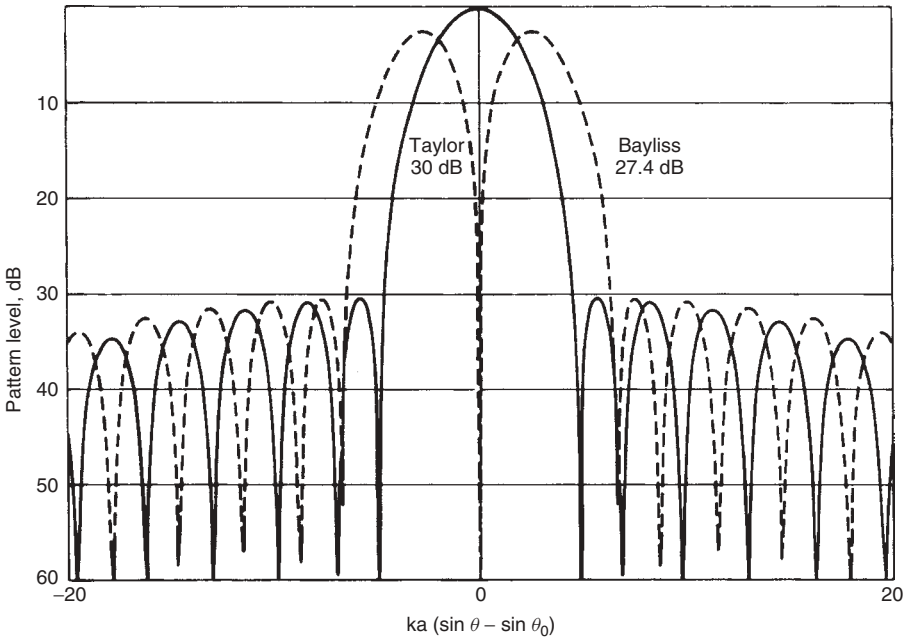

FIGURE 4-28 Taylor and Bayliss circular aperture distributions to give 30-dB sidelobes ($\overline{n} = 6$).

Tables 4-32 to 4-34 list the characteristics for a few designs of the circular Taylor distribution. Table 4-32 shows that for each sidelobe level there is an optimum $\overline{n}$. As the sidelobes are lowered, the optimum value of $\overline{n}$ increases. The blanks are unsuitable designs. The beamwidth factor (Table 4-33) and the null beamwidth factor (Table 4-34) continue to decrease as $\overline{n}$ increases at a given sidelobe level. In all three tables the values depend primarily on the sidelobe level.

TABLE 4-31 Fourier–Bessel Series Coefficients for Taylor Distribution: 30 dB, $\overline{n} = 6$

No.	B_m	B_m Normalized	Function
0	1.0000	0.53405	1
1	0.93326	0.49841	$J_0(x_{11}r)$
2	0.038467	0.01808	$J_0(x_{12}r)$
3	−0.16048	−0.08570	$J_0(x_{13}r)$
4	0.16917	0.09035	$J_0(x_{14}r)$
5	−0.10331	−0.05517	$J_0(x_{15}r)$

TABLE 4-32 Amplitude Taper Losses of Taylor Circular-Aperture Distribution (dB)

	Sidelobe Level (dB)					
$\overline{n}$	25	30	35	40	45	50
4	0.30	0.71	1.14	1.51	1.84	
6	0.28	0.59	1.03	1.48	1.88	2.23
8	0.43	0.54	0.94	1.40	1.82	2.21
12	1.03	0.62	0.86	1.28	1.71	2.12
16	1.85	0.86	0.87	1.22	1.64	2.05
20		1.20	0.94	1.20	1.60	2.01

TABLE 4-33 Beamwidth Factor of Taylor Circular-Aperture Distribution

	Sidelobe Level (dB)					
$\overline{n}$	25	30	35	40	45	50
4	1.0825	1.1515	1.2115	1.2638	1.3095	
6	1.0504	1.1267	1.1957	1.2581	1.3149	1.3666
8	1.0295	1.1079	1.1796	1.2457	1.3067	1.3632
12	1.0057	1.0847	1.1580	1.2262	1.2899	1.3499
16	0.9927	1.0717	1.1451	1.2137	1.2782	1.3391
20		1.0634	1.1367	1.2054	1.2701	1.3314

TABLE 4-34 Null Beamwidth Factor of Taylor Circular-Aperture Distribution

	Sidelobe Level (dB)					
$\overline{n}$	25	30	35	40	45	50
4	1.1733	1.3121	1.4462	1.5744	1.6960	
6	1.1318	1.2775	1.4224	1.5654	1.7056	1.8426
8	1.1066	1.2530	1.4001	1.5470	1.6928	1.8370
12	1.0789	1.2244	1.3716	1.5197	1.6680	1.8162
16	1.0643	1.2087	1.3552	1.5029	1.6514	1.8003
20		1.1989	1.3442	1.4920	1.6402	1.7890

4-20 BAYLISS CIRCULAR-APERTURE DISTRIBUTION [8]

We can also design a Bayliss distribution (difference pattern) for circular apertures. This gives us the pattern necessary for monopulse tracking along one axis. The U-space pattern has modified zeros to produce nearly equal sidelobes close in to the main lobes:

$$f(U,\phi) = \cos\phi\,\pi U J_1'(\pi U)\frac{\prod_{N=1}^{\overline{n}-1}(1-U^2/U_N^2)}{\prod_{N=0}^{\overline{n}-1}(1-U^2/\mu_N^2)} \tag{4-96}$$

where U_N are the new zeros and $\pi\mu_N$ are zeros of $J_1'(\pi U)$. Bayliss lists those zeros μ_N (Table 4-35). The inner zeros have been removed and replaced by new ones, U_N. We compute the zeros in a manner similar to that used for a linear distribution (Section 4-7):

$$U_N = \begin{cases} \mu_{\overline{n}}\sqrt{\dfrac{\xi_N^2}{A^2+\overline{n}^2}} & N = 1,2,3,4 \\ \mu_{\overline{n}}\sqrt{\dfrac{A^2+N^2}{A^2+\overline{n}^2}} & N = 5,6,\ldots,\overline{n}-1 \end{cases} \tag{4-97}$$

The four inner zeros had to be adjusted to achieve the desired sidelobe level. Bayliss found these through a computer search. The values for ξ_N and A can be found through the polynomial approximations [Eq. (4-40)].

TABLE 4-35 Bessel Function Zeros, $J_1'(\pi\mu_N)$

N	μ_N	N	μ_N	N	μ_N	N	μ_N
0	0.5860670	5	5.7345205	10	10.7417435	15	15.7443679
1	1.6970509	6	6.7368281	11	11.7424475	16	16.7447044
2	2.7171939	7	7.7385356	12	12.7430408	17	17.7450030
3	3.7261370	8	8.7398505	13	13.7435477	18	18.7452697
4	4.7312271	9	9.7408945	14	14.7439856	19	19.7455093

Like the Taylor circular aperture distribution, the aperture distribution is expanded in a finite-length Fourier–Bessel series:

$$E(r,\phi) = \cos\phi' \sum_{m=0}^{\overline{n}-1} B_m J_1(\pi\mu_m r) \qquad r \le 1 \tag{4-98}$$

where the coefficients are found by transforming Eq. (4-98) and comparing it with a U-space pattern [Eq. (4-96)]. The coefficients are given by

$$B_m = \frac{\mu_m^2}{j J_1(\pi\mu_m)} \frac{\prod_{N=1}^{\overline{n}-1}(1-\mu_m^2/U_N^2)}{\prod_{N=0,N\neq m}^{\overline{n}-1}(1-\mu_m^2/\mu_N^2)} \tag{4-99}$$

Example Design a Bayliss circular-aperture distribution with 30-dB sidelobes and $\overline{n} = 6$.

We start with Eq. (4-40) to compute coefficients A and ξ_N:

$$A = 1.64126 \qquad \xi_1 = 2.07086 \qquad \xi_2 = 2.62754 \qquad \xi_3 = 3.43144 \qquad \xi_4 = 4.32758$$

We substitute these constants into Eq. (4-97) along with the zeros from Table 4-35 to calculate the modified zeros:

N	1	2	3	4	5
U_N	2.2428	2.8457	3.7163	4.6868	5.6994

We use the zeros in Eq. (4-96) to calculate the pattern. The U-space pattern peak can be found by using Eq. (4-41):

$$U_{\max} = 0.7988 \qquad ka\sin\theta_{\max} = \pi U_{\max} = 2.5096$$

where a is the aperture radius. The coefficients of the Fourier–Bessel series are found from Eq. (4-99) (Table 4-36). The normalized coefficients give an aperture distribution peak of 1. The 3-dB pattern points can be found by searching the pattern:

$$ka\sin\theta_1 = 1.3138 \qquad ka\sin\theta_2 = 4.2384$$

TABLE 4-36 Fourier–Bessel Series Coefficients for Bayliss Distribution: 30 dB, $\overline{n} = 6$

No.	B_m	B_m Normalized	Function
0	0.62680	1.2580	$J_1(\pi\mu_0 r)$
1	0.50605	1.0157	$J_1(\pi\mu_1 r)$
2	−0.06854	−0.03415	$J_1(\pi\mu_2 r)$
3	−0.0028703	−0.005761	$J_1(\pi\mu_3 r)$
4	0.014004	0.028106	$J_1(\pi\mu_4 r)$
5	−0.011509	−0.02310	$J_1(\pi\mu_5 r)$

TABLE 4-37 Characteristics of a Bayliss Circular-Aperture Distribution, $\overline{n} = 10$

Sidelobe Level (dB)	Beam Peak, $ka/2 \sin \theta_{\max}$	3-dB Beam Edge		ATL (dB)	PEL (dB)
		$ka/2 \sin \theta_1$	$ka/2 \sin \theta_2$		
20	2.2366	1.165	3.700	1.47	1.80
25	2.3780	1.230	3.940	1.15	1.89
30	2.5096	1.290	4.160	1.32	1.96
35	2.6341	1.346	4.363	1.62	2.01
40	2.7536	1.399	4.551	1.95	2.05

Figure 4-28 contains a plot of a Bayliss circular-aperture distribution ($\overline{n} = 6$) designed to have sidelobes 30 dB below those of the Taylor distribution with 30-dB sidelobes. The losses to the difference pattern are about 2.6 dB higher than the sum pattern. The amplitude taper efficiency is calculated from

$$ATL = \frac{\left[\int_0^1 4 \left| \sum_{m=0}^{\overline{n}-1} B_m J_1(\pi \mu_m r) \right| r \, dr \right]^2}{\pi^2 \int_0^1 4 \left| \sum_{m=0}^{\overline{n}-1} B_m J_1(\pi \mu_m r) \right|^2 r \, dr} \tag{4-100}$$

where the integrals over ϕ' have been separated and evaluated. An integral expression for the phase error efficiency can be found similarly by evaluating the separable $\cos \phi'$ integrals along the coordinate $\phi = 0$, the peak:

$$\text{PEL}(U) = \frac{\left| 2\pi \int_0^1 \sum_{m=0}^{\overline{n}-1} B_m J_1(\pi \mu_m r) J_1(\pi U r) r \, dr \right|^2}{\left[\int_0^1 4 \left| \sum_{m=0}^{\overline{n}-1} B_m J_1(\pi \mu_m r) \right| r \, dr \right]^2} \tag{4-101}$$

Table 4-37 lists the parameters of Bayliss circular-aperture distributions with $\overline{n} = 10$ and various sidelobe levels. The optimum design for $\overline{n} = 10$ occurs for 25-dB sidelobes.

4-21 PLANAR ARRAYS

We design planar arrays with nearly circular boundaries by sampling circular distributions. Given enough sample points in the array, a distribution such as the circular Taylor will be modeled adequately to produce a similar pattern. We can use pattern multiplication to combine the designs for linear arrays into a planar array, but in the special case of a square array, a true Chebyshev design can be obtained in all planes. A technique has been developed to allow the synthesis from pattern nulls provided that some of the possible nulls are not specified. We are still left with the problem of specifying the numerous nulls possible with a planar array.

Chebyshev Array [23] When we combine two Dolph–Chebyshev linear arrays through pattern multiplication, it produces a pattern that has lower sidelobes than

those specified in all planes except the principal ones along the axes. These designs give beamwidths in the diagonal planes that are wider than necessary. The pattern deviates from the optimum because sidelobes are suppressed more than necessary.

We use a technique on a square array to produce equal sidelobes in all constant ϕ cuts around the array. The array is square in the number of elements, but different spacings along the axes can produce a rectangular array. We expand the pattern in a single Chebyshev polynomial:

$$T_{L-1}(x_0 \cos \psi_1 \cos \psi_2) \tag{4-102}$$

where $\psi_1 = kd_x \cos\theta \cos\phi + \delta_1$ and $\psi_2 = kd_y \cos\theta \sin\phi + \delta_2 L = 2N$ or $L = 2N + 1$ for L^2 elements in the array. We compute x_0 from Eq. (4-51) for a given sidelobe level. The pattern for an odd number of elements in each row and column is

$$E(\theta, \phi) = \sum_{m=1}^{N+1} \sum_{n=1}^{N+1} \varepsilon_m \varepsilon_n I_{mn} \cos 2(m-1)\psi_1 \cos 2(n-1)\psi_2 \qquad L = 2n + 1$$

where $\varepsilon_m = 1$ for $m = 1$ and $\varepsilon_m = 2$ for $m \neq 1$. Similarly,

$$E(\theta, \phi) = 4 \sum_{m=1}^{N} \sum_{n=1}^{N} I_{mn} \cos(2m-1)\psi_1 \cos(2n-1)\psi_2 \qquad L = 2n$$

The element excitations I_{mn} are given by

$$I_{mn} = \left(\frac{2}{L}\right)^2 \sum_{p=1}^{N+1} \sum_{q=1}^{N+1} \varepsilon_p \varepsilon_q T_{L-1}\left[x_0 \cos\frac{(p-1)\pi}{L} \cos\frac{(q-1)\pi}{L}\right] \times \cos\frac{2\pi(m-1)(p-1)}{L} \cos\frac{2\pi(n-1)(q-1)}{L} \qquad L = 2N+1 \tag{4-103}$$

or

$$I_{mn} = \left(\frac{4}{L}\right)^2 \sum_{p=1}^{N} \sum_{q=1}^{N} T_{L-1}\left[x_0 \cos\frac{\left(p-\frac{1}{2}\right)\pi}{L} \cos\frac{\left(q-\frac{1}{2}\right)\pi}{L}\right] \times \cos\frac{2\pi\left(m-\frac{1}{2}\right)\left(p-\frac{1}{2}\right)}{L} \cos\frac{2\pi\left(n-\frac{1}{2}\right)\left(q-\frac{1}{2}\right)}{L} \qquad L = 2N \tag{4-104}$$

4-22 CONVOLUTION TECHNIQUE FOR PLANAR ARRAYS

We may synthesize a desired pattern through multiplication of two or more simpler patterns. Because patterns derive from Fourier transforms of distributions in space, the distribution to produce the product of two simpler patterns is the convolution of the

simpler distributions [24, p. 30]. We find it easier to synthesize by using a few elements and then build up patterns through multiplication.

Consider the convolution of a linear array with another linear array on the same axis. We describe the array as a distribution consisting of weighted impulse functions, $\delta(x - x_i)$:

$$A_1(x) = \sum_{i=1}^{N_1} a_{1i}\delta(x - x_i)$$

where a_{1i} are the feeding coefficients and x_i are the locations for an N_1-element array. To determine the array that gives the product of two array patterns, we convolve the second array, $A_2(x)$, with the first:

$$A_1(x) * A_2(x) = \int A_1(\tau)A_2(x - \tau)\, d\tau \tag{4-105}$$

We evaluate a function at the argument of the impulse function when we convolve the two arrays [25, p. 237]. Equation (4-105) reduces to

$$A_1(x) * A_2(x) = \sum_{i=1}^{N_1}\sum_{j=1}^{N_2} a_{1i}a_{2i}\delta(x - x_i - x_j) \tag{4-106}$$

Example Consider the two 2-element arrays in Figure 4-29 and the graphical solution of the convolution. Figure 4-29*a* shows the location of the elements in the arrays on the x-axis. To perform the convolution, we reflect the x-axis of one array and move it across the other array while performing the integral at each location x, the coordinate of the convolution. We have a net result to the integral only when two impulse functions are aligned, $x = x_i + x_j$. We have four elements in the resulting array (Figure 4-29*c*). If the elements are equally spaced in the two arrays, two elements will sum into one.

Patterns are the result of a three-dimensional Fourier transform. For a general array with element locations $\mathbf{r}_i$, we must perform a convolution along all three axes to find the distribution that gives the product of the patterns of two simpler distributions. For the general array, Eq. (4-106) becomes

$$A_1(\mathbf{r}) * A_2(\mathbf{r}) = \sum\sum a_{1i}a_{2j}\delta(\mathbf{r} - \mathbf{r}_i - \mathbf{r}_j) \tag{4-107}$$

where $\mathbf{r}$ is the location vector and $\mathbf{r}_i$ and $\mathbf{r}_j$ are the locations of elements in the two arrays.

A rectangular array can be described as the convolution of a linear array on the x-axis with a linear array on the y-axis. When $y = y_j$ there is a string of values $x = x_i$ that satisfy the impulse argument [Eq. (4-107)]. These are the locations of the elements. We step through all values of y_j until the entire array is formed. Equation (4-107) gives the feeding coefficient of each element $a_{1i}a_{2j}$ since no two elements of the convolution are in the same place. The pattern of the rectangular array is the product of the linear array patterns along the axes.

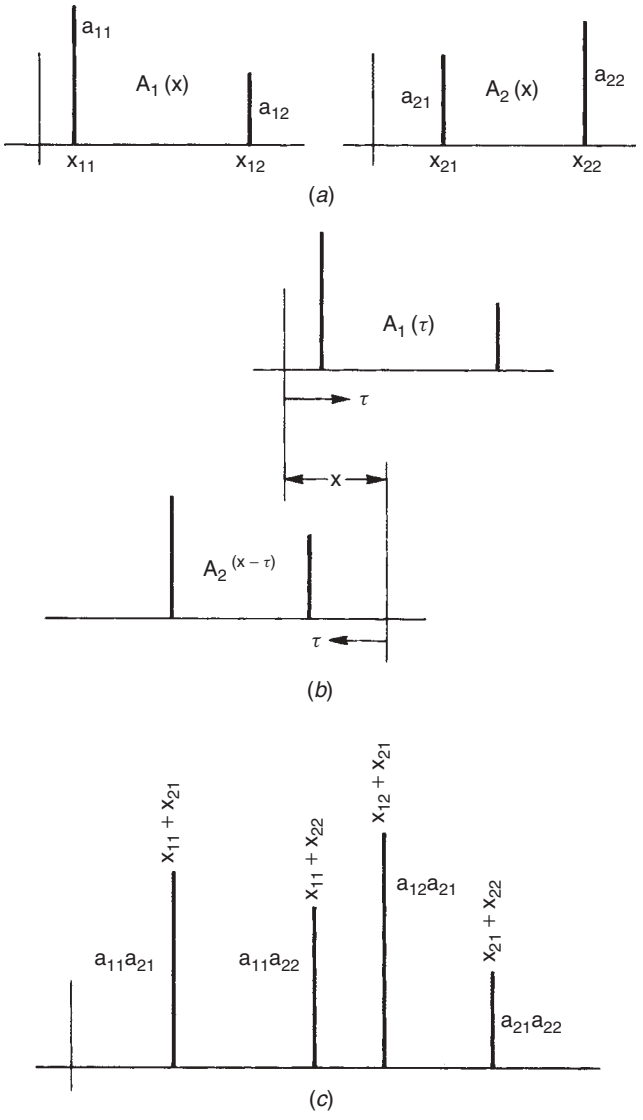

FIGURE 4-29 Convolution of two linear arrays: (*a*) separate arrays; (*b*) graphical convolution; (*c*) convolution.

Given an array, we compute the pattern from a Fourier transform containing N terms each of which corresponds to one element. Ignoring the element pattern, we have

$$E = \sum_{i=1}^{N} a_i e^{j\mathbf{k}\cdot\mathbf{r}_i'} \tag{4-108}$$

The array has $N - 1$ independent nulls (zeros) in the pattern. Given the set of nulls $\mathbf{k}_j$ we can substitute them into Eq. (4-108) to form a matrix equation in $N - 1$ unknowns a_i. We must normalize one coefficient, $a_i = 1$, to solve the set of equations for the

feeding coefficients:

$$[B]\begin{bmatrix} a_2 \\ a_3 \\ \vdots \\ a_N \end{bmatrix} = -\begin{bmatrix} e^{j\mathbf{k}_1\cdot\mathbf{r}_1} \\ e^{j\mathbf{k}_2\cdot\mathbf{r}_1} \\ \vdots \\ e^{j\mathbf{k}_{N-1}\cdot\mathbf{r}_1} \end{bmatrix} \tag{4-109}$$

where $b_{ij} = e^{j\mathbf{k}_i\cdot\mathbf{r}_{j+1}}$. We find the direct solution of Eq. (4-109) unwieldy for a large array. We can subdivide the array into smaller arrays whose convolution is the total array and use pattern multiplication. We reduce the number of nulls we need to specify in the synthesis of an array.

Convolution can be used in the synthesis of planar arrays by using a rhombic array (four elements) as the basic building block [26] (Figure 4-30). If we convolve two identically shaped rhombic arrays, we obtain a nine-element (three on a side) array (Figure 4-30*b*). By continuing to convolve the resulting array with other rhombic arrays, we can build up a large array in the shape of the rhombus. Each rhombic array has three pattern nulls without the symmetry of the linear array about some axis. The rhombic array has symmetry only about the plane of the rhombus. We build up an array of $N + 1$ by $N + 1$ elements through the convolution of N rhombic arrays. The original array has $(N + 1)(N + 1) - 1$ independent nulls. The convolution of N rhombic arrays reduces the number of independent nulls to $3N$. Similarly, when we use the convolution of two linear arrays to form a square array, $N + 1$ by $N + 1$, the number of independent nulls is $2N$, or N for each array.

We denote a single rhombic array as RA_1 and the convolution of two rhombic arrays as RA_2. The number of elements on each side of an RA_N array is $N + 1$. We can convolute a rhombic array with a linear array to form an $M \times N$ array ($M > N$). Denote the linear array by L_N, where the array has $N + 1$ elements. The planar array $PA_{M,N}$ becomes

$$PA_{M,N} = L_{M-N} * RA_{N-1} \tag{4-110}$$

We specify $3(N - 1)$ nulls in space for the rhombic arrays and $M - N$ nulls about the axis of the array. Like all convolutions, the pattern is the product of the individual array patterns.

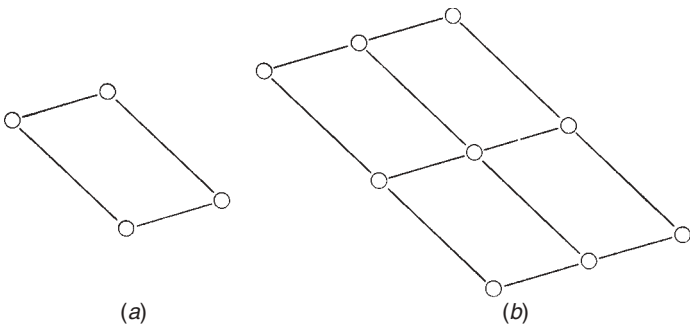

FIGURE 4-30 Rhombic array with its convolution: (*a*) rhombic array RA_1; (*b*) convolution of two rhombic arrays RA_2.

This method allows the specification of nulls in space with other than linear symmetry. Second, it reduces the required specification of nulls. Third, it provides a method for synthesis of triangularly or hexagonally spaced elements.

Example Consider the six-element rectangular array shown in Figure 4-31*a*. It can be broken down into the convolution of a four-element rectangular array (rhombic) and a two-element linear array from Eq. (4-110):

$$PA_{3,2} = L_1 * RA_1$$

Pick the three nulls of the rhombic array at

θ	90°	90°	90°
ϕ	110°	-60°	180°

We measure the pattern nulls from the normal of the plane containing the rhombus and the x-axis (ϕ). For an array of broadcast towers, the nulls point toward the horizon. We restrict θ to less than or equal to 90°. We substitute the positions of the elements (Figure 4-31*b*) and the nulls into Eq. (4-109) to solve for the feeding coefficients of the rhombic array (Table 4-38).

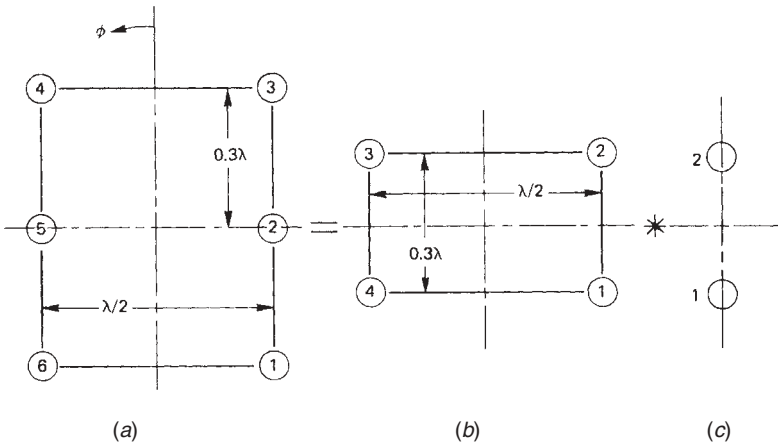

FIGURE 4-31 Rectangular array from convolution of rhombic and linear arrays: (*a*) six-element rectangular array; (*b*) rhombic array; (*c*) linear array.

TABLE 4-38 Coefficients of Rhombic Array for Horizon ($\theta = 90^\circ$) Nulls at $\phi = 100^\circ, -60^\circ$, and 180°

Element	Amplitude (dB)	Phase (deg)
1	0.00	0.0
2	4.12	−79.2
3	0.00	−109.2
4	4.12	−30.2

TABLE 4-39 Coefficients of Six-Element Rectangular Array with Pattern of Figure 4-32*b*

Element	Amplitude (dB)	Phase (deg)
1	0.00	0.0
2	8.13	−88.5
3	4.12	177.2
4	0.00	147.2
5	8.13	−124.3
6	4.12	−30.1

We pick the single null of the two-element array at 135°. This null has symmetry about the axis of the array. With the first element at zero phase, we pick the element phase to cancel the first element voltage when $\theta = 135°$:

$$\text{phase} = 180° - 360°(0.3)\cos 135° = 256.37°$$

When we convolute the two arrays, we obtain the feeding coefficients from Eq. (4-107) (Table 4-39). The elements in the center that result from two convolutions have summed feeding coefficients producing a six-element array. Figure 4-32 shows the patterns of the convolution. We obtain the six-element array pattern (Figure 4-32*b*) by multiplication of the patterns of the individual subarrays (Figure 4-32*a*).

4-23 APERTURE BLOCKAGE

Blocking an aperture reduces the gain and raises the sidelobes. The blockage either scatters the aperture power in unwanted directions in a broad pattern or is just an area without fields. Scattered blockage causes higher sidelobes and greater loss than the

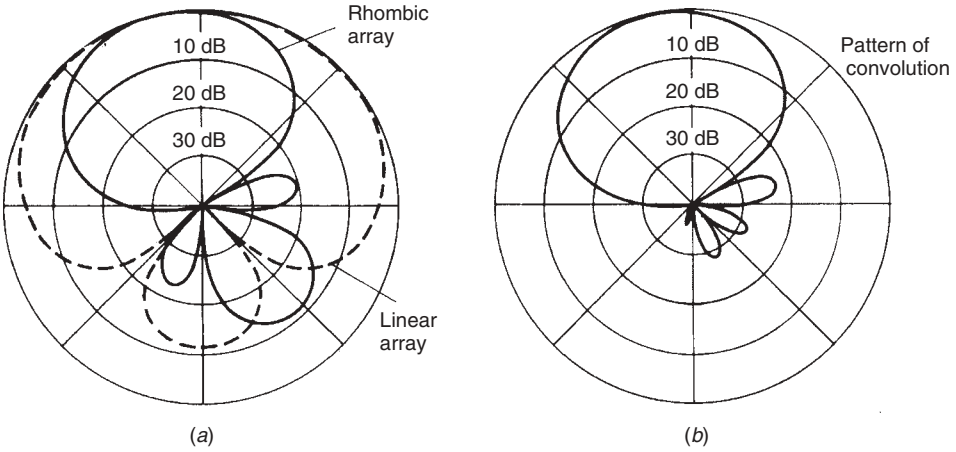

FIGURE 4-32 Patterns of the convolution of a rhombic and a linear array to form the six-element rectangular array of Figure 4-31.

nonexcitation blockage. Scattered blockage has the same power input as the unblocked aperture, but fields scattered off the blockage do not contribute significantly to the maximum field. Compared to the unblocked aperture, the blockage efficiency becomes

$$\text{blockage efficiency} = \frac{\left| \iint_{\text{blocked}} E e^{j\mathbf{k}\cdot\mathbf{r}'} \, ds' \right|^2_{\max}}{\left| \iint_{\text{unblocked}} E e^{j\mathbf{k}\cdot\mathbf{r}'} \, ds' \right|^2_{\max}} \qquad \text{scattered} \tag{4-111}$$

We use Eq. (2-16) to compute the directivity of each distribution by using the total power radiated from the unblocked aperture [denominator of Eq. (2-16)] for the blocked aperture. A centrally blocked circular aperture with a uniform distribution has the blockage efficiency $(1 - b^2)^2$ (scattered), where b is the normalized blockage radius. The blockage of a circular Gaussian distribution has a simple blockage function:

$$\text{blockage efficiency} = \left(\frac{e^{-\rho b} - e^{-\rho}}{1 - e^{-\rho}} \right)^2$$

The second type of blockage is an area without fields. The blockage does not waste power in the aperture. When we take the ratio of the two directivities, we must account for the power in each aperture:

$$\text{blockage efficiency} = \frac{\left| \iint_{\text{blocked}} E e^{j\mathbf{k}\cdot\mathbf{r}'} \, ds' \right|^2_{\max} \iint_{\text{unblocked}} |E|^2 \, ds'}{\left| \iint_{\text{unblocked}} E e^{j\mathbf{k}\cdot\mathbf{r}'} \, ds' \right|^2_{\max} \iint_{\text{blocked}} |E|^2 \, ds'} \qquad \text{nonexcitation} \tag{4-112}$$

The blockage of a uniformly excited centrally blocked circular aperture where the center is not excited reduces the directivity only by the area lost from the aperture, $1 - b^2$ (nonexcitation). In a sense, nonexcitation blockage is not a true loss; it is a loss of potential radiation aperture.

Table 4-40 lists the blockage losses of centrally blocked circular apertures calculated by Eq. (4-111), the more severe case. The uniformly excited aperture is affected least by blockage. All points are equally important. The tapered distributions suffer more loss with increased taper toward the edge. The lists for different tapered distributions track each other fairly closely, and any one of them gives a good estimate of the blockage loss. Blockage causes sidelobes. In the case of scattered blockage the exact sidelobes cannot be found without an analysis of the scatterer. A Cassegrain reflector would need a geometric theory of diffraction (GTD) analysis to locate the directions of scattering from the subreflector. We can handle the nonexcitation blockage in a general fashion. Consider the aperture to be broken into two radiating apertures. The first is the unblocked aperture; the second is the blockage. If we take the blockage aperture to be 180° out of phase with respect to the unblocked aperture distribution, the sum gives us the blocked distribution.

We use this analysis as an approximation to scattered blockage with the realization that scattering may produce unpredicted lobes.

TABLE 4-40 Blockage Losses of Circular-Aperture Distributions (dB)

Central Blockage (%)	Uniform	Gaussian 12-dB Edge	Taylor 30 dB, $\overline{n} = 6$	Taylor 40 dB, $\overline{n} = 6$	Hansen 30 dB	Hansen 40 dB
5	0.02	0.04	0.04	0.05	0.05	0.07
6	0.03	0.06	0.06	0.08	0.07	0.09
7	0.04	0.08	0.08	0.11	0.09	0.13
8	0.06	0.10	0.10	0.14	0.12	0.17
9	0.07	0.13	0.13	0.18	0.16	0.21
10	0.09	0.16	0.16	0.22	0.19	0.26
11	0.11	0.19	0.20	0.26	0.23	0.32
12	0.13	0.23	0.24	0.31	0.28	0.38
13	0.15	0.27	0.28	0.37	0.33	0.44
14	0.17	0.32	0.32	0.43	0.38	0.51
15	0.20	0.36	0.37	0.49	0.43	0.59
16	0.22	0.41	0.42	0.56	0.49	0.67
17	0.26	0.47	0.48	0.63	0.56	0.76
18	0.29	0.52	0.54	0.71	0.63	0.85
19	0.32	0.58	0.60	0.79	0.70	0.95
20	0.36	0.65	0.67	0.88	0.77	1.06
21	0.39	0.71	0.74	0.97	0.86	1.17
22	0.43	0.78	0.81	1.07	0.94	1.28
23	0.47	0.86	0.88	1.17	1.03	1.40
24	0.52	0.94	0.96	1.27	1.12	1.53
25	0.56	1.02	1.05	1.38	1.22	1.66

We can calculate an upper bound on the sidelobes easily. Assume that the blockage distribution is uniform and compared to the main aperture, produces a broad, flat beam. Since the blockage aperture fields are 180° out of phase from the unblocked aperture fields, their radiation subtracts from the main beam and adds sidelobes 180° out of phase with respect to the main lobe. The sidelobe due to the blockage is proportional to the area: sidelobe level $= 20 \log b$. This formula estimates values much higher than are realized. Table 4-41 lists the sidelobes of a centrally blocked Taylor circular aperture distribution with 40-dB design sidelobes. They are far less than predicted by the upper bound.

TABLE 4-41 Sidelobe Level Due to Central Blockage of a Circular Aperture with Taylor Distribution (40 dB, $\overline{n} = 6$)

Blockage (% of Diameter)	Sidelobe Level (dB)	Blockage (% of Diameter)	Sidelobe Level (dB)	Blockage (% of Diameter)	Sidelobe Level (dB)
7	34.5	13	26.1	19	21.1
8	32.8	14	25.6	20	20.4
9	31.3	15	24.2	21	19.7
10	29.8	16	23.3	22	19.1
11	28.5	17	21.7	23	18.5
12	27.3	18	21.7	24	18.0

Ludwig [27] has found distributions to reduce the sidelobes of blocked apertures. The first sidelobe can be reduced only a little, but the outer sidelobe levels can be controlled. In many applications one high sidelobe next to the main beam is acceptable. A Taylor distribution for circular apertures with a zero edges value, like Section 4-5 for linear apertures, reduces the far-out sidelobes. A second aperture function with a doughnut distribution also reduces all but the first sidelobe. Reducing the edge taper of the blockage distribution lowers the blockage-caused sidelobes.

Sachidananda and Ramakrishna [28] use a numerical optimization technique to reduce the sidelobes of a blocked aperture for both the sum and difference patterns of a monopulse excitation. They start with the Taylor and Bayliss circular-aperture distribution functions [Eqs. (4-94) and (4-98)]. The coefficients B_m are determined through the numerical optimization, which restrains the sidelobes while optimizing the monopulse tracking coefficients and sum pattern gain.

4-24 QUADRATIC PHASE ERROR

A linear phase error function scans the aperture beam with some loss of gain because of the shrinking of the projected aperture in the direction of the main beam. Quadratic phase error (order 2) does not scan the beam but causes loss and a change in the sidelobe levels and the depth of the nulls between them. This phase error arises mainly from defocusing when the source of radiation appears as a point source. A feed axially displaced from the focus of a parabolic reflector produces quadratic phase error in the aperture. The flare angle of a horn changes the distance from the assumed point source in the throat to different points in the aperture at the end of the flare. We can approximate the phase distribution as quadratic.

We express the quadratic phase error in a line-source aperture as

$$\text{linear:} \quad e^{-j2\pi S(2x/a)^2} \qquad |x/a| \le 0.5 \tag{4-113a}$$

where S is a dimensionless constant, cycles and a is the aperture width. Similarly, the circular-aperture phase is

$$\text{circular:} \quad e^{-j2\pi Sr^2} \qquad r \le 1 \tag{4-113b}$$

where r is the normalized radius. We use Eq. (4-7) with the linear-source aperture phase error [Eq. (4-113a)] and use Eq. (4-9) with the quadratic phase error [Eq. (4-113b)] in a circularly symmetrical aperture distribution to compute phase error loss:

$$\text{PEL}_x = \frac{\left| \int_{-a/2}^{a/2} E(x) e^{-j2\pi S(2x/a)^2}\, dx \right|^2}{\left[\int_{-a/2}^{a/2} |E(x)|\, dx \right]^2} \qquad \text{linear} \tag{4-114}$$

$$\text{PEL} = \frac{\left| \int_0^1 E(r) e^{-j2\pi Sr^2} r\, dr \right|^2}{\left[\int_0^1 |E(r)| r\, dr \right]^2} \qquad \text{circular} \tag{4-115}$$

A few distributions have simple formulas for the phase error efficiency when excited with quadratic phase error [29]:

$$\text{uniform linear:} \quad \text{PEL}_x = \frac{1}{2S}\left[C^2(2\sqrt{S}) + S^2(2\sqrt{S})\right] \tag{4-116}$$

where $C(t)$ and $S(t)$ are the Fresnel integrals, tabulated functions:

$$\text{uniform circular: PEL} = \left(\frac{\sin \pi S}{\pi S}\right)^2 \tag{4-117}$$

$$\text{Circular Gaussian}(e^{-\rho r^2}): \quad \text{PEL} = \frac{\rho^2[1 - 2e^{-\rho}\cos(2\pi S) + e^{-2\rho}]}{[\rho^2 + (2\pi S)^2](1 - e^{-\rho})^2} \tag{4-118}$$

We use numerical integration for the general distribution.

Table 4-42 lists quadratic phase error losses for various linear-aperture distributions. We will use the lists for uniform and cosine distributions to evaluate the gains of rectangular horns. The effect of quadratic phase error decreases as the distribution taper increases. Table 4-43 lists results for a few circularly symmetrical aperture distributions. Quadratic phase error raises the sidelobes of low-sidelobe antennas. Figure 4-33 shows the effects on a circular Taylor distribution with 35-dB design sidelobes. The first lobe increases, and the null between the main lobe and the first sidelobe disappears as the quadratic phase error increases. A source antenna spaced a finite distance, as on

TABLE 4-42 Quadratic Phase Error Loss of Linear-Aperture Distributions (dB)

Cycles, S	Uniform	Cosine	Cosine^2	Cosine^2 + 19.9-dB Pedestal
0.05	0.04	0.02	0.01	0.02
0.10	0.15	0.07	0.04	0.07
0.15	0.34	0.16	0.09	0.16
0.20	0.62	0.29	0.16	0.28
0.25	0.97	0.45	0.25	0.44
0.30	1.40	0.65	0.36	0.63
0.35	1.92	0.88	0.49	0.84
0.40	2.54	1.14	0.64	1.08
0.45	3.24	1.43	0.80	1.34
0.50	4.04	1.75	0.97	1.62
0.55	4.93	2.09	1.16	1.90
0.60	5.91	2.44	1.36	2.19
0.65	6.96	2.82	1.57	2.48
0.70	8.04	3.20	1.79	2.76
0.75	9.08	3.58	2.01	3.04
0.80	9.98	3.95	2.23	3.29
0.85	10.60	4.31	2.46	3.52
0.90	10.87	4.65	2.69	3.73
0.95	10.80	4.97	2.91	3.92
1.00	10.50	5.25	3.13	4.09

TABLE 4-43 Quadratic Phase Error Loss of Circular-Aperture Distributions (dB)

Cycles, S	Uniform	Gaussian 12-dB Edge	Taylor 30 dB	Taylor 40 dB	Hansen 30 dB	Hansen 40 dB
0.05	0.04	0.03	0.04	0.03	0.03	0.02
0.10	0.14	0.13	0.15	0.11	0.11	0.08
0.15	0.32	0.29	0.33	0.26	0.25	0.19
0.20	0.58	0.53	0.59	0.46	0.45	0.34
0.25	0.91	0.82	0.93	0.72	0.70	0.53
0.30	1.33	1.20	1.36	1.03	1.01	0.76
0.35	1.83	1.64	1.86	1.41	1.38	1.03
0.40	2.42	2.16	2.46	1.84	1.81	1.34
0.45	3.12	2.76	3.16	2.33	2.30	1.69
0.50	3.92	3.44	3.95	2.87	2.85	2.08
0.55	4.86	4.22	4.86	3.47	3.46	2.50
0.60	5.94	5.08	5.88	4.11	4.16	2.95
0.65	7.20	6.04	7.01	4.79	4.85	3.43
0.70	8.69	7.10	8.25	5.50	5.63	3.94
0.75	10.46	8.24	9.56	6.21	6.43	4.46
0.80	12.62	9.44	10.87	6.91	7.26	4.98
0.85	15.39	10.66	12.01	7.56	8.09	5.51
0.90	19.23	11.81	12.80	8.14	8.88	6.03
0.95		12.75		8.62	9.60	6.53
1.00		13.36		8.99	10.20	6.99

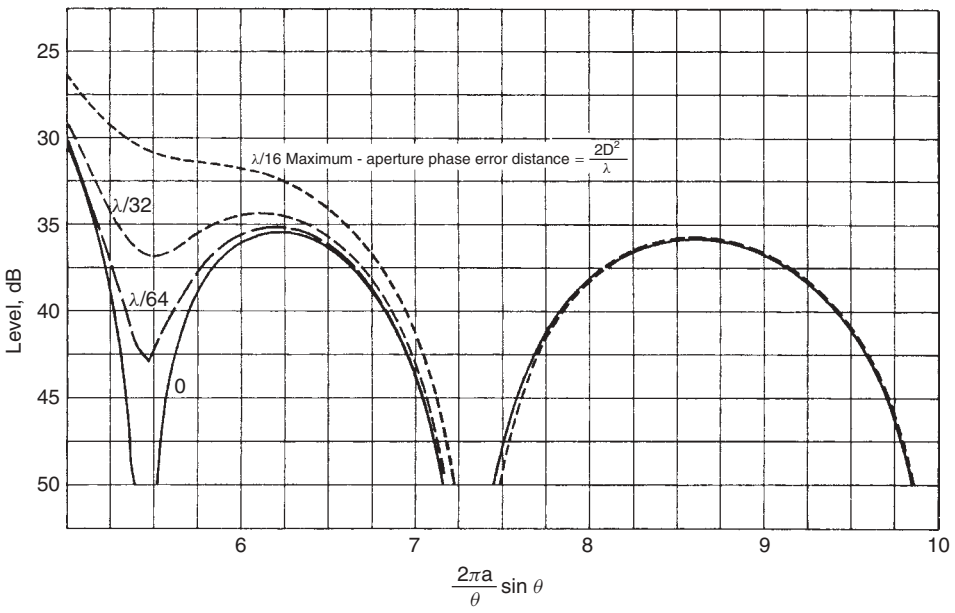

FIGURE 4-33 Effects of quadratic phase error on 35-dB circular Taylor distribution ($\overline{n} = 6$).

an antenna measurement range, feeds the aperture with a quadratic phase error. The source would have to be spaced $8D^2/\lambda$ to measure the sidelobe level within 0.5 dB. Low-sidelobe antennas require greater distances than the usual $2D^2/\lambda$ for accurate sidelobe measurement [30].

4-25 BEAM EFFICIENCY OF CIRCULAR APERTURES WITH AXISYMMETRIC DISTRIBUTION

From Eq. (1-27) we can derive an approximate formula for axisymmetric distributions that depends on the normalized variable k_r (or U). For large apertures we can approximate $\cos\theta \approx 1$ in the main beam, integrate the ϕ integral to obtain 2π, and incorporate the $(ka)^2$ directivity factor into the integral:

$$\text{beam efficiency} = \frac{\text{ATL} \cdot \text{PEL} \int_0^{k_{r1}} |f(k_r)|^2 k_r \, dk_r}{2|f(0)|^2} \tag{4-119}$$

$$= \frac{\text{ATL} \cdot \text{PEL} \int_0^{u_1} |f(U)|^2 U \, dU}{2|f(0)|^2} \tag{4-120}$$

where k_r is the factor $(2\pi a \sin\theta)/\lambda$, U (the Taylor distribution factor) is $(2a \sin\theta)/\lambda$, and a is the aperture radius. U_1 and k_{r1} correspond to the beam edge θ_1. The integrals of Eqs. (4-119) and (4-120) cause underestimations of beam efficiency for small apertures when we ignore the $\cos\theta$ factor, which should divide the argument of the integral.

Table 4-44 lists beam edges in k_r-space $(2\pi a \sin\theta)/\lambda$ for various distributions along with the beam efficiency at the null beam edge. We can use it to determine the aperture size required for a given beam efficiency beamwidth specification.

Example Calculate the aperture radius to give a 90% beam efficient beamwidth of 5° for the distribution: parabolic on 12-dB pedestal.

TABLE 4-44 Beam Efficiencies of Axisymmetric Circular-Aperture Distributions

			$k_r = 2\pi a \sin\theta/\lambda$ Specified Beam Efficiency (%)			
Distribution	Null, k_r	Beam Efficiency at Null (%)	80	85	90	95
Uniform	3.83	83.7	2.82	4.71	5.98	
Parabolic	5.14	98.2	2.81	3.03	3.31	3.75
Parabolic + 12-dB pedestal	4.58	96.4	2.60	2.81	3.10	3.64
Taylor						
30 dB, $\overline{n} = 6$	4.90	96.2	2.65	2.88	3.19	3.82
30 dB, $\overline{n} = 10$	4.74	91.4	2.76	3.06	3.65	
40 dB, $\overline{n} = 6$	6.00	99.5	2.90	3.13	3.42	3.85
Hansen						
30 dB	5.37	99.3	2.79	3.01	3.28	3.69
40 dB	6.64	99.9	3.17	3.42	3.73	4.19

From Table 4-43,

$$k_r(90\%) = 3.10 = \frac{2\pi a}{\lambda} \sin \frac{5^\circ}{2}$$

$$\frac{a}{\lambda} = \frac{3.10}{2\pi \sin(5^\circ/2)} = 11.31$$

The beam edge has $\cos 2.5^\circ = 0.999$, which justifies the approximation in Eq. (4-119).

REFERENCES

1. T. T. Taylor, Design of line source antennas for narrow beamwidth and low sidelobes, *IEEE Transactions on Antennas and Propagation*, vol. AP-4, no. 1, January 1955, pp. 16–28.
2. C. L. Dolph, A current distribution for broadside arrays which optimizes the relationship between beamwidth and sidelobe level, *Proceedings of IEEE*, vol. 34, June 1946, pp. 335–348.
3. R. C. Hansen, Linear arrays, Chapter 9 in A. W. Rudge et al., eds., *The Handbook of Antenna Design*, Vol. 2, Peter Peregrinus, London, 1982.
4. D. R. Rhodes, On a new condition for physical realizability of planar antennas, *IEEE Transactions on Antennas and Propagation*, vol. AP-19, no. 2, March 1971, pp. 162–166.
5. D. R. Rhodes, On the Taylor distribution, *IEEE Transactions on Antennas and Propagation*, vol. AP-20, no. 2, March 1972, pp. 143–145.
6. R. S. Elliott, *Antenna Theory and Design*, Prentice-Hall, Englewood Cliffs, NJ, 1981.
7. D. A. Pierre, *Optimization Theory with Applications*, Wiley, New York, 1969.
8. E. T. Bayliss, Design of monopulse antenna difference patterns with low sidelobes, *Bell System Technical Journal*, vol. 47, May–June 1968, pp. 623–650.
9. P. M. Woodward, A method of calculating the field over a plane aperture required to produce a given polar diagram, *Proceedings of IEE*, vol. 93, pt. IIIA, 1947, pp. 1554–1558.
10. S. A. Schelkunoff, A mathematical theory of linear arrays, *Bell System Technical Journal*, vol. 22, 1943, pp. 80–107.
11. J. Kraus, *Antennas*, McGraw-Hill, New York, 1950.
12. R. S. Elliott, Beamwidth and directivity of large scanning arrays, *Microwave Journal*, vol. 6, no. 12, December 1963, pp. 53–60.
13. A. T. Villeneuve, Taylor patterns for discrete arrays, *IEEE Transactions on Antennas and Propagation*, vol. AP-32, no. 10, October 1984, pp. 1089–1092.
14. R. S. Elliott, On discretizing continuous aperture distributions, *IEEE Transactions on Antennas and Propagation*, vol. AP-25, no. 5, September 1977, pp. 617–621.
15. H. J. Orchard, R. S. Elliott, and G. J. Stern, Optimising the synthesis of shaped beam antenna patterns, *IEE Proceedings*, vol. 132, pt. H, no. 1, February 1985, pp. 63–68.
16. Y. U. Kim and R. S. Elliott, Shaped-pattern synthesis using pure real distributions, *IEEE Transactions on Antennas and Propagation*, vol. AP-36, no. 11, November 1988, pp. 1645–1648.
17. F. Ares-Pena, Application of genetic algorithms and simulated annealing to some antenna problems, Chapter 5 in Y. Rahamat-Samii and E. Michielssen, eds., *Electromagnetic Optimization by Genetic Algorithms*, Wiley, New York, 1999.
18. C. H. Walters, *Traveling Wave Antennas*, Dover, New York, 1970.
19. G. Doundoulakis and S. Gethin, Far field patterns of circular paraboloidal reflectors, *IRE National Convention Record*, pt. 1, 1959, pp. 155–173.

20. R. C. Hansen, Circular aperture distribution with one parameter, *Electronic Letters*, vol. 11, no. 8, April 17, 1975, p. 184.
21. R. C. Hansen, A one-parameter circular aperture with narrow beamwidth and low sidelobes, *IEEE Transactions on Antennas and Propagation*, vol. AP-24, no. 4, July 1976, pp. 477–480.
22. T. T. Taylor, Design of circular apertures for narrow beamwidth and low side lobes, *IEEE Transactions on Antennas and Propagation*, vol. AP-8, no. 1, January 1960, pp. 17–22.
23. F. I. Tseng and D. K. Cheng, Optimum scannable planar arrays with an invariant side-lobe level, *Proceedings of IEEE*, vol. 56, no. 11, November 1968, pp. 1771–1778.
24. D. Steinberg, *Principles of Aperture and Array System Design*, Wiley, New York, 1976.
25. D. K. Cheng, *Analysis of Linear Systems*, Addison-Wesley, Reading, MA., 1959.
26. S. R. Laxpati, Planar array synthesis with prescribed pattern nulls, *IEEE Transactions on Antennas and Propagation*, vol. AP-30, no. 6, November 1982, pp. 1176–1183.
27. A. C. Ludwig, Low sidelobe aperture distributions for blocked and unblocked circular apertures, *IEEE Transactions on Antennas and Propagation*, vol. AP-30, no. 5, September 1982, pp. 933–946.
28. M. Sachidananda and S. Ramakrishna, Constrained optimization of monopulse circular aperture distribution in the presence of blockage, *IEEE Transactions on Antennas and Propagation*, vol. AP-31, no. 2, March 1983, pp. 286–293.
29. A. W. Love, Quadratic phase error loss in circular apertures, *Electronics Letters*, vol. 15, no. 10, May 10, 1979, pp. 276, 277.
30. P. S. Hacker and H. E. Schrank, Range requirements for measuring low and ultralow sidelobe antenna patterns, *IEEE Transactions on Antennas and Propagation*, vol. AP-30, no. 5, September 1982, pp. 956–966.